

Assessing the hydro-logic performance of the Aquaflow in Rotterdam

A monitoring case study of the Agniesebuurt area of Rotterdam

Mikki Metz

Assessing the hydrologic performance of the AquafLOW in Rotterdam

A monitoring case study of the Agniesebuurt area of Rotterdam

by

Mikki Metz

In partial fulfilment of the requirements for the degree of

Master of Science
in Civil Engineering

at the Delft University of Technology,
to be defended publicly on Tuesday September 27, 2022 at 13:00 PM.

Supervisor: Prof. Dr. Zoran Kapelan
Thesis committee: Dr. Thom Bogaard (TU Delft)
Ir. Ella van der Hout (Municipality of Rotterdam)
Dr. Nikola Stanic (Municipality of Rotterdam)

Preface

This thesis is the product of a years work with the involvement many interesting, knowledgeable people at both the municipality of Rotterdam and the TU Delft. The Municipality of Rotterdam (IBR) provided me with the resources to conduct this research. I would like to start of by thanking Ella van der Hout and Nikola Stanic for their constant support, feedback and motivational meetings. Ella, thank you for the help in securing the budget for all the monitoring, for applying your years of experience and the interpretation of the field work data. Thanks to you in part, I was able to use the flowmeter. Nikola, thank you for all your help in the processing of the data, the thesis writing and your advice to just have a beer once in a while. Thanks goes to my TU Delft graduation committee members Zoran Kapelan and Thom Bogaard, for your patience, constructive feedback, expert knowledge and enthusiasm of this topic.

For all the people involved in the purchasing and installation of the flowmeter: thank you and your efforts are not forgotten! Francois Kamminga, thank you for the constant supply and organisation of monitoring equipment, all your explanations, and your tireless input for the orchestration of the flowmeter installation. The flowmeter ordering, set-up design and calibration is thanks to Willem van Bommel, thank you for all your advice in relation to the monitoring equipment and output. Special thanks to Bas Koolhaas of the municipality, Pierre, Don and Sven from Kloens for making the entire installation of the flowmeter possible. And thank you Bert de Doelder for organising the financing. Lastly, without Sacha, Gino and the rest of the field team, I would not have all the groundwater, manhole and gully-pot level data available, so thank you.

Thank you to my parents, my sister and the people close to me for the patience, peptalks and advice and good distractions. Tijn, thanks for all your tips, tricks, laughs and food, best roomie ever. And last but not least, Thor, thanks for all you did and do and for being my biggest supporter.

Working on this thesis in a spring/summer period with little rain and a large precipitation deficit, has underlined the importance of finding solutions to restore the natural hydrologic cycle and to create climate resilient cities. I look forward to continue to work in this field!

Mikki Metz
Delft, August 2022

Summary

The municipality of Rotterdam is increasingly applying sustainable urban drainage systems in its urban drainage network. Sustainable urban drainage systems, or SUDS, aim to replicate the natural, pre-development drainage from a site, and are usually applied in a sequence of stormwater practices and technologies. The Aquaflow system is a type of SUDS that combines stormwater runoff retention with road functionality and infiltration, by storing runoff in its road foundation. In the Agniesebuurt area of Rotterdam, the Aquaflow system was applied in combination with a renewed, separated sewer system and perforated drainage-infiltration-transport pipes (DIT pipes). To determine the possibilities for future implementation of the Aquaflow in Rotterdam, it is important to quantify the functioning of the system. In this study, the hydrological performance of the Aquaflow system was assessed.

The case study area of this study was the Agniesebuurt area, in the North of Rotterdam. The Meester Marrestraat, to the South-West of the case study area was the test area. At the test area, gully-pot water levels, groundwater levels, flow at the DIT pipe and water temperatures in manholes and gully-pots were measured, using equipment provided by the municipality. To quantify the hydrologic performance, eight performance criteria were defined related to the ponding at surface level, emptying time of the granulate foundation layer, peak delay, volume retention and groundwater recharge. The Aquaflow performance at the test location was quantified using naturally occurring rain events, monitored by three weather stations provided by the Royal Netherlands Meteorological Institute, Sky-Echo and a tipping bucket rain gauge. The monitoring period spanned from November 2021 to June 2022, resulting in the selection of 6 rain events. These events varied in intensity (20 - 65 mm/hour), volume (8 - 30 m^3), antecedent dry days and initial groundwater table. In addition to the naturally occurring events, a full scale test was conducted, to provide information regarding intense rainfall events. The monitoring results provided insight to the Aquaflow performance. The Aquaflow system performed well in terms of peak delay, volume retention and peak reduction. The total peak delay was 3:45 to 8:30 hours, for all monitored events. The total volume retention was between 50.5% and 97%, depending on the soil saturation prior to the event and the rainfall volume. The peak reduction capacity of the Aquaflow system was found to depend mainly on the rainfall intensity and initial soil conditions, and ranged from 15% to 76%.

In addition to monitoring results related to the aforementioned metrics, a model was created using Hydrus 2D, to estimate the subsurface groundwater flows from Aquaflow infiltration. The model was calibrated using the full-scale test data and estimated van Genuchten parameters, from soil experiments. The created, calibrated Hydrus 2D provides a means to determine the effects of Aquaflow infiltration on the groundwater table, the delay of the system and the total runoff through the DIT pipe. The model performed well in showing the trend in the system response. From the modelling, parameters for future implementation were found:

The hydrologic performance of the Aquaflow system at the test area Meester Marrestraat in the Agniesebuurt area in Rotterdam is high for all the defined performance criteria. The Aquaflow system performs well in delaying peak runoff (4-8 hours), volume retention (50 - 97%) and peak reduction (15% for wet initial conditions to 76% for dry initial conditions.). The road cunet below the Aquaflow foundation was found to be critical in delaying peak runoff and providing groundwater recharge. The gully-pots were found to be sensitive to clogging and subsidence. When applying perforated drain pipes in combination with the Aquaflow, groundwater recharge and fluctuations are achieved, while maintaining the specified drainage level. The monitoring period proved to be an extremely dry period, with long dry spells. Therefore the results provide great insight into the Aquaflow and DIT performance under dry, low groundwater level conditions.

Contents

Preface	i
Nomenclature	v
1 Introduction	1
1.1 Motivation	1
1.2 Background	2
1.3 Problem Statement	2
1.3.1 Goal and Objectives	3
2 Literature Review	4
2.0.1 Natural Hydrologic Cycle	4
2.1 Urban Hydrologic Cycle	5
2.1.1 Hydrologic Cycle in the Netherlands	6
2.2 SUDS: future of urban hydrologic cycle	7
2.2.1 Aquaflow	11
3 Case study area	13
3.1 Rotterdam	13
3.2 Agniesebuurt area	15
3.2.1 Introduction	15
3.2.2 Test area	16
3.2.3 Urban drainage system	16
3.2.4 Subsurface	18
3.2.5 Groundwater	20
4 Performance criteria	22
4.1 Performance criteria definition	22
4.1.1 Stormwater Runoff	22
4.1.2 Filling- and emptying time	23
4.1.3 Peak delay and volume retention	23
4.1.4 Groundwater recharge	24
4.1.5 Criteria Summary	25
5 Methods	26
5.1 Monitoring	26
5.1.1 Precipitation	27
5.1.2 Full scale test	28
5.1.3 Ponding and Aquaflow emptying time	29
5.1.4 Peak delay and volume retention	29
5.1.5 Groundwater table	33
5.1.6 Barometric pressure	34
5.2 Modeling	35
5.2.1 Required input	36
5.2.2 Model set-up	37
6 Results	40
6.1 Event selection	40
6.2 Aquaflow response	40
6.2.1 Event 1: Full scale test	40
6.2.2 Event 2: May 20	47
6.2.3 Event 3: 23 May 2022	51

6.2.4	Event 4: 5 June 2022	55
6.2.5	Event 5: 7 April 2022.	58
6.2.6	Aquaflow response: overview	61
6.3	Model results	62
6.3.1	Model calibration and validation: full-scale test	62
6.3.2	Aquaflow event model response.	64
6.3.3	Hydrus for Aquaflow: overview	67
7	Conclusions & Recommendations	69
7.1	Conclusions.	69
7.1.1	Hydrological performance of the Aquaflow system	69
7.1.2	Performance limiting factors	69
7.1.3	Model performance.	70
7.1.4	Monitoring.	70
7.2	Recommendations	70
	Bibliography	71
A	Appendix A: Subsurface	78
B	Rainfall analysis	90
C	Hydrus	92

Abbreviations

Abbreviation	Definition
NAP	Nationaal Amsterdams Peil. Reference level used in The Netherlands. NAP 0m is approximately the average sealevel of the North Sea [Ministerie van Infrastructuur en Waterstaat, 2021]
KNMI	Koninklijke Nederlandse Meteorologisch Instituut (Royal Dutch Meteorological Institute).
SUDS	Sustainable Urban Drainage Systems
LID	Low Impact Development
GI	Green Infrastructure
BGI	Blue-Green Infrastructure
UHI	Urban Heat Island
SVF	Sky View Factor
WRC	Soil Water Retention Curve

Introduction

1.1. Motivation

Climate change by global warming is a worldwide phenomenon and calls for transformative change [Ripple et al., 2021, Oo et al., 2019]. The effects of climate change have worldwide impact on the economy, food security, human- and ecological health and overall livelihood [Patz et al., 2014, Watts et al., 2021]. In 2021, effects of climate change were visible in all continents, with extreme rainfall in China and Europe causing fatal floods, the deep freeze in Texas and the extreme heat waves in Canada and the Pacific Northwest as clear examples [Boers and Rypdal, 2021, Ramirez et al., 2021, WMO, 2021]. And still, scientists are warning there is more to come [Brenner, 2019, Ripple et al., 2020]. The 2022 IPCC report predicts a further increase of extreme weather events and natural disasters, as global temperatures continue to rise.

Another worldwide phenomenon is urbanisation. As of 2022, more than 50% of the world's population is living in urban areas. While in Europe, this percentage is approximately 75% [Nabiliek, 2016] and this number is projected to increase [Chen et al., 2014, Gašparović et al., 2021]. Urban areas can be defined as areas with very high level of human interference with natural processes [Klungniam, 2016]. There is a clear relation between global warming and urbanisation. The global warming heats up urban areas, while increasing urbanisation leads to the generation of the urban heat island and CO₂ emissions [Kumar, 2021, Eugenia and Ming, 2003, Zhou et al., 2004]. Consequently, approximately 70% of the global CO₂ emissions originate from urban areas [Ribeiro et al., 2019]. Furthermore, urbanisation affects not only the natural hydrologic cycle and ecosystems, but also overall human well-being and health [Maheshwari et al., 2020].

Urban areas are typically densely populated, with extensive infrastructure, high mobility, high impermeability and the presence of urban drainage systems. Conventional urban drainage systems were designed to rapidly transport stormwater and waste water away from urban areas. The increased imperviousness and enhanced connectivity of drainage networks has altered the hydrologic cycle in these urban areas, and led to vulnerability for higher stormwater runoff volumes and peaks compared to the natural situation [Sarkar et al., 2018, Li et al., 2016, Li et al., 2018].

Climate change is expected to affect urban areas in the future, with hazards from flash/surface flooding, sea level rise, heat waves, rain storms, droughts and fires [Harrington et al., 2022]. These extremes have become very visible in Europe over the past years, with catastrophic flooding in Germany, Belgium and the Netherlands in summer 2021 [Kreienkamp et al., 2021]. And, the extreme water deficit, heat waves and forest fires in summer 2022 [Toreti et al., 2022, Satoh et al., 2022]. The vulnerability and contribution of urban areas to global warming play a central role in pursuing solutions and mitigation and adaptation strategies against climate change. The increased awareness of climate change threats to urban areas, has led to various climate adaptation strategies internationally. Climate adaptation in urban areas has been widely reported and seven adaptation strategies can be summarized, regarding the potential of: (i) the lay-out of cities, (ii) building design and materials (iii) urban materials and sur-

faces to influence absorption, heat storage and emissivity, (iv) the amount of greenery, (v) lowering of anthropogenic heat production, (vi) green- and blue infrastructure and (vii) ecosystem-based adaptation [Lenzholzer et al., 2020, Mauree et al., 2019, Geneletti and Zardo, 2016, Mees and Driessen, 2011]. In this thesis, the focus lies on green- and blue infrastructure and ecosystem-based adaptation.

1.2. Background

As a densely populated country, in the Netherlands, the focus has shifted from conventional urban drainage systems to more sustainable urban drainage systems, by focusing on the reuse and retention of stormwater through 'retention, storage, discharge' (Figure 1.1). The Netherlands is the most densely populated country in Europe, with an urban population of more than 90%. It is expected the urban populations will increase by 2035 by 15-20% in Amsterdam and Rotterdam respectively [PBL, 2019]. In the Netherlands, responsibilities regarding water management in urban areas are divided among the government, municipalities, Water Boards and residents. Water Boards are responsible for the surface water, municipalities for public ground- and rainwater and residents for ground- and rainwater at their own properties.

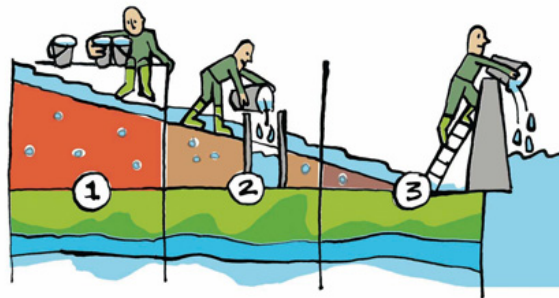


Figure 1.1: retention, storage, discharge (Dutch Government)

The municipality of Rotterdam is the second largest municipality of the Netherlands. It has a total area of 32,414 hectares and 650,000 inhabitants. The total impermeable surface area is approximately 13,000 hectares. In Rotterdam, the urban water system is divided in four segments: the sewer system and sewage treatment plants, surface water system, subsurface and groundwater system (groundwater table, aquifers, drainage and infiltration) and the public area consisting of all permeable and impermeable surfaces. An area of 4,400 hectares is connected to the urban drainage system, with a total length of 2,600 km.

The Municipality of Rotterdam is focused on five goals for the near future of the urban drainage system [Rotterdam, 2021]:

1. To create a functioning urban drainage system for public health and attractive living conditions;
2. Creating a climate resilient water system by focusing on collection, retention, transport, processing and reuse of rainwater to prevent (pluvial) flooding;
3. Creating a robust groundwater system by applying measures that prevent structural negative effects from high or low groundwater table;
4. Active communication between all parties;
5. Focus on innovation, digitalization en automatization.

1.3. Problem Statement

For urban drainage renewal in Rotterdam, the above aspects must be considered. Sustainable Urban Drainage Systems (**SUDS**), Low Impact Development (**LID**) and Green Infrastructure (**GI**) are measures to meet the urban drainage goals of the Municipality of Rotterdam. Such systems (e.g. bioswales, permeable pavements and green roofs), combine urban drainage functions with climate adaptation. Another example of such measures is the Aquaflow system [AquaflowB.V., 2014]. This

system combines road functionality with stormwater retention, by storing stormwater runoff in the road's foundation. The Aquaflow system meets the Municipality's climate adaptation requirements by combining stormwater retention, peak delay and infiltration.

The positive effects of SUDS are not only known in Rotterdam. In recent years, SUDS have been applied globally for more climate resilient cities. The increasing application of SUDS, like the Aquaflow system, has led to more research on the subject and possible positive and negative effects. Aquaflow knows several application types; permeable pavements, permeable bottoms, impermeable pavements and impermeable bottoms. The storage and protection of rainfall runoff by Aquaflow was investigated by [Coupe et al., 2009]. In 2006, Wijtze et al. studied the potential application of Aquaflow with a focus on the sub-base, by addressing road construction stability, heavy metal attenuation and storing capacity, among others [Boomsma and ir Marinus Huurman, 2006]. The potential for multipurpose roads, to adverse the effect on the local hydrology was discussed by Puertas et al [Puertas et al., 2014]. The effect of infiltrating SUDS on the water balance was investigated by many. [Wang and Guo, 2020] derived equations for the dynamic water balance of infiltration based BMPs (or SUDS). [Leimgruber et al., 2018] assessed sensitivity of water balance components to the parameters of LIDs (or SUDS).

The potential effects on the water balance, filtering of heavy metals and contaminants, and potential positive effects of infiltrating road foundations have been investigated in previous research. However, to the author's knowledge, an in-detail research of the positive effect of Aquaflow on runoff retention and peak delay, in combination with model predictions for different events of the subsurface effects and hydrologic performance has not been performed yet. The application of SUDS, like the Aquaflow, is expected to rapidly increase in the future, therefore understanding of the effects of SUDS on the local hydrologic system and urban drainage system is of interest.

1.3.1. Goal and Objectives

The goal of this research is to assess the effects of the Aquaflow infiltrating road foundation on the local hydrologic system. As a result, four research questions were formulated:

1. What is the hydrologic performance of the Aquaflow system in the Agniesebuurt area of the Municipality of Rotterdam?
2. What are the limiting factors to the Aquaflow system hydrologic performance in the Agniesebuurt area?
3. Can Hydrus 2D be used to model Aquaflow response to monitored rainfall events in the Agniesebuurt area and Rotterdam?
4. What are recommendations for future implementation of the Aquaflow system in Rotterdam?

2

Literature Review

Sustainable urban drainage systems (SUDS), like Aquaflow have an effect on the local hydrologic cycle. To quantify these effects, a literature review was conducted. First, the natural hydrologic cycle and the associated fluxes are introduced. Then, the hydrologic cycle is related to the urban hydrologic cycle. SUDS provide a future of the urban hydrologic cycle. The most popular SUDS are explained in the final section.

2.0.1. Natural Hydrologic Cycle

The natural hydrologic cycle describes the cycle of water through many phases driven by solar radiation and gravity [Hordon, 1998, Yang et al., 2021, Singh et al., 2020, Marsalek et al., 2006]. This process is illustrated in Figure 2.1. Water evaporates from the large water bodies: oceans and seas. The solar radiation causes evaporation, after which the water in the gaseous phase is part of the atmosphere. Evaporation is the phase change from liquid to vapor and is affected by temperature and ambient humidity [U.S. EPA, 2008]. By cooling of the vapor, condensation occurs, from which precipitation is formed. Precipitation can be in many states like rain or snow. Precipitation falls on the Earth's surface and surface water bodies and is stored at the surface and absorbed by vegetation, soil, leaves etc [Kuchment, 2004]. Part of this stored water evaporates directly from the wet surface, this process is interception. Net precipitation (after interception) can infiltrate, depending on the soil saturation, or runoff over land.

Infiltration is the movement of water from above ground into the subsurface. Infiltrated water enters the unsaturated zone, where it is available for plant uptake. Transpiration is the movement of water to the atmosphere by plant respiration. Plants take up water from the soil through their roots and emit it through their leaves and water evaporates from the soil. Precipitation that does not evaporate and exceeds soil's infiltration capacity, flows away overland [Pagano and Sorooshian, 2002]. Three types of runoff are defined: surface runoff, subsurface runoff and base-flow [Geography Notes and Riya, 2018]. The excess water in the unsaturated zone percolates down to the water table [Poeter et al., 2020]. When recharge occurs, the water table rises. The factors that affect infiltration are: (i) water table depth, (ii) hydraulic properties of the soil, (iii) surface entry possibilities of the soils, (iv) soil moisture [Balasubramanian and Nagaraju, , Ferré and Warrick, 2005]. On steep slopes, part of the infiltration can runoff quickly underground (subsurface runoff). The groundwater flow eventually seeps to the surface water (base flow). Groundwater outflow is defined as the seepage of water from the groundwater system into the surface waters. Groundwater outflow can be both horizontal and vertical. The infiltrated water is stored in the groundwater system and flows slowly toward surface water bodies.

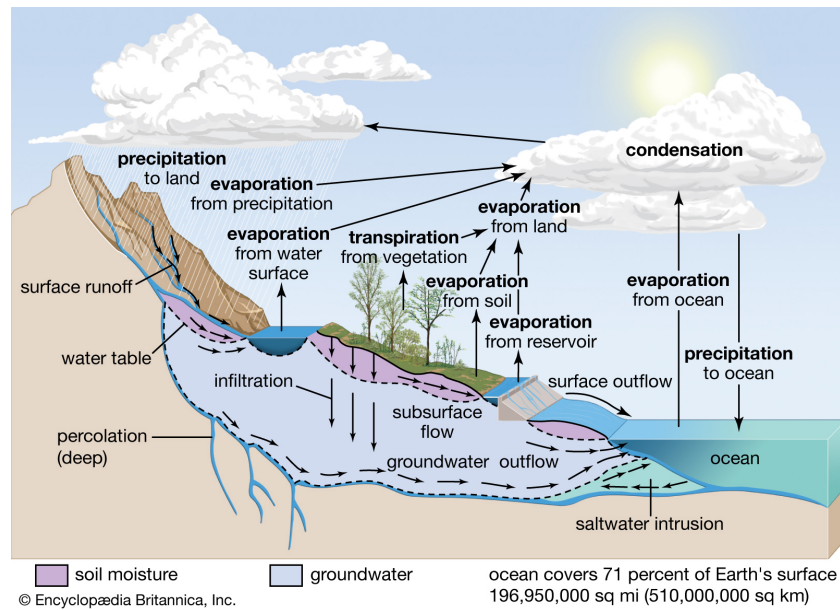


Figure 2.1: The hydrologic cycle and its associated fluxes [Encyclopaedia Britannica,]

2.1. Urban Hydrologic Cycle

The urban hydrologic cycle differs from the natural water cycle. This is mainly due to the presence of engineered water systems and the high percentage of impermeable surfaces [Dow and DeWalle, 2000, Jacobson, 2011]. Water enters urban areas in many ways: through precipitation, surface water, groundwater and through pipes (drinking water). Regarding the natural water cycle, urbanisation impacts all fluxes [McGrane, 2016].

Urban Heat Island

The main difference between the natural- and urban hydrologic cycle is the Urban Heat Island phenomenon (UHI). The UHI is caused by a range of external factors: (i) urban structure determined by the ratio of buildings and the Sky View Factor (SVF), (ii) increased emissions of anthropogenic heat flux, (iii) land cover change due to increasing imperviousness and decreasing green areas [Azevedo et al., 2016, Oke, 2006, Soltani and Sharifi, 2017]. Buildings absorb solar radiation and built areas evaporate less water, which contributes to elevated surface and air temperatures [Rahman et al., 2020] (Figure 2.2). The change in ground cover results in less shade and moisture to keep urban areas cool. Urban areas emit heat due to the high mobility and density of inhabitants [Soltani and Sharifi, 2017]. The SVF is often used to show the radiation from surfaces and defines the ratio of unobstructed sky hemisphere visible from the ground. The SVF affects the UHI since the long-wave radiation term is directly impacted by its value: the higher the SVF, the lower the long-wave radiation flux emitted by built surfaces to the sky during night-time [Bernard et al., 2018]. Typically, the UHI effect is strongest at night [Azevedo et al., 2016].

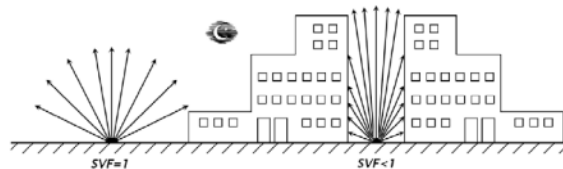


Figure 2.2: Reduced surface cooling in the urban areas, causing UHI. From [Bessembinder et al., 2013]

Precipitation

Urbanisation affects precipitation [Liu and Niyogi, 2019, Singh et al., 2020]. Potential reported causes of precipitation differences are thermal effects due to the urban heat island, air flow obstructions and

increased turbulence and a higher aerosol concentration due to pollution [Huff and Changnon, 1973, Han et al., 2014]. Liu and Niyogi showed the effects of urbanisation on rainfall (precipitation) modification. According to their research, the mean precipitation is enhanced by 18% downwind of cities and 16% over cities [Liu and Niyogi, 2019]. Steensen et al., assessed the effect of the UHI effect on precipitation and found the UHI leads to an updraft that increased moisture convection which could result in an increase in precipitation downwind [Steensen et al., 2022].

Evaporation and transpiration

The alteration of the evaporation and transpiration process in the urban hydrologic cycle, depends on different factors and is mainly caused by the increase of impermeable surfaces in the built environment, in combination with a decrease of green areas [Barron et al., 2013]. The increased impermeability, affects the runoff flux, and the potential evaporation. The limiting of green areas affects the transpiration in urban areas, and consequently, limits the cooling of urban areas [Marsalek et al., 2006, Rahman et al., 2020]. Higher temperatures increase the evaporation flux, so the increasing temperature, in turn, positively affects the evaporation. To summarize, the alteration of the evaporation and transpiration fluxes depends on the surface cover, presence of surface water and greenery and affects infiltration and runoff fluxes.

Runoff

Urbanisation affects the surface cover, and the runoff process [Li et al., 2018]. The increased impervious land cover from roads, pavements and buildings in urban areas highly increases the runoff flux compared to the natural hydrologic cycle. In urban areas, runoff is typically conveyed by the urban drainage system. These drainage systems have the ability to transport runoff at high velocities. The urban drainage systems transports runoff away from cities, and water ends up in surface water after treatment. Such systems affect the lag times and peaks of runoff. In rural areas, storm hydrographs are typically low rising with a low peak discharge. Urbanisation affects surface runoff in three ways: the reduced evaporation, transpiration and infiltration increases the runoff volumes, the speed of runoff is increased by impervious covers and by reducing the catchment response time and thereby increasing the maximum rainfall intensity causing the peak discharge [Marsalek et al., 2006, Ress et al., 2020].

Infiltration

The infiltration is strongly affected by urbanisation. In comparison to the natural hydrologic cycle, the infiltration flux in urban areas is altered by the increased imperviousness, compaction of soil and the presence of urban drainage systems [McGrane, 2016]. The groundwater flow depends on the infiltration. The altered infiltration flux in urban areas thus alters the groundwater flow flux. The decreasing infiltration results in a decreasing groundwater flow flux. However, the presence of urban drainage systems has been shown to have an additional effect on the groundwater [Wakode et al., 2018, Eiswirth and Hötzl, 1997, Foster, 2001]. In areas with low groundwater table, leaky mains allow for ex-filtration from drainage pipes, recharging the groundwater table. Conversely, the leaky mains also act as extra drainage of the groundwater table, when groundwater tables are higher than pipe level [Marsalek et al., 2006, Barron et al., 2013]

2.1.1. Hydrologic Cycle in the Netherlands

The Netherlands is characterised by deltas and former flood plains of the rivers Rhine, Meuse and Scheldt. The Western and Northern parts of the the country have elevations of approximately 6 m below NAP. The Netherlands is sloped from south-east to north-west with the highest point in the south-east at 322 m NAP and 100 m NAP in the central part of the Netherlands [Huisman, 1998]. The meteorologic climate in Netherlands is classified as Cfb, with maritime temperate climates [Steenefeld et al., 2011]. The Cfb term describes a dry, fully humid, warm summer climate [Kalvová et al., 2003]. The Dutch climate has high average precipitation in all months and an average temperature below 22 degrees Celsius in the warmest month, and at least 4 months above 10 degrees Celsius. The KNMI reports average yearly precipitation and evaporation values, the average precipitation is 900 mm and the average evaporation is 600 mm [CBS et al., 2020]. There is a yearly precipitation excess in the Netherlands. However, in recent years there has been an increasing precipitation deficit in the months from April to September, as shown in Figure 2.3. The yearly precipitation excess is related to the yearly infiltration [mm].

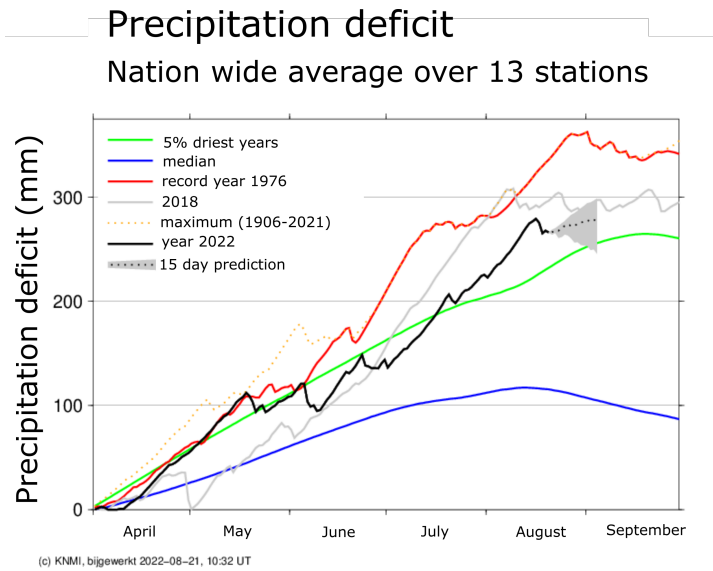


Figure 2.3: Precipitation deficit in 2022 as recorded by the Royal Netherlands Meteorological Institute [KNMI, 2022]

The Urban Heat Island effect in the Netherlands was researched by Steeneveld et al (2011) and Bessembinder et al (2013). In extreme events with calm weather, the UHI in the most urbanised areas (>25.000 inhabitants/km²) can be as high as 8-10 degrees Celsius. In other urban areas, the UHI is up to 5-7 degrees Celsius. On average, this value is approximately 0.6-1.1 degrees Celsius for urban areas with >4000 inhabitants [Bessembinder et al., 2013]. The Rotterdam area is highly urbanised and sensitive to extreme weather [Bessembinder et al., 2013]. With climate change the effects are expected to increase. According to research by the Municipality of Rotterdam, by the year 2050, the average temperature is expected to increase to 23.5 degrees with maximum temperatures of 39 degrees Celsius, and more than three weeks of >20 degrees Celsius. Regarding climate change, the KNMI predicts an overall increase of temperature and rainfall by 2050, with more heatwaves and periods of droughts [KNMI, 2015]. The KNMI predictions for 2050 and 2085 are summarized in the table in Figure 2.4.

Variabele	Indicator	Climate 1981-2010	Scenario changes for the climate around 2050				Scenario changes for the climate around 2085				Natural variations averaged over 30 years
			G _L	G _H	W _L	W _H	G _L	G _H	W _L	W _H	
Global temperature rise:			+1 °C	+1 °C	+2 °C	+2 °C	+1.5 °C	+1.5 °C	+3.5 °C	+3.5 °C	
Change in air circulation pattern:			low value	high value	low value	high value	low value	high value	low value	high value	
Sea level at North Sea coast	absolute level	3 cm above NAP	+15 to +30 cm	+15 to +30 cm	+20 to +40 cm	+20 to +40 cm	+25 to +60 cm	+25 to +60 cm	+45 to +80 cm	+45 to +80 cm	±1.4 cm
	rate of change	2.0 mm/yr.	+1 to +5.5 mm/yr.	+1 to +5.5 mm/yr.	+3.5 to +7.5 mm/yr.	+3.5 to +7.5 mm/yr.	+1 to +7.5 mm/yr.	+1 to +7.5 mm/yr.	+4 to +10.5 mm/yr.	+4 to +10.5 mm/yr.	±1.4 mm/yr.
Temperature	mean	10.1 °C	+1.0 °C	+1.4 °C	+2.0 °C	+2.3 °C	+1.3 °C	+1.7 °C	+3.3 °C	+3.7 °C	±0.16 °C
Precipitation	mean amount	851 mm	+4 %	+2.5 %	+5.5 %	+5 %	+5 %	+5 %	+7 %	+7 %	±4.2 %
Solar radiation	solar radiation	354 kJ/cm ²	+0.6 %	+1.6 %	-0.8 %	+1.2 %	-0.5 %	+1.1 %	-0.9 %	+1.4 %	±1.6 %

Figure 2.4: Climate predictions by the Royal Netherlands Meteorological Institute (2015) for 2050 and 2085 [KNMI, 2015]

2.2. SUDS: future of urban hydrologic cycle

Traditionally, urban drainage systems were designed to convey urban water away from urban areas, as quickly as possible. With increasing effects from climate change, urban drainage systems are required to increase in size to meet expected runoff demands. Due to climate change, a paradigm shift has led to more awareness for sustainable urban drainage systems, like SUDS and LID.

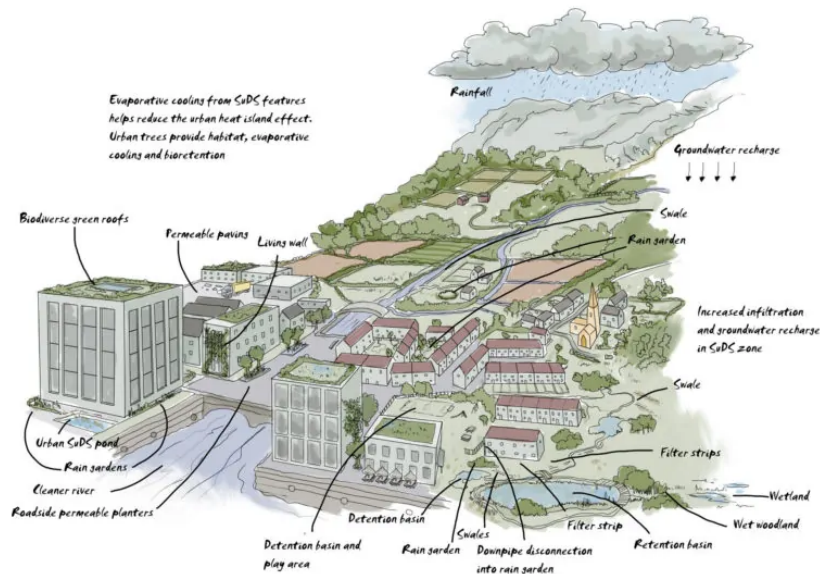


Figure 2.5: An illustration of possible SUDS to be applied in an urban catchment. [Graham et al., 2012]

SUDS, LID and BGI are all widely used terms. These systems aim to replicate the natural, pre-development drainage from a site, and are usually applied in a sequence of stormwater practices and technologies (Figure 2.5). These systems are focused on a design with nature approach to achieve a more natural hydrology of infiltration, evaporation, transpiration and runoff [Fletcher et al., 2015]. Blue-Green Infrastructure, BGI, refers to the use of blue elements, like rivers and canals and green elements, such as trees in urban planning for the retention stormwater runoff [Dar et al., 2021].

All strategies aim to combine stormwater runoff treatment and natural hydrologic phenomena like infiltration, groundwater recharge and evaporation to limit the effects of urbanisation and climate change, like heating and flooding to increase the livelihood in cities and further adapt to climate change. In this thesis, the term SUDS is used. Research has shown the capabilities of SUDS to reduce peak flow and hydrological recovery in urban areas [Charlesworth, 2010, Chan et al., 2019, Sørensen and Emilsson, 2019, Støvring et al., 2018, Paithankar and Taji, 2020, Kim and Kim, 2021]. The design and selection of SUDS is dependent of soil characteristics (i.e. infiltration rate, porosity), retention storage and available space. Examples of SUDS are listed below and the relevant research is briefly discussed in the following sections.

- Ponds
- Permeable pavements
- Green roofs
- Rainwater harvesting (rain barrels)
- Bioswales
- Wetlands
- Water Squares
- Infiltration trenches

Permeable pavements

Permeable pavement (Figure 2.6) is a porous urban surface and is applied in many forms by e.g. open pore bricks, concrete, or asphalt with an underlying stone reservoir [USGS, 2020]. Applying permeable pavements decreases the effects of impermeable road surfaces on the runoff. Water can infiltrate through the pavement.

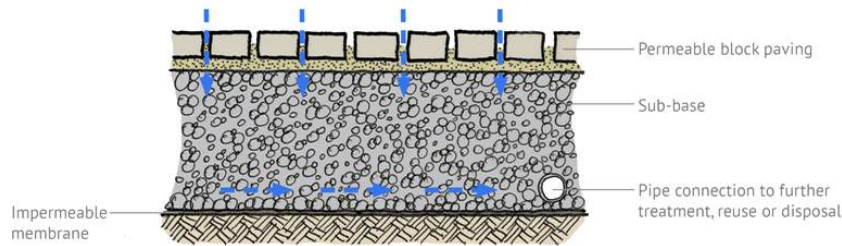


Figure 2.6: Typical permeable pavement construction from Susdrain [susdrain,].

Permeable pavement hydrologic performance has been researched by many (e.g. [Abdalla et al., 2021, Støvring et al., 2018, Marchioni and Becciu, 2014]). In the Municipality of Rotterdam, since 2003, approximately 12 hectares of permeable pavements have been applied. In addition, extensive monitoring of the permeable pavement has been done at five monitoring locations. Groundwater levels and water levels in the drain below the system were monitored. This led to the following conclusions:

- Permeable pavements provide a means for storage-retention-discharge by allowing for 100% infiltration.
- The retention time between rainfall peak and groundwater peak is 3.38 to 3.63 hours for 20-30 mm rainfall. The retention time decreases to approximately 2 hours for shorter events.

Støvring et al (2018) assessed the hydraulic performance of lined permeable pavement by measuring outflow. The total volume reduction ranged from 3% to 37%. Precipitation measured had a return period of two years, with a median volume reduction of 40%, and median lag time of 1:38 hours, ranging from 0:39 to 3:16 hours [Støvring et al., 2018]. In 2021, Abdalla et al., conducted research to lined permeable pavements (PP) in Norway, with no infiltration. For peak reduction, the PP achieved a median peak reduction of 89%, with a peak delay of 40 to 86 minutes, depending on initial conditions and rain volume [Abdalla et al., 2021].

Green roofs

Green roofs incorporate vegetation, growth medium and other landscape components on the rooftops of buildings [Vijayaraghavan, 2016]. Green roofs imitate the natural hydrologic cycle at a very small scale. When precipitation falls on the roofs, a portion of the water is absorbed or retained in the pore space and remaining water enters green roof drains. Green roofs have the potential for water storage, cooling and greening of the city. Two types of green roofs are typically defined: intensive and extensive. Intensive green roofs typically have an intensive growing media allowing for more plants and filtering. The two types are shown in Figure 2.7.

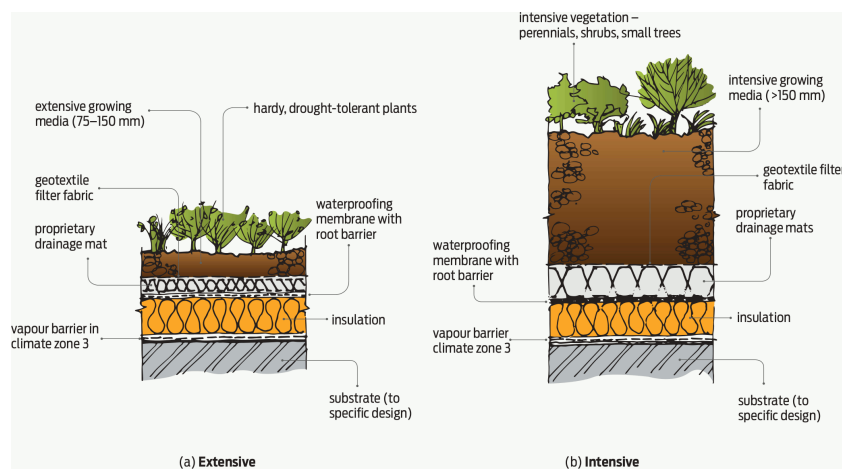


Figure 2.7: Typical green roof construction showing both extensive (a) and intensive (b) [Elkink, 2017]

Since 2006, green roofs have been increasingly applied in the city of Rotterdam. Rotterdam has 14.5 km² of flat roof surface. As of 2019, the total green roof area was 400,000 m² [Gemeente Rotterdam, 2019]. Due to the limited retention area, the green roofs hydrological effects are limited [Mobron et al., 2022].

Bioswales

Bioswales are ditches filled with filter material (plants) and granulate. Runoff passes through the different layers of bioswales and is both retained and filtered. Xiao et al described the bioswale as (1) interception from vegetation; (2) increasing subsurface storage capacity by transpiration and; (3) root channels improve infiltration [Xiao et al., 2017].

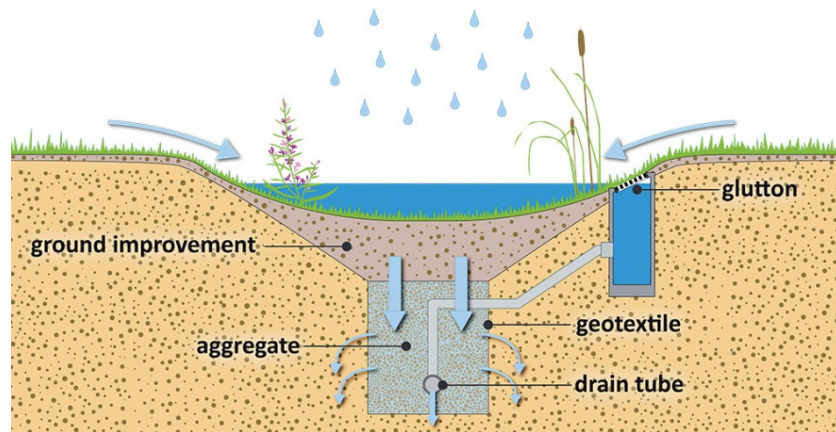


Figure 2.8: Bioswale design as illustrated by atelier GROENBLAUW [© atelier GROENBLAUW, Marlies van der Linden,].

Runoff infiltrates in the ground in a few ways. In addition to the filtering and peak retention functions, bioswales can have positive the ecosystem by using different types of plants. Bioswales have been the research topic of many papers. The performance has been shown to be promising (e.g.) in retention, but bioswales are also susceptible to clogging. Besides, these systems are high-maintenance [Xiao et al., 2017]. Davis et al, among others, assessed the hydrologic performance of bioswales with a length of 15 meters, 0.61m bottom width and a slope of 33% and 25% with a connected surface of 0.27 hectares. The attenuation was found to be 40% for small events (3 cm). Most limiting factors of bioswales was found to be the storage space. Once the soil has become saturated, very little volume is attenuated [Davis et al., 2012].

Infiltration trenches

Infiltration trenches are shallow excavations filled with gravel or other coarse materials, that create temporary subsurface storage of stormwater runoff. Stored water can exfiltrate into surrounding soils from these trenches. Infiltration trenches retain and stormwater, delay peak flows and allow for infiltration. et al conducted a study to assess the hydrological performance of infiltration trenches by comparing the infiltration trenches to traditional pipe drainage. The monitoring results indicated 77% peak discharge reduction and 98% volume reduction and showed the increased infiltration and recharge of soil and groundwater [Lucas et al., 2009].

Water squares

Water squares (Figure 2.9), combine leisure with stormwater retention. Typically, basins collect and store runoff from the area. Water squares can be applied with the sole function of peak retention, storage and/or combined with infiltration functions. Water squares have been applied in Rotterdam with the explicit aim for multi-functional solutions, such as rainwater buffering, visible urban water management and enhancement of public space [Ilgen et al., 2019].

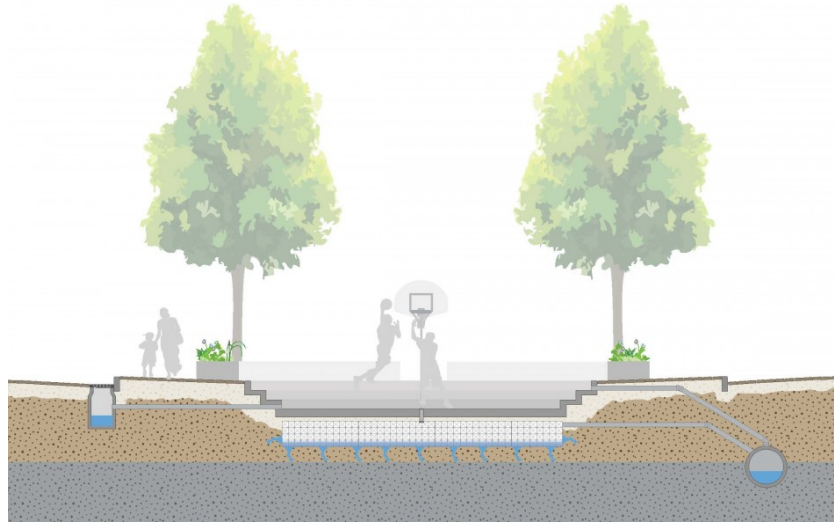


Figure 2.9: Water square design in Rotterdam [atelier GROENBLAUW,]

2.2.1. Aquaflow

Aquaflow is an innovative solution for rainwater runoff in areas where space is limited i.e. urban areas. It is a form of SUDS that combines road functionality with stormwater retention and infiltration, by storing stormwater in the road's foundation [AquaflowB.V, 2022]. Stormwater runoff enters the system through gully pots and flows into the road foundation layer. This layer is built up with freestone (8-32+mm (type (MHK53)) [AquaflowB.V., 2014], with a porosity of 40%. On placement, the granulate layer is condensed to a stiffness of 1200-1400 MPa, allowing for a horizontal displacement of 100 m/hr in the granulate layer [AquaflowB.V., 2012]. With the high level of stiffness and absence of fine materials, water tension and possibly "quicksand" can be prevented, thus underlining the potential for Aquaflow application in roads. The permeable bottom of the system allows for infiltration through percolation. The total height of the foundation layer is typically smaller than 50 cm, meaning application is possible even for very high groundwater tables [AquaflowB.V, 2022]. The Aquaflow system design is shown in Figure 2.10.

The functioning of the Aquaflow system depends on the following factors:

- The stormwater runoff to the gully-pots;
- Inflow from gully-pots to granulate layer;
- The emptying of the granulate layer via infiltration;
- Infiltration and percolation in the road cunet;
- Groundwater drainage by the drain pipe (entry to the urban drainage system)

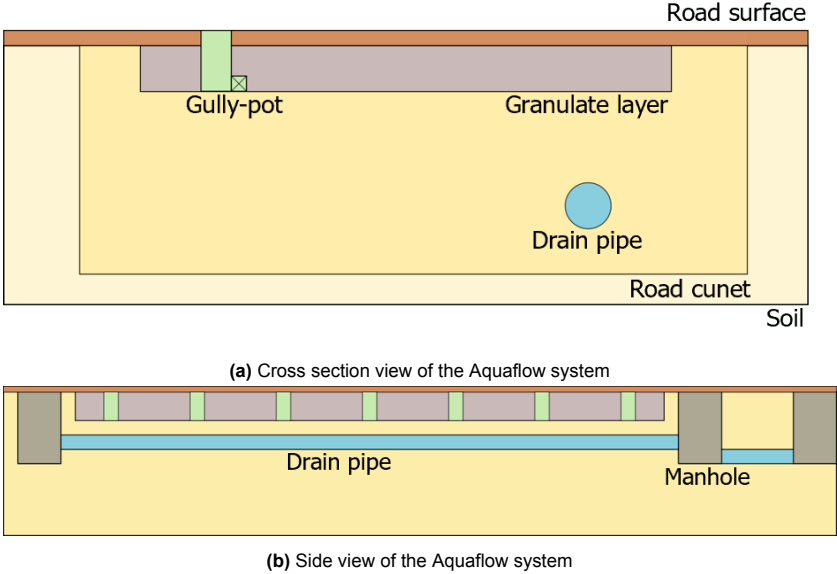


Figure 2.10: Aquaflow cross section (top figure) and Aquaflow side view (bottom figure)

3

Case study area

The Agniesebuurt area in the North of Rotterdam is the case study area of this thesis.

3.1. Rotterdam

The city of Rotterdam is a metropolitan area in het Randstad, in het West of the Netherlands. It is situated in a delta (Rijn-Maasdelta) where the North Sea meets the Maas, Rijn and Waal rivers. The Nieuwe Maas, a river branch of the Rijn, splits the city in two, creating the Northern and Southern parts of the city. To the West of the city, at the North Sea border lies the Port of Rotterdam, the largest seaport in Europe. For the most part, Rotterdam lies below sea level. In the Netherlands the reference level is the average sea level of the North Sea, meters relative to sea level (**m NAP**). The city is protected by dikes along rivers, and dunes and storm surge barriers along the North Sea coast. A system of water storage and pumping stations, transports water to and from the polder area behind the dikes and dunes. As a result of peat excavations for fuel, many water bodies were created, these water bodies were dried up by windmills and pumping stations, forming polders. As a result of the peat excavations in the area and water drainage out of the area, land subsidence occurred. The Western part of the Netherlands, with the exception of the dune area, can be characterised as mainly low-lying polder area.

The city of Rotterdam was built around 1270, when the river Rotte was dammed and a small fishing village was created. The city obtained city rights on 7 June 1340. After the 'Nieuwe Waterweg' was constructed in 1872, the city grew rapidly. One of the most crucial aspects of the history of Rotterdam is the bombing on May 14 1940, burning down a large part of the city (Figure 3.1). After this, a lot of new constructions were built which has given Rotterdam the modern image it has today. After the damming of the river Rotte in the 13th century, the Rotterdam area was increasingly made habitable by polder development. The subsurface area of Rotterdam was built up over thousands of years from various sediments by alternating sedimentary environments under the influence of the river (sand and clay), the sea (clay), and marshes. As a result of urbanisation, areas have been raised with external materials and subsidence has occurred, in combination with contamination of the soil. The intense use of the subsurface and surface in the city, has affected the natural characteristics of the soil regarding bearing capacity, permeability and groundwater.



Figure 3.1: The map shows the area of the bombing in 1940, the so called 'burning boundary'

The subsurface of Rotterdam can be summarized as followed, as illustrated in Figure 3.2:

- The upper anthropogenic layer in the urban area has been influenced by human intervention, such as embankment, underground infrastructure and soil improvement. This layer has been highly affected regarding composition and conductivity.
- The phreatic groundwater (shallow groundwater) is fed by precipitation, infiltrating surface water and seepage from underlying soil layers.
- The Holocene layer below consists mainly of clay and peat and generally has poor permeability. The thickness varies between 5 and 25 metres. In some places, the top layer is more sandy (gully fillings or old river dunes), which increases permeability.
- Below this lies the first aquifer. The top of this aquifer lies at NAP -15 to -20 m, with a total depth between 10 to 20 m. This layer is highly permeable and consists of sand and gravel. The head in the aquifer is directly affected by the Nieuwe Maas and affects the local seepage.
- The layer below has low permeability, with a depth of approximately 5 m.
- The second aquifer has a varying depth of 30 to 100 m, with high permeability.

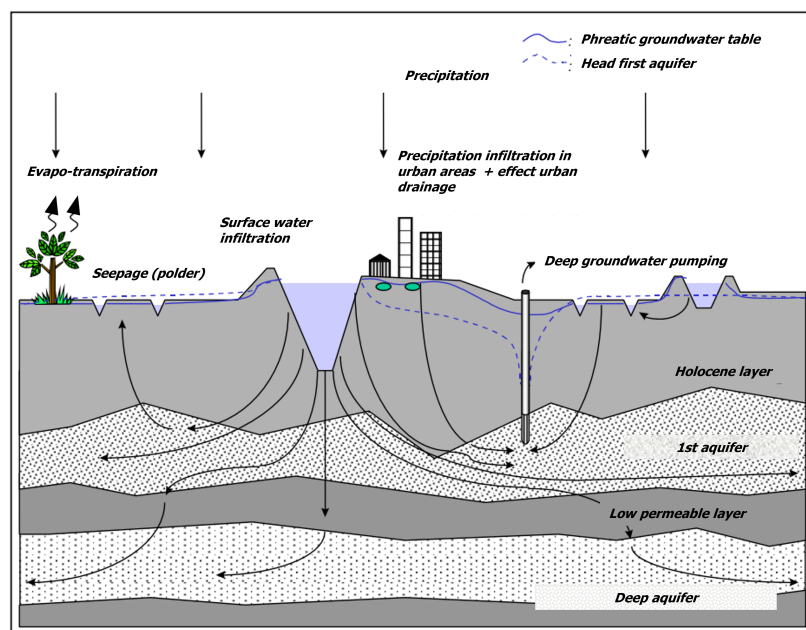


Figure 3.2: The subsurface and hydrologic system of Rotterdam. Adapted from source: IBR, 2012

The delta area of Rotterdam is strongly dependent on its rivers, groundwater and surface water. Rotterdam has many rivers and streams in and around the city; the Maas being its largest water body in the city. The city center, however, is mainly urbanised with little surface water bodies and canals. Around 1900, Rotterdam was characterized by canals. Due to urbanisation over the years, waterbodies were subdued. After the bombing in 1940, this was intensified and more water bodies were subdued with the bombing rubble. The city center (330 ha) is highly urbanised (210 ha impermeable). There is one main surface water body in this area, the Westersingel, resulting in approximately 2% surface water in the city center area. The Northern part of the city is characterised by more canals. The existing canals in Rotterdam are used for stormwater overflows and excess groundwater overflows from the urban drainage system [Pieneman and Goedbloed, nd]. The surface water bodies are maintained by the water boards and the Dutch Government. Rotterdam falls under management of three Water Boards:

1. Hoogheemraadschap van Delfland
2. Hoogheemraadschap van Schieland en de Krimpenerwaard
3. Waterschap Hollandse Delta

The Rotterdam groundwater system depends on seasonal effects, urban drainage systems and other urban activities. The municipality is responsible for all groundwater in the public domain,

there is an effort-based obligation. For the rainwater collection, the municipality has a duty of care for the collection of rainwater runoff and is responsible for the processing of the collected rainwater.

Due to climate change, intensively built-up areas and areas with soil subsidence are particularly vulnerable to flooding. Rotterdam is focused on the disconnection of rainwater from the sewer systems and more local, on-site processing of rainwater. This is partially to limit the flow of 'clean' water to treatment plants, and to limit the overflows from the sewer system onto surface water, to adverse negative effects on the surface water. This process can be summarized by local retention and storage of rainwater. For the runoff collection, the new system is designed to retain rainwater and infiltrate it locally. Excess groundwater (from infiltration) is drained by delayed discharge. The Rotterdam drainage system is designed to process rainwater from a rain event that occurs once every 2 years (return period $T = 2$). The system is designed to overflow in case of more extreme events.

3.2. Agniesebuurt area

3.2.1. Introduction

The Agniesebuurt area is situated in the North of the city of Rotterdam (Oude Noorden), to the North of the city center. The area is bounded by the Noordsingel (surface water), Bergweg, Schiekade and Heer Bokelweg (Figure 3.3). The Agniesebuurt is built on the former Oost-Blommersdijk polder. Most construction dates back from around 1850 up to around 1940. The first development in the Oude Noorden was the building of the railway viaduct, nowadays known as the Hofbogen, which started in 1898. Soil investigations from that period point out that for these construction works a thick layer of sand (up to 4 m) was deposited which resulted in several meters of subsidence. The Hofbogen is one of the characterising constructions for the Agniesebuurt area. The buildings are built in a block-like urban design, with inner-gardens. Part of the Agniesebuurt area lies within the burn zone of the 1940 bombing, and some of the residential block date from early 1850's. At that time, also the Rotterdamse Schievaart was subdued with rubble and transformed in the current Schiekade. Due to urbanisation of Rotterdam and the housing demand, the Agniesebuurt area was highly developed in the late 20th century. From 1892 to 1975 a large hospital was situated at the Schiekade. This hospital was torn down and as a result, new apartment blocks were built. In the 1980's the Oude Noorden area was largely renewed. Subsequently, a lot of new construction was built.

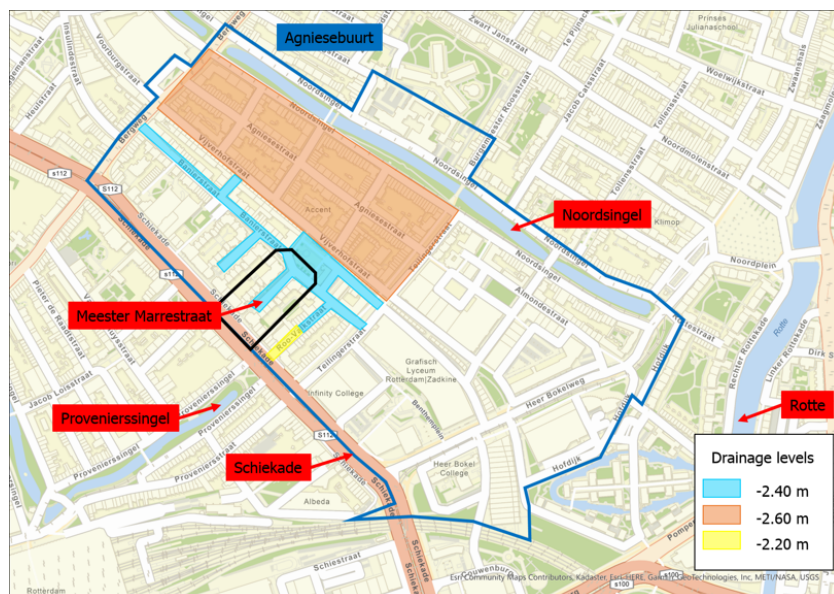


Figure 3.3: Drainage levels of the urban drainage system and groundwater levels in the Agniesebuurt

3.2.2. Test area

The specific test area of this study is the Meester Marrestraat area, to the South-West of the Agniesebuurt area (Figure 3.3). At the test location, the constructions dates from 1980 and buildings have concrete foundations. There are no vulnerable wooden foundations at the test area. The surface level is designed at -1.05 m NAP.



Figure 3.4: Meester Marrestraat impressions

3.2.3. Urban drainage system

For the renewal of the urban drainage system in the Agniesebuurt area, the municipality received the European SPONGE subsidy from the Interreg 2 Seas Mers Zeeën 2014-2020. SPONGE2020 is a multilateral collaboration between Dutch, British and Belgian governments [Interreg 2 Mers Seas Zeeën 2014-2020,]. Collectively the governments work towards measures that help to deal with the impacts of climate change, especially in urban areas. The Sponge2020 is focused on the task: "How can we improve water buffering in urban areas and thus have the city function as a sponge". To obtain the sponge like function, Aquaflow was placed in the Agniesebuurt in combination with the urban drainage renewal. As a result, a separated sewer system was created with two sewer systems: waste water and rainwater system (Figure 3.6).

- Dry weather system (DW) with all waste water from buildings in the area and rainwater from roofs of some buildings. In the Agniesebuurt area, several buildings' downspouts are directly connected to the sewer system. These connections have been maintained in the new system. Other buildings have been 'disconnected', meaning the downspouts are disconnected from the sewer system and as a result rainwater is discharged onto the surface for infiltration, detention or runoff.
- Wet weather system (WW) transporting 'clean' water to the surface water bodies. Rainwater is collected in the Aquaflow gully-pots and infiltrated to the subsurface. Perforated drain pipes (Drainage-Infiltration-Transport pipes (**DIT**)) form the drainage system. Prior to the total completion of the Agniesebuurt area urban drainage system, rainwater is transported to the waste water treatment plant (via pumping station in Figure 3.7.) After completion, the drainage system is connected to the surface water of the Noordsingel by means of pumping stations.

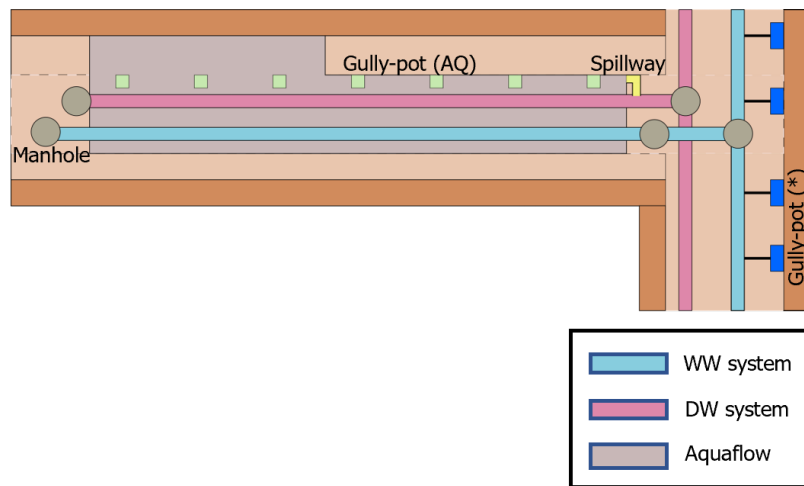


Figure 3.5: Top view of the Aquaflow system

The drainage level in the Agniesebuurt area is set at three levels: -2.40 m NAP (blue areas in Figure 3.3), -2.60 m NAP for the areas still to be completed around the Noordsingel (orange areas in Figure 3.3) and -2.20 m NAP locally at the Roo-Valkstraat (yellow area in Figure 3.3). In areas where Aquaflow is placed, gully-pots transport runoff towards the granulate layer (green gully-pots in Figure 3.5). In other areas, gully-pots are directly connected to the WW drainage pipes (blue gully-pots(*) in Figure 3.5).

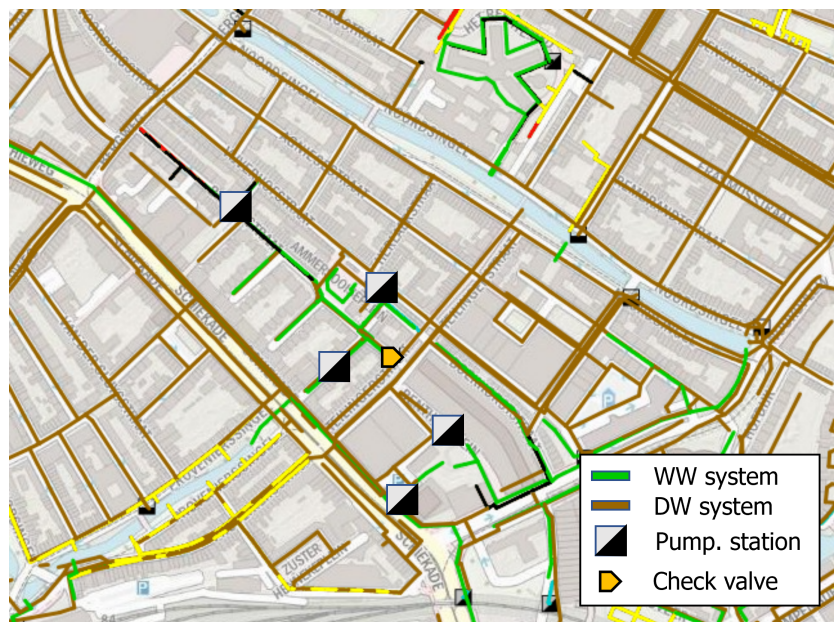


Figure 3.6: Urban drainage system as is in the Agniesebuurt area. The system consists of a separated sewer system in the completed area in the South East of the area, and a combined system in the remaining part of the system. Pumping stations transport the water to the Waste Water Treatment Plant (WWTP).

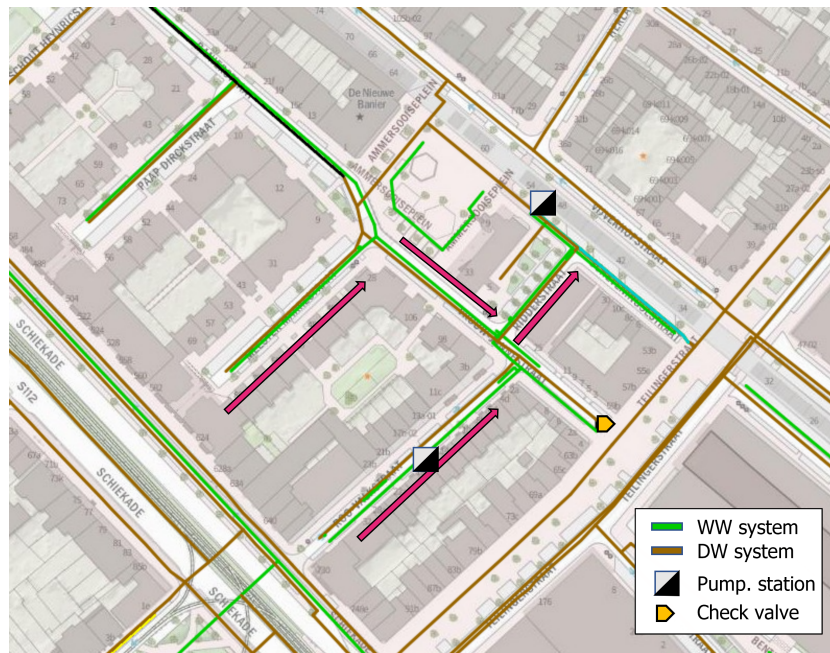


Figure 3.7: Zoom of the separated sewer system as completed in 2020. At the check valve, both WW and RW systems are connected. At the pumping station it is transported to the WWTP, until the entire system is completed and water is transported to the Noordsingel.

The Aquaflow design at the Agniesebuurt is a granulate layer with a height of 35 cm, below the road surface. The road surface pavement and the granulate layer are separated by a shallow sand layer. The main connection between the road surface and the granulate layer is through the gully-pots. The gully-pots have a depth of 72 cm, with the invert level of the pipe 38 cm above the bottom of the gully-pot. The pipe connects the gully-pot with the granulate layer by means of an infiltrating grate. The sand filter (Figure 4.1) is placed to filter rubble from the stormwater runoff. The Aquaflow system is equipped with a small spillway at the end of the system, to empty the system in case of extreme rainfall volumes and/or limited emptying capacity of the system. This spillway is connected to the DW sewer as seen in Figure 3.5. The Aquaflow system in the Agniesebuurt area is equipped with an impermeable foil, preventing the flow of water to the neighbouring houses. At the bottom, the permeable foil allows for infiltration. The Aquaflow system is designed to store extreme summer rainfall events.

3.2.4. Subsurface

In the Agniesebuurt, the surface level is NAP -1.05 m. This level is the design ground level at the sidewalk level. The road surface level lies 10 to 30 centimeters below this level (-1.20 m NAP to -1.30 m NAP). The gully-pots are placed at the lowest points. The gully-pot surface levels are summarized in Table 3.1.

Table 3.1: GP dimensions and depths with respect to m NAP

<i>Gully-pot</i>	<i>GP surface level [m NAP]</i>	<i>Filter top [m NAP]</i>	<i>Pipe invert level [m NAP]</i>	<i>GP depth</i>
K1	-1.412	-1.492	-1.792	0.72
K2	-1.405	-1.485	-1.785	0.72
K3	-1.422	-1.487	-1.802	0.72
K4	-1.424	-1.504	-1.802	0.72
K5	-1.422			0.72
K6	-1.431	-1.511	-1.811	0.72
K7	-1.250	-1.495	-1.785	0.72
MA	-1.173			3.50
MB	-1.287			1.80

The subsurface of the Agniesebuurt is characterised by a top layer of sand with a depth ranging from 3 to 5 m, the anthropogenic layer (Figure 3.8). Below the sand layer with varying depth lies the clay layer. In the area, cone penetration tests were conducted to a depth of 30 m. The findings for locations in the proximity of the test area are summarized in Table 3.2. Prior to the construction of the urban drainage system in 2016, soil experiments were conducted and piezometers were installed. The boreholes had depths ranging from 1.5 to 3.0 m. The findings are summarized in Table A.1. At the test area, the top soil layer is sand with varying depth up to 3 meters. In the North-East of the test area, more clay is found. These drill states are summarized in Appendix A.

Table 3.2: Cone penetration tests in the proximity of the test area to a depth of -35 m NAP.

	Scheveningsestraat	Soil	Roo-Valk	Soil
<i>Section 1</i>	-1.34 to -8.34 m NAP	Sand	-1.38 to -16.38 m NAP	Clay
<i>Section 2</i>	-8.34 to -11.34 m NAP	Peat	-16.38 to -31.38 m NAP	Sand
<i>Section 3</i>	-11.34 to -17.34 m NAP	Clay		
<i>Section 4</i>	-17.34 to -35 m NAP	Sand		

There is clay present in the area, mostly on the South side of the test area. The cone penetration test at the Roo-Valkstraat shows the top 15 meter of the soil consists of clay. At location 57 and 105 in addition to P3, clay was found in the boreholes. Towards the downstream end of the test area, the soil is characterised by sandy soil to a depth of 3 m. The summary of the soil characterisation and depth is presented in Table A.1. The associated locations are shown in Figure A.12. To determine whether the Agniesebuurt area was suitable for the application of permeable pavements, additional soil experiments were conducted. These tests included grain size distribution and falling head tests. The location of these tests falls outside of the test area. In addition to existing knowledge of the subsurface, additional testing was done of the local subsurface at the test area road cunet. These results are further explained in section 5.1.5 and section 5.2.1.

Table 3.3: Soil characteristics to a depth > 30 m for the Agniesebuurt

Depth below surface (m-mv)	Composition	Definition	Parameters
0 - 10/15	Clay, peat, silty sand	Top layer	$c = 500-1000d$
10 /15 - 20/30	Medium coarse to coarse sand	First aquifer	$kD = 500 \text{ m}^2/d$
>20/30	Clay, silty sand	Low permeable layer	

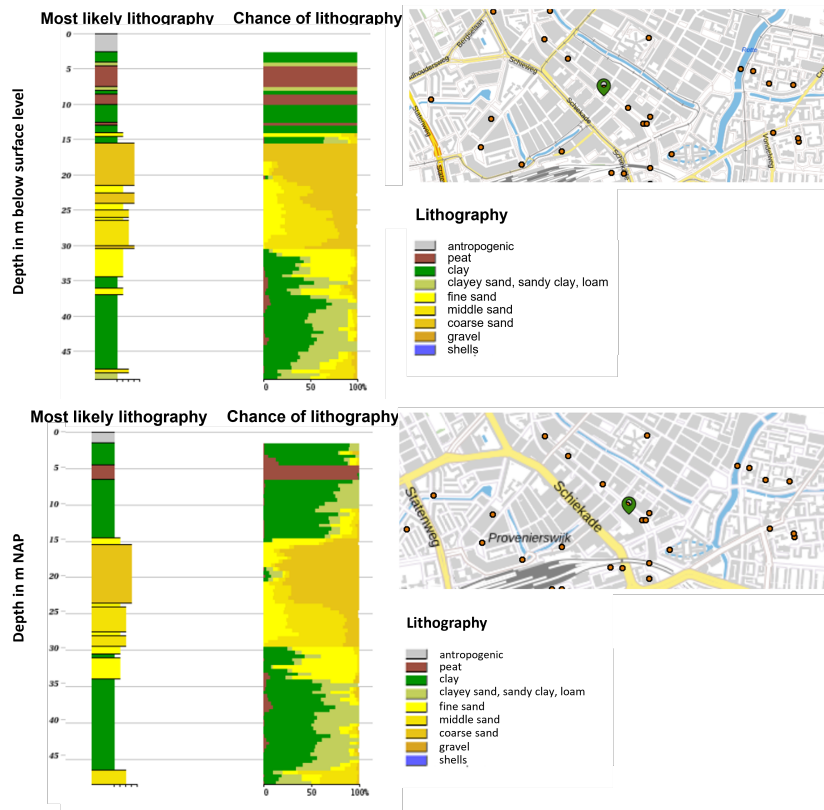


Figure 3.8: Lithography of the subsurface in the Agniesebuurt area to a depth of 50 m below surface level

3.2.5. Groundwater

The groundwater levels vary throughout the year due to the DIT pipe, infiltration and natural groundwater flows. Long-term groundwater table elevations above the set drainage levels should be drained by the DIT system. In the Agniesebuurt area, the perforated pipes are placed below the groundwater table, these pipes maintain a more natural groundwater response (Figure 3.9).

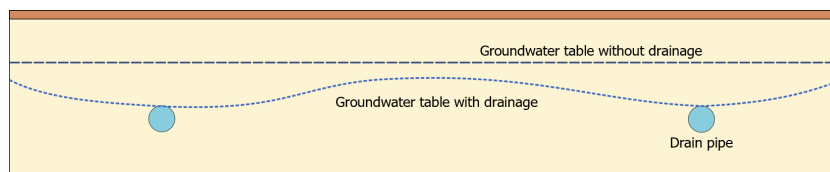


Figure 3.9: Effect of subsurface drainage pipes on the unsaturated zone

In Figure 3.10, the groundwater levels at the case study area are shown for the period between January 2019 and January 2022. As observed, after Aquaflow installation, the water levels follow more natural fluctuations, and the groundwater table was lowered by an average of 20 cm.

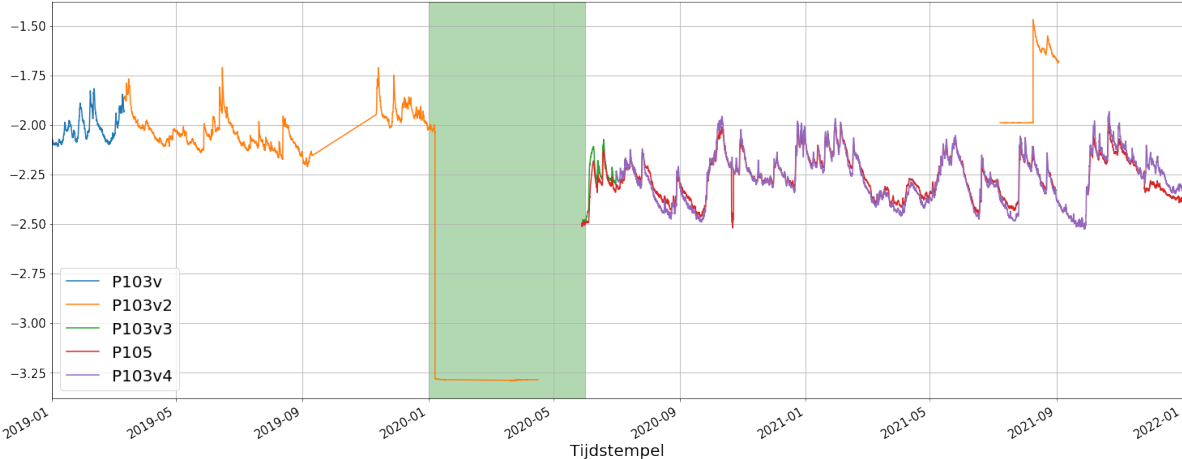


Figure 3.10: Groundwater levels in the Agniesebuurt area. Between 01-2020 and 06-2020 works on the Aquaflow system were in progress.



Performance criteria

In this thesis, the performance of the Aquaflow system in the Agniesebuurt is quantified. To do so, performance criteria are defined. The aim of the research is to monitor the performance with available resources of the Municipality of Rotterdam. In this chapter, the performance criteria are defined.

4.1. Performance criteria definition

To assess the hydrologic performance of the Aquaflow system, performance criteria must be defined. The performance criteria are based on the demands for the water system and drainage by the Municipality and the key performance indicators as discussed in literature e.g. [Santos et al., 2019, Bhimanadhuni et al., 2015, Gilissen, 2014]. The performance criteria are grouped in the following categories: (i) stormwater runoff, (ii) emptying- and filling time, (iii) peak reduction and volume retention and (iv) groundwater recharge.

4.1.1. Stormwater Runoff

To design urban drainage systems, design storms are typically used. In the Netherlands, the reference storm event is a rainfall event with a return period of $T = 2$ (Bui08) [RIONED, 2019, Rotterdam, 2021]. With climate change and increasing expected rainfall intensity, the design storm events are changing. The Municipality has defined criteria for the performance of the drainage system for storms $T=2$, $T=10-25$ and $T=100$, regarding rainfall intensity (mm/hour), and the tolerable hindrance. Where the tolerable hindrance depends on the duration, and depth of water on the street (ponding) for each event. Small hindrance is defined as lightly submerged streets for limited time ($t < 1$ hour), extreme hindrance is defined as large scale disturbance from rainfall from large scale failure of vital public infrastructure. The municipality's performance metrics are related to rain events and associated return period, related to rainfall intensity [mm/hr]. Since the monitoring period of this research was 8 months, it is unlikely all three rain events; $T = 2$, $T = 10-25$ and $T = 100$, will occur in this period. Therefore, the ponding metrics were adapted, to create 5 performance criteria for ponding (PC1 - PC5), as defined in Table 4.1 for rainfall duration of maximum 12 hours.

Table 4.1: Ponding performance criteria for the Aquaflow system based on the hindrance criteria defined by the municipality.

	PC1	PC2	PC3	PC4	PC5	
<i>Intensity</i>	>100	>70	>48	>20	<20	mm/hr
<i>Water equivalent</i>	>30	>30	>10	>10	>0	mm
<i>Max. pond. depth</i>	20	10	10	10	None	cm
<i>Max. pond duration</i>	60	20	20	10	None	min

Based on the limits as defined in Table 4.1, the performance criteria can be summarized as:

- For rain events with an intensity below 20 mm/hour, zero ponding is accepted.

- For rain events with high intensity rainfall (>100 mm/hour) ponding is allowed for a maximum duration of 60 minutes.
- For mid range rainfall intensities (20 - 70 mm/hour) with a minimum of 10 m³, the maximum ponding duration is 20 minutes.
- For rain intensities > 20 mm/hour with low volumes (> 10 m³) ponding is accepted for a maximum duration of 10 minutes.

The rain intensities as defined in Table 4.1 form the basis for the remaining criteria definition.

4.1.2. Filling- and emptying time

The purpose of the Aquaflow system in the Agniesebuurt area is to delay the runoff peak as much as possible and limit the stormwater loading of the sewer system. The emptying time of the Aquaflow system is a component of two factors: (i) the granulate layer and (ii) the road cunet. The filling time is important regarding the ponding criteria as defined in section 4.1.1. For the emptying time and ponding time, two limits are defined:

1. Empty limit
2. Ponding limit

The empty limit is the invert level of the connecting pipe between gully-pot and granulate layer. Water levels above the empty limit, indicate filling of the system. Conversely, water levels below the empty limit indicate an empty system. The ponding limit is set at the top of the gully-pots, at surface level. When water levels exceed this, water ponds at the street level.

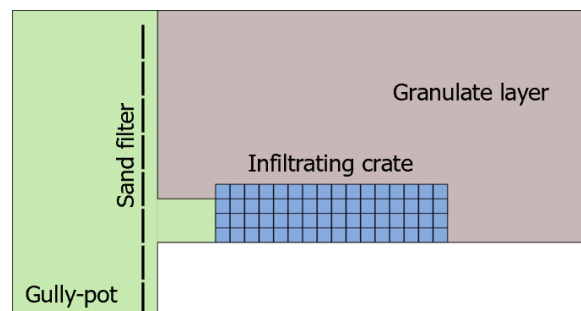


Figure 4.1: Gully-pot and granulate layer cross section view showing the connection between the two components.

The emptying time is defined as the time between the time of first filling $t_{fill,1}$ and the first empty time $t_{empt,1}$, where first empty time is the first instance where water levels in the gully-pot fall below the empty limit, after filling. The emptying time is a factor of the degree of filling and the infiltration capacity of the soil [Chahar et al., 2012]. In addition, clogging of the system affects the emptying time.

$$t_{empty} = t_{empt,1} - t_{fill,1} \quad (4.1)$$

The performance criterion regarding emptying and filling can be summarised as:

- The emptying time t_e should be smaller than 24 hours for fully filled systems, for any event (Equation 4.1)

4.1.3. Peak delay and volume retention

LID systems like the Aquaflow are often applied to relieve the urban drainage system by spreading the water load over a longer period. The Aquaflow system combines stormwater runoff retention, with infiltration. The unsaturated zone between the Aquaflow and the groundwater table acts as additional storage. Peak delay and peak retention are possible metrics to assess the spreading of the water load [Abdalla et al., 2021, Lucas et al., 2009, Xiao et al., 2017, Støvring et al., 2018]

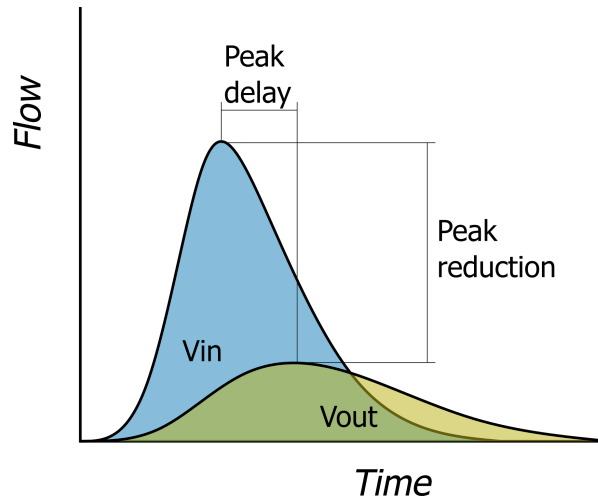


Figure 4.2: Peak reduction, peak delay and volume retention illustration

The peak delay is defined as the time between the runoff peak and the peak in the urban drainage system (Figure 4.2). For the Aquaflow, this is determined by the time between the peak inflow in the gully-pots and the peak in the outflow, as measured in the drain (DIT pipe), at the end of the case study area. The volume retention, or volume reduction, represents the stormwater runoff that does not end up in the urban drainage system. The volume reduction was defined by Støvring et al. (2017), and Abdalla et al. (2021), as the percentage of precipitation not immediately discharged and is determined by comparing the inflow volumes to outflow volumes (Equation 4.4), as illustrated in Figure 4.2. Another equation for the determination of retention volume (m^3) was defined by Szota et al (2019) (Equation ??). The Aquaflow system is designed for short, high intensity summer storm events. For these events, a delay of 1 hour is considered sufficient by the municipality. However, for long duration events, a peak delay time of 4 to 6 hours is desirable.

$$Peak_{delay} = t_{p,DIT} - t_{p,GP} \quad (4.2)$$

$$Peak_{reduction} = \frac{Q_{p,GP} - Q_{p,DIT}}{Q_{p,GP}} 100\% \quad (4.3)$$

$$VR_{total} = \frac{V_{precipitation} - V_{discharge}}{V_{precipitation}} 100\% \quad (4.4)$$

The LID performance regarding peak delay, volume retention and peak reduction rely heavily on initial conditions and the rainfall volume and intensity [Abdalla et al., 2021]. Based on the research regarding LID performance, the performance criteria for the peak delay, volume retention and volume reduction are defined as:

- The peak delay should be more than 1 hour for any rain event.
- The volume retention should be more than 35% for any rain event.

4.1.4. Groundwater recharge

The Aquaflow system combines a mixture of nature based and traditional stormwater management solutions to reduce flood risk and attenuate surface water runoff [Fletcher et al., 2015]. An advantage of applying such systems in urban areas is the increased groundwater recharge. The combination with the perforated pipe (DIT) allows for more short-term groundwater fluctuations in the area. In traditional sewage systems, groundwater typically leaks through cracks which drains the groundwater from the area. Increased groundwater recharge by LIDs or SUDS, in combination with sewage system renewal has the potential to increase the groundwater table above the acceptance limit. This acceptance limit is determined by the level of basements (sous-terrains), foundation types, average groundwater levels and surface levels. For the Agniesebuurt area of the Municipality of Rotterdam the groundwater acceptance limit is set at 80 cm below the surface level:

- The groundwater table around the road cunet should be minimum 0.80 m below surface level in response to any event.

4.1.5. Criteria Summary

The performance criteria selected to assess the hydrologic functioning of the Aquaflow system are as followed:

- For rain events with an intensity below 20 mm/hour, zero ponding is accepted.
- For rain events with high intensity rainfall (>100 mm/hour) ponding is allowed for a maximum duration of 60 minutes.
- For mid range rainfall intensities (20 - 70 mm/hour) with a minimum of 10 m³, the maximum ponding duration is 20 minutes.
- For rain intensities > 20 mm/hour with low volumes (> 10 m³) ponding is accepted for a maximum duration of 10 minutes.
- The emptying time t_e should be smaller than 24 hours for a fully-filled system for any event (Equation 4.1)
- The peak delay should be more than 1 hour for any rain event.
- The volume retention should be more than 35% for any rain event.
- The groundwater table around the road cunet should be minimum 0.80 m below surface level in response to any event.

5

Methods

5.1. Monitoring

To assess the performance criteria, monitoring was conducted during the period from January to June 2022. Monitoring was conducted to quantify the effects of the Aquaflow on local the hydrologic system by monitoring: (i) precipitation, (ii) Aquaflow filling, (iii) groundwater levels, and (iv) drainage (Figure 5.1). The monitoring equipment relevant information is summarized in Table 5.1.

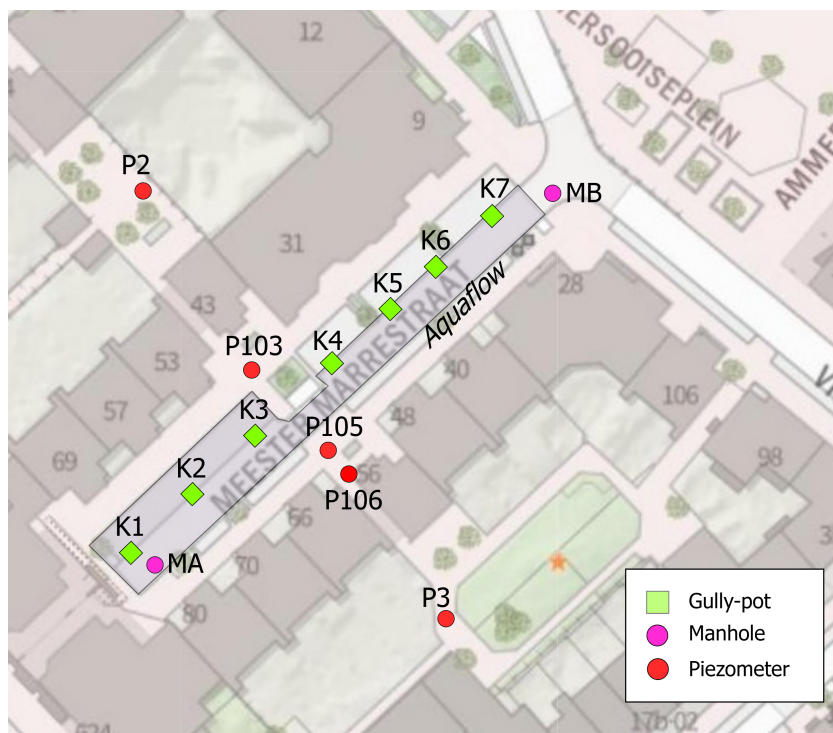


Figure 5.1: Monitoring locations at the test area.

Table 5.1: Monitoring equipment relevant information

	GP water levels	Groundwater levels	Outflow
<i>Material</i>	Pressure sensor	Pressure sensor	Electro-magnetic flowmeter
<i>Accuracy</i>	0.01 cm	Pressure: 0.5 cmH ₂ O; Temperature: 0.1 C	0.02%
<i>Parameter</i>	hPa	hPa	dm ³
<i>Temporal resolution</i>	5 minutes	15 minutes	15 seconds
<i>Output resolution</i>	5 minutes	15 minutes	5 minutes
<i>Locations</i>	6 (K1-K7)	5 (P2, P3, P103, P105, P106)	1 (Manhole MB)

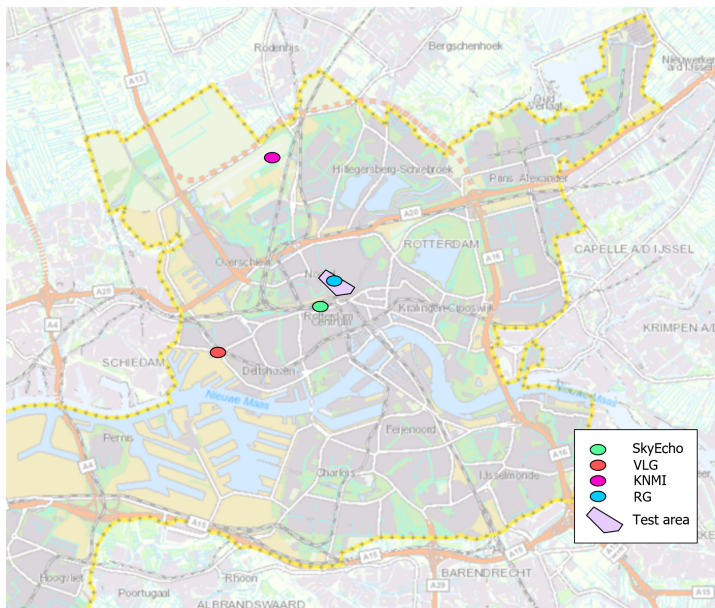
5.1.1. Precipitation

The aim of this thesis is to assess the performance of the Aquaflow in natural conditions, using naturally occurring rain events. Precipitation was monitored at three locations: Royal Netherlands Meteorological Institute (KNMI), SkyEcho, near the Delftse Poort building at the Rotterdam Central Station, and the test area (Rain Gauge (RG)), the locations of these stations are presented in Figure 5.2. Each station used different monitoring techniques and intervals, as summarized in Table 5.2. The rain gauge at the test location is a volume measuring tipping bucket placed for this thesis to provide rainfall data at close proximity (<100 m) to the test location. The tipping bucket is maintained by the Municipality and was placed in January. The output interval is 5 minutes, with a sensitivity of 0.02 mm. The raw data output is in European/Amsterdam timezone. The SkyEcho weather station placed near Rotterdam Central station at an elevation of 600 m. The station is maintained by the TU Delft and owned by the municipality of Rotterdam. The station provides pressure, rainfall volume, rainfall intensity, wind speed and wind direction among others. The output monitoring interval is 15 minutes. The raw data is in European/Amsterdam timezone. The KNMI station provides an additional rainfall data source in hourly output data. The raw data is in UT timezone (UTC + 1).

Precipitation monitoring is prone to errors related to underestimation of rainfall data, the location of installation and external effects like wind and rubble [Foelsche, 2015, Vieux and Vieux, 2005, Habib et al., 2008]. By using different weather stations, these errors can be identified more easily. The three selected stations vary in distance to the test site, installation height and monitoring equipment. An assessment of best fit was conducted between monitoring data at the test location and the precipitation measurement. For this assessment, the measured volume of rain and the rainfall intensity were considered most important. For this, the rainfall intensity, the rainfall volume and the rainfall period were assessed for the three stations. Based on the assessment (Appendix B) it was decided to use the local rain gauge data as rainfall measurements and to use the SkyEcho radar as a source for the rainfall intensity, due to the close proximity to the test location (max. 600 meters). The KNMI data is used as verification of the monitored data, and as an additional data source in case either station fails to record rainfall.

Table 5.2: Precipitation data sources available for study

Precipitation	Rain Gauge	KNMI	SkyEcho
<i>File format</i>	.csv	.txt	.csv
<i>Temporal resolution</i>	Instant	10 min	15 min
<i>Output resolution</i>	5 min	60 min	15 min
<i>Parameter</i>	Rain depth (mm)	Rain depth (mm)	Rain intensity (mm/hr)
<i>Distance to test area</i>	100 m	4000 m	650 m



(a) Available precipitation monitoring locations. SkyEcho weather station at Rotterdam Central Station, VLG (barometric pressure data) at Marconiplein, KNMI weather station (Royal Dutch Meteorological Institute) at park Zestienhoven and RG (Rain Gauge tipping bucket) at the test location.



(b) Rain gauge (RG) location with respect to the test area.

Figure 5.2: Precipitation monitoring locations

5.1.2. Full scale test

In addition to the natural rain events, a full scale test was conducted to calibrate and validate the monitoring results and to observe the Aquaflo response. Aside from the observations, the full scale test provides insight in the response to intense rainfall events. The full scale test consisted of four loads with a total of $30m^3$ (L1 - L4), with varying duration, as summarized in Table 5.3. The test area (Meester Marrestraat) was separated in two sections, section 1 and section 2 (Figure 5.3). Each section received $15 m^3$ spread out over two loads.



Figure 5.3: Sections for full scale test load discharge

The full scale test was conducted in a period with more than 7 antecedent dry days and initial groundwater levels at the drainage level (-2.40 m NAP). There was an interval of 30 minutes between each load. The field observations provided supplementary information regarding clogging of the system, flow direction at the surface and ponding.

Table 5.3: Full-scale test data

<i>Load</i>	<i>Start time</i>	<i>Section</i>	<i>Volume</i>	<i>Time</i>	<i>Area</i>	<i>Total area</i>	<i>Intensity</i>	<i>Water equivalent</i>
	CET		m ³	min	m ²	m ²	mm/hour	mm
<i>L1</i>	07:19	1	10	4	400	1500	100	6.7
<i>L2</i>	07:53	2	10	4	300	1500	100	6.7
<i>L3</i>	08:24	1	5	1.5	400	1500	133	3.33
<i>L4</i>	08:26	2	5	2.5	300	1500	80	3.33
<i>Total</i>			30	60				20

5.1.3. Ponding and Aquaflow emptying time

The ponding time and volume and Aquaflow system emptying time are important metrics of the Aquaflow performance as defined in section 4.1. These metrics rely on the discharge capacity of the gully-pots and the degree of filling and infiltration rate of the granulate layer. To measure these metrics, water levels were monitored in the gully-pots (K1 - K7 in Figure 5.1). The water levels were measured using both compensated (for barometric pressure) and absolute pressure sensors. The monitoring period of these gully-pots was between November 2021 and July 2022. The monitoring interval of the gully-pot water levels was 5 minutes, with a sensitivity of 0.5 cmH₂O (Table 5.1). The sensors were attached to the sand filter of the gully-pots, below the invert level of the connecting pipe between gully-pots and Aquaflow granulate layer. The output of the sensors is hPa at the monitoring height. The sensors are manually calibrated in the field, at the location of installation. For the calibration, the reference level, the sensor height and the sensor output are related with the water pressure equation. The raw data was converted to water height with respect to the reference level (invert level of the pipe) and with respect to meters NAP. Then, raw data from the absolute sensors was compensated with air pressure to represent actual water levels. The monitoring interval of the air pressure is 10 minutes, the monitoring interval of the pressure sensors is 5 minutes. Due to the interval difference, the monitored air pressure data was adapted with forward interpolation, to achieve the lower interval of 5 minutes. The pressure sensor output is in UTC timezone, the air pressure is in CET timezone. The relevant dimensions of the gully-pots are presented in Table 3.1.

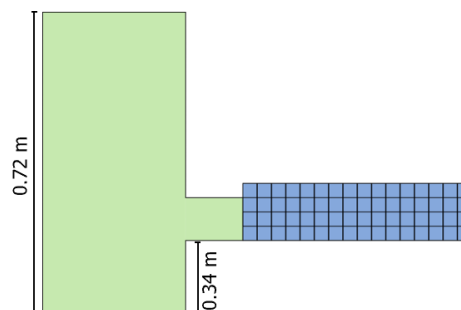


Figure 5.4: Ponding and gully-pot heights

5.1.4. Peak delay and volume retention

To assess the criteria regarding peak delay and volume retention, both inflow and outflow must be determined. In this thesis, the inflow is the stormwater runoff. The outflow is defined as the flow through the drainage pipe below the Aquaflow system. For the runoff, the rational method is used to determine the inflow using $Q=CiA$ where $C = 1$, to obtain the maximum volume retention and peak delay. To determine the peak inflow in the gully-pots, the volume difference in the gully-pots over time (dV/dt) is calculated (Figure 5.5).

The outflow is the water flow that enters the drain pipe. To determine this flow, an Electro-Magnetic flowmeter was installed in the outlet of the drain pipe at manhole MB (Figure 5.1). The Electro-Magnetic (EM) flowmeter was selected over other flowmeters because the drain pipe is always filled (DIT below

groundwater table). The flowmeter has high sensitivity (0.02%) and can measure the flow velocity and the volume of flow over a selected period. The temporal resolution is 15 seconds and the output is volume of water (m^3) every 5 minutes. The EM flowmeter uses Faraday's Law and the conductivity of fluid to measure the flow.

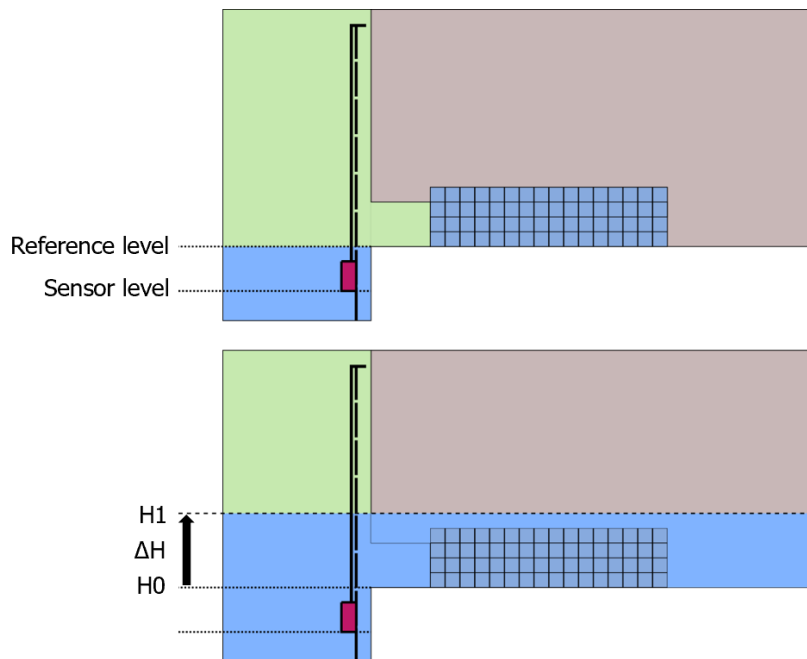


Figure 5.5: Pressure sensor installation and reference height and inflow measurements

The flowmeter was installed in a drainage manhole, in a fully submerged perforated drain pipe. As can be seen in Figure 5.6, the flow from the outlet of the drain pipe (perforated DN350) is diverted through a smaller pipe (DN150) which is connected to the flowmeter. The flowmeter is connected to an outflow pipe. The outflow pipe discharges water to the manhole. Manhole MB is connected to a second manhole, manhole MC, by a diver pipe (concrete DN350) and so connected to the urban drainage system. Part of the Aquaflow design is an emergency spillway at the downstream end of the system. This spillway overflow is connected to the sewer pipe and becomes active when Aquaflow system is filled and the infiltration is hindered (3.5). The exact flow from the spillway is difficult to quantify, this value must be considered when interpreting the monitoring results.

The flowmeter data consists of a lot of noise, due to measuring of groundwater in a drain pipe. By filtering this data, the results are more clear. However, this removes the peakedness in the results. The Savitzky Golay filter, reduces the noise using a simplified least-squares procedure and was applied to the data [Savitzky and Golay, 1964]. The filtered signal is presented with the raw data.

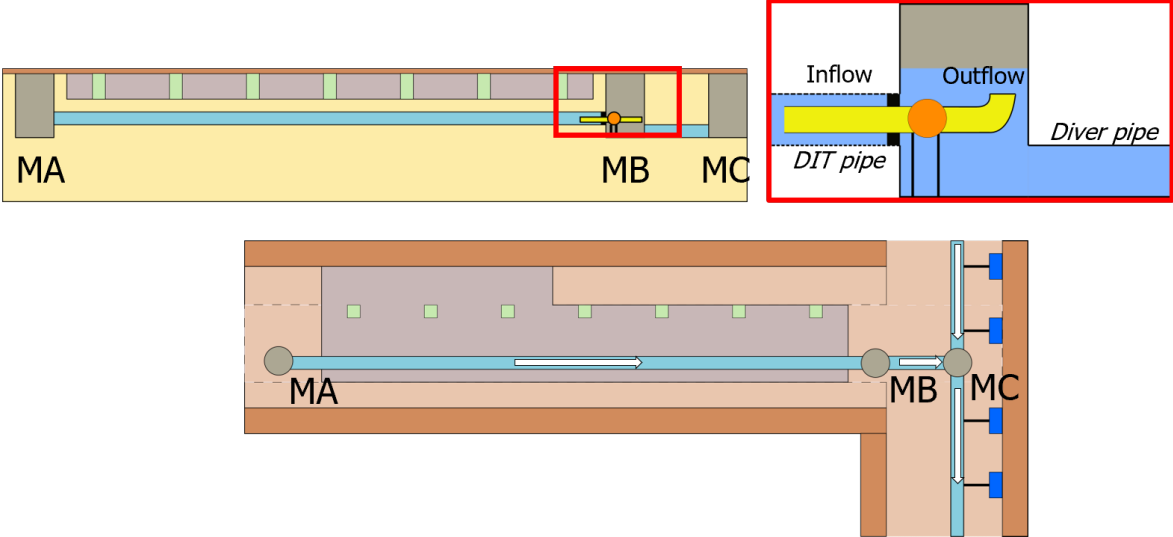


Figure 5.6: Set-up of the EM flowmeter (orange circle) in manhole MB and overview of the position with respect to drainage system



(a) Flowmeter installed in the manhole



(b) Flowmeter structure

Figure 5.7: Flowmeter installation process at the test location, showing the final installation (a), and the structure placement (b).

Manhole water levels

In addition to the flow measurements, manhole water levels were measured in the manholes at MB and MA. The sensors have the capacity to measure both pressure and water temperature. The manhole water temperature is connected to the groundwater temperature. Fluctuations in temperature can indicate the time of first flow reaching the manholes. Arianna Bucci et al. (2017) assessed the shallow groundwater temperature fluctuations in Turin city [Bucci et al., 2017]. The study observed lower values in the shallow portions and a gradual increase in the spring measurements. Conversely, the values are higher in the first few metres and decrease with depth in autumn. In Figure 5.8, the manhole water temperature at Manhole A and Manhole B are shown. From this figure, the temperature fluctuations between February and July are clearly observed.

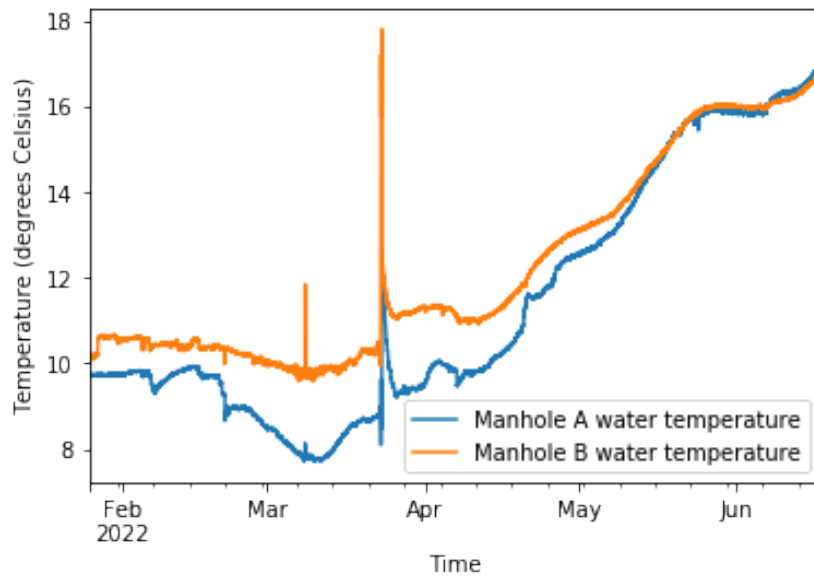


Figure 5.8: The manhole water temperature fluctuations between February and July. The temperature peaks (March 20th) indicate the sensor taken out of the manhole to read the monitored data

Theoretically, manhole water level fluctuations provide additional information regarding flow in the drainage from manhole MA to manhole MB (downstream direction). As the connecting pipe between MA and MB is the perforated (DIT) drain pipe, assumptions have to be made regarding the inflow over the length (over the full diameter) and the friction factor. The drain pipe is placed under the drainage level and lies below the groundwater table, and is thus filled. The Darcy-Weisbach equation provides a solution to determine the turbulent flow using the pressure difference. The Darcy-Weisbach connects the head loss caused by friction along a given length of pipe to the average fluid flow velocity for an in-compressible fluid.

$$\frac{\Delta p}{L} = f_D \frac{\rho}{2} \frac{v^2}{D_H} \quad (5.1)$$

Where: ρ , the density of the fluid (groundwater \sim kg/m³); D_H , the hydraulic diameter of the pipe (Diameter of the DIT pipe = 400 mm); v , mean flow velocity or Q per unit cross-sectional wetted area; f_D , the Darcy friction factor.

5.1.5. Groundwater table

The groundwater is monitored extensively at the case study area of the Agniesebuurt. Groundwater level measurements depend on several factors [Spane, 1999]:

- The sensitivity of the sensor
- The soil in and around the borehole
- Barometric pressure

At the test location, Meester Marrestraat, groundwater is monitored at six locations, as shown in Figure 5.1 (Piezometers). All piezometers are placed in the top soil layer (anthropogenic), mostly consisting of sand, as described in section 3.2.4. The groundwater monitoring locations are placed in a line perpendicular to the direction of the street. The groundwater measurement output is in meters NAP with a measuring interval of 15 minutes. The borehole descriptions of the piezometers are displayed in Appendix A.

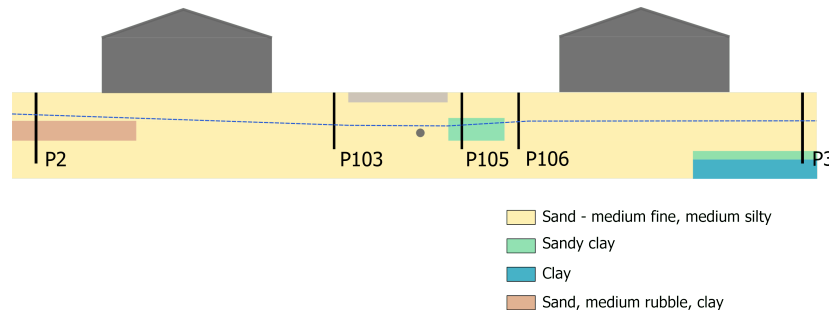


Figure 5.9: Cross sectional view of the subsurface characterisation and monitoring locations.

The monitoring locations as shown in Figure 5.9 and Figure 5.1 are described in more detail in this section. The accompanying borehole descriptions are found in Appendix A. Location P2 is situated at the inner gardens. Here, the soil is mainly characterised by sand. At -2.06 m NAP there is a layer of sand with rubble and clay with a depth of 0.70 meters (Figure A.5). The soil structure is medium fine with low to medium silt present. The average groundwater level at P2 is between -2.10 and -2.20 m NAP. The presence of the rubble and clay layer could affect monitored groundwater levels. At the location of P3, also at the inner gardens, the soil is characterised mainly by sand. At -3.266 m NAP there is a layer of clay with rubble and gravel with a depth of 0.30 meters (Figure A.6). The soil structure is medium fine with low to medium silt present. The average groundwater level at P3 is around -2.30 m NAP. Location P103 is situated to the West of the Aquaflow in the pavement. At P103, the soil is characterised by sand of medium fine, medium silty structure. P105 and P106 are placed to the East of the Aquaflow system in the test area, also in the pavement. At the location of P105, there is a clay layer with a depth of 0.80 m). The remaining soil is sand of medium fine structure, with light silt and loam levels. The average groundwater level is -2.40 m NAP. At the location of P106, the soil is characterised as sand. The soil structure is medium fine with light silt and loam levels. The average groundwater level is -2.30 m NAP.

5.1.6. Barometric pressure

Barometric pressure is monitored (inside) at Marconiplein, approximately 3.5 km from the case study area. Barometric pressure (mBar) is measured using the same devices as the monitoring equipment at the case study area. The monitoring interval is 15 minutes. This barometric pressure is automatically applied to compensate absolute groundwater measurements in all of Rotterdam. Barometric pressure affects the groundwater measurements at piezometers. This phenomenon was investigated by FA Spane (1999) and Rasmussen & Crawford (1997). The barometric pressure affects both groundwater measurements and groundwater levels. There is an inverse relation between barometric pressure and water levels: increase in barometric pressure creates declines in observed water levels and vice versa [Spane, 1999, Rasmussen and Crawford, 1997]. In order to assess the groundwater level fluctuations, barometric pressure effects must be considered.

In addition, aquifer characteristics are important. Two types of aquifers can be defined: unconfined and confined aquifers. Since groundwater levels are measured in piezometers with boreholes to a depth of 2 meters below surface level, in this thesis, the unconfined aquifers are considered. Groundwater levels fluctuate due to influxes from infiltration and groundwater flows and outfluxes from evapo-transpiration and groundwater flows. Additionally, due to seasonal fluctuations, groundwater levels change. Aside from barometric effects, sensor sensitivity and installation can affect accuracy of groundwater measurements, with a potential error of up to a few cm. The sensor sensitivity is typically high (mm). The installation relies on the reference levels and installation levels, which can lead to high

deviations (cm).

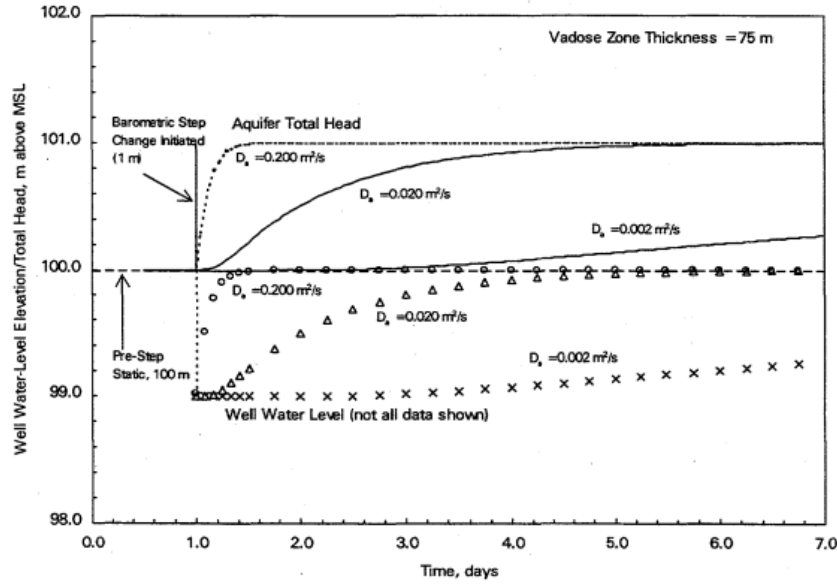


Figure 5.10: Hydraulic head response and unconfined aquifer water levels in relation to 1m step change in atmospheric pressure [Spaen, 1999].

Dan Zhao and Guangcai Wang (2013) developed a method to identify the delay between barometric fluctuations and groundwater response. One method is to use linear regression method. This process is based on the assumption that the water level lags behind the barometric pressure for different times. The barometric pressure and the water pressure are plotted on the same diagram and calculate the correlation coefficients. The largest correlation coefficient time is then selected as the lag time. The equation to remove the barometric pressure was determined as [Zhao and Wang, 2013]:

$$y_{ic} = y_i - b_P(x_i - x) \quad (5.2)$$

With y_{ic} the water level after correction, y_i the observed water level, b_P is the barometric pressure coefficient, x_i is measured barometric value and x is average barometric pressure.

5.2. Modeling

To confirm the understanding of the subsurface processes, Hydrus 2D was used to model the unsaturated and saturated zone at the test area. Hydrus is a modeling environment for the analysis of water flow and solute transport in variably saturated porous media [by J Šimůnek et al., 1999]. The model is based on solving the Richards equation for saturated-unsaturated water flow [Šimůnek et al., 2012].

The van Genuchten parameters are related to the water retention curve [Hilberts et al., 2005, by J Šimůnek et al., 1999]. The water retention curve (**WRC**) is the relationship between the water content, θ , and the soil water suction, h [Likos et al., 2014]. Hydrus2D solves the hydraulic model using the van Genuchten function (van Genuchten 1980) (Equation 5.3), and the combination with Mualem's (1970) pore-size model (Equation 5.4):

$$\theta(h) = \theta_r + \frac{(\theta_s - \theta_r)}{(1 + (\alpha h)^n)^{1 - \frac{1}{n}}} \quad (5.3)$$

$$K(S_e) = K_0 S_e^L (1 - (S_e^{\frac{n}{n-1}})^{1 - \frac{1}{n}})^2 \quad (5.4)$$

$$S_e = \frac{\theta(h) - \theta_r}{\theta_s - \theta_r} \quad (5.5)$$

Where:

$\theta(h)$ is the volumetric water content (cm^3/cm^3), at suction h [cm]

θ_s saturated water content [-];

θ_r residual water content [-];

α is related to the inverse of the air entry suction, $\alpha > 0$ [$\frac{1}{cm}$]; and;

n is a measure of the pore-size distribution, $n > 1$ [-];

K_0 is a fitted matching point at saturation [cm/d];

L is an empirical parameter (Mualem 1970) [-].

The water retention curve can be obtained through various methods, in the field and laboratory. However, it is usually determined under laboratory conditions using the porous plate apparatus or tensiometers. Obtaining soil hydraulic parameters, such as the WRC, either in the field or laboratory, is often demanding, in both time and labor [Ícaro Vasconcelos do Nascimento et al., 2018]. A solution lies in obtaining the grain size distribution of the soil, the bulk density, the organic matter and the soil saturated conductivity [Wang et al., 2017]. Once obtained, two sources can be used to predict the Van Genuchten parameters, as shown in Table 5.4. These sources being Rosetta Lite [Schaap et al., 2001] and StaringReeks [Heinen et al., 2020]. Rosetta, is a pedo-transfer function which allows the estimation of the van Genuchten (1980) water retention parameters, saturated hydraulic conductivity (K_s), and their uncertainties. StaringReeks, provides estimation of the parameters from a Dutch soil database. The required inputs for these programmes are:

- Rosetta Lite: % Sand, Silt, Clay and Bulk Density
- StaringReeks: % Organic matter, lutum, loam and median sand fraction.

The output of these programmes provides the following parameters:

- r : the water content for which the gradient becomes zero;
- s : the water content of the soil when it becomes completely saturated;
- m : scaling parameter, inversely proportional to mean pore diameter and the air-entry value of the pF curve;
- n : shape parameter of the soil water characteristic.
- K_s : the saturated hydraulic conductivity.

5.2.1. Required input

Aside from the van Genuchten parameters, the required input of the model are soil parameters, geometry, initial conditions and boundary conditions. To identify the precipitation effects, atmospheric fluxes are added, related to the rainfall in the area. This data is provided by the Rain Gage as the monitoring interval is smallest [5 minutes]. The atmospheric flux is applied at the atmospheric boundary with a factor of 3.5. This factor was added to account for the concentration of runoff from the connected area at the Aquaflow granulate layer. To apply the soil parameters, additional testing was required. Soil samples were collected at four locations. Of these four, three locations (L1, L2 and R2 in Figure 5.11) were analysed in the Rotterdam Soil Laboratory. The fourth sample (R1) was not analysed as the sample was contaminated with tree soil. The results are presented in Table 5.4.



Figure 5.11: Soil sample locations at the test area.

The samples taken from the sampling locations (Figure 5.11) were disturbed samples, taken to a depth of 3 meters below surface level. These samples were analysed by means of: (i) a sieve test and grain size distribution, including sand, silt and loam percentage (Figure A.3) and (ii) burning to determine the organic content. Additionally, the saturated hydraulic conductivity (K_s) and the dry bulk density (BD) were determined. The following methods were used:

1. K_s disturbed: Permeability constant head (NEN 5123);
2. Soil-texture: Sieving analysis (NEN-EN-933-1);
3. Dry-bulk density: Wet and dry volumetric weight determination (NEN 5111);
4. Organic content: RAW 2015, test 28 ('gloeiverlies')

5.2.2. Model set-up

Geometry

The 2D model was created in the horizontal x-z-plane with a width of 50 meters and a total depth of 5 meters. The model represents the cross-section of the Aquaflow system between P2 and P3. At the top middle, a 40 cm inlet was created over a length of 7 meters to mimic the Aquaflow granulate layer. The drain (40 cm diameter) is modelled by an opening with a radius of 20 cm.

The FE Mesh (Figure 5.13) is the Finite Element Mesh. Hydrus models use the method of Finite Differences to integrate the governing equations (the Richards equation and the convection-dispersion equation) in time [Šimůnek et al., 2012]. The Finite Elements method solves the governing equations in space. In the model, the FE-Mesh was created with high density around the domain of interest: the area of the Aquaflow system and the drainage pipe. For the remainder of the model area, lower densities were applied. A higher density FE-Mesh improves the accuracy of the model.

Domain properties

Three types of soil are applied in the model for material distribution as displayed in Figure 5.12: Links 1 (from soil samples) consisting of fine sand, Links 2 (from soil samples) consisting of medium fine sand and Clay (standard Hydrus parameters). The distribution of the material is based on the soil experiments in the area as described in section 5.2.1.



Figure 5.12: Material distribution of soils applied in the Hydrus model: L1, L2 and clay

To account for the delay in the system, the effect of the granulate layer and to provide reasonable results, scaling factors were applied at the atmospheric boundary (Aquaflow) and the seepage face boundary. At the atmospheric boundary a scaling factor of 1.5 x hydraulic conductivity at Material 1 was applied, to simulate the permeable foil at the bottom of the Aquaflow foundation layer between the granulate and sand of the unsaturated zone. Around the seepage face boundary a scaling factor of 0.19 was applied to account for the inflow friction of water to the perforated drainage pipe (DIT), at the seepage face a scaling factor of 0.05 was applied. The scaling factors are displayed in Figure C.5. To identify the effects in the unsaturated zone, observation points can be added to the model at which pressure head data is recorded. Along the drainage level, 7 points were added to observe the circle of influence of infiltrated water. 5 points coincide with piezometer locations, the additional points are for additional observations.

Table 5.4: Measured (M) soil characteristics and predicted (P) van Genuchten parameters at the three sampling locations.

	<i>L1</i>	<i>L2</i>	<i>R2</i>	<i>units</i>	<i>P/M</i>
<i>gravel</i>	0.7	1.6	0.6	%	M
<i>sand</i>	92.7	94	94.1	%	M
<i>silt</i>	4.1	3.1	3.6	%	M
<i>lutum</i>	2.6	1.3	1.7	%	M
<i>D50</i>	0.215	0.205	0.199	mm	M
<i>D60/D10</i>	3.2	2.6	2.7	mm	M
<i>M50</i>	0.227	0.21	0.206	mm	M
<i>rho_b</i>	16.5	16.5	16.6	kN/m ³	M
<i>rho_b</i>	1.682534179	1.682534	1.692731	g/cm ³	M
<i>porosity</i>	37	36	36	%	M
<i>k10</i>	2.20E-05	5.50E-05	4.10E-05	m/s	M
	0.13	0.33	0.25	cm/min	M
<i>dry volumetric weight</i>	15	15	14.9	kN/m ³	M
<i>Output</i>					
<i>theta_r</i>	0.0482	0.0487	0.0482		P
<i>theta_s</i>	0.3329	0.3312	0.3289		P
<i>alpha</i>	0.0347	0.0338	0.0343	1/cm	P
<i>n</i>	2.8788	3.3067	3.1236		P
<i>Ksat</i>	365.5288	548.0282	457.218	cm/d	P
<i>Ksat</i>	0.253839444	0.380575	0.317513	cm/min	P
<i>Ksat</i>	4.23066E-05	6.34E-05	5.29E-05	m/s	P

Initial conditions

To apply the local conditions regarding soil moisture and rainfall, initial conditions and boundary conditions have to be defined. The initial conditions are related to the groundwater levels. The initial condition is defined as the bottom pressure head from the lowest located nodal point. For simplicity, the groundwater table at P103 is used as the reference groundwater table. At the test area groundwater levels at the inner gardens are much higher than the road cunet. The initial condition is the groundwater level at the start of the event (T=1000).

Boundary conditions

In the model, four boundary conditions are applied:

1. Atmospheric boundary at the Aquaflow
2. Seepage face
3. No flux

The 'Atmospheric Boundary' condition relates directly to the stormwater runoff entering the Aquaflow system. It is presented in units [cm/min]. For this boundary condition, the monitored rainfall volume is used as measured at Rain Gage [mm in 5 minutes]. This boundary is applied at the Aquaflow layer level. The 'Seepage Face' boundary condition states that "there is no flux across the boundary as long as the boundary is unsaturated, and that the pressure head is fixed to the zero value once saturation is reached" [by J Šimůnek et al., 1999]. The flux across the boundary is calculated from the flow field by solving the governing flow equations. The 'Seepage Face' flux presents the outflow information at the drainage pipe. The 'Seepage Face' flux unit is [cm³/min]. The drainage pipe lies below the groundwater table, with a positive pressure head at the drainage pipe as a result. Since the seepage face b.c. becomes active when pressure heads are positive, a pressure head needs to be specified at the 'Seepage Face' to activate the boundary condition when the specified pressure head is reached at the seepage face. The drainage level at the test area is -2.40 m NAP and the drainage pipe lies at -3.20 m NAP. The specified internal pressure head is 80 cm. The 'No Flux' boundary condition is applied at the remaining boundaries of the model. The 'No Flux' boundary condition was selected due

to the distance from the zones and to separate the Aquaflow system at the test area from the rest of the Agniesebuurt area.

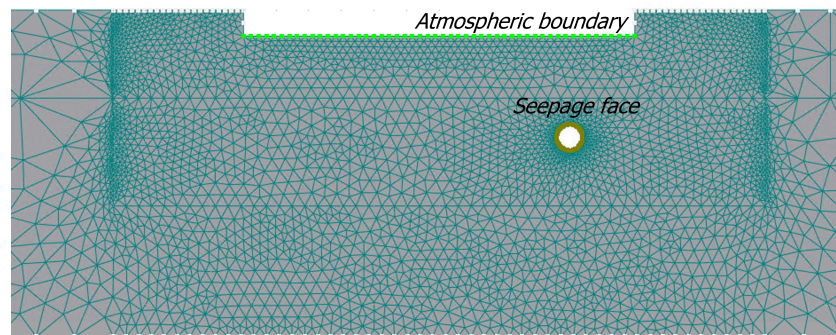


Figure 5.13: Boundary conditions applied in the model. At all other boundaries, the 'No Flux' boundary condition was applied.

6

Results

The results obtained from the monitoring at the case study area are presented in this chapter. First, the events were selected with varying intensity, duration and antecedent dry days. In the following sections, results from the Aquaflow response to these selected events are presented and discussed.

6.1. Event selection

Naturally occurring rain events were selected in addition to the full-scale test performed on 20-04-2022 (Event 1). The events 2 to 5 were selected due to the availability of the full range of monitoring data. The selected rain events are summarized in Table 6.1, with the associated rainfall intensity, and rainfall depth.

Table 6.1: Selected events over the monitoring period

Event	Period start	Water equivalent	Max. rain intensity	Volume rain	Performance criteria
	<i>[yyyy-mm-dd]</i>	<i>[mm]</i>	<i>[mm/hr]</i>	<i>[m³]</i>	
1.	2022-04-20	20	100	30	PC1
2.	2022-05-20	12.6	45	18.9	PC4
3.	2022-05-23	15.2	34	22.8	PC4
4.	2022-06-05	25.8	49.5	38.7	PC3
5.	2022-04-07	5.8	21.8	8.7	PC5

6.2. Aquaflow response

After the rain events were selected in the previous section, the monitored response results are presented in this section. The performance is assessed using the performance criteria as defined in section 4.1.5.

6.2.1. Event 1: Full scale test

The full scale test (2022-04-20) as discussed in section 5.1.2 presents information regarding high intensities and thus, high return period events. The event is characterised by four high intensity peaks with volumes ranging from 5 to 10 m³ for each peak. The response of the Aquaflow to Event 1 is summarized in Table 6.2 in section 6.2.1. In the following sections, the performance regarding ponding, emptying time, inflow and outflow and groundwater recharge are discussed. The mentioned monitoring locations are presented in Figure 5.1 in section 5.1.

Ponding

The ponding time and depth in response to Event 1 are shown in Figure 6.1 for all gully-pots with respect to the reference level: the pipe invert level.

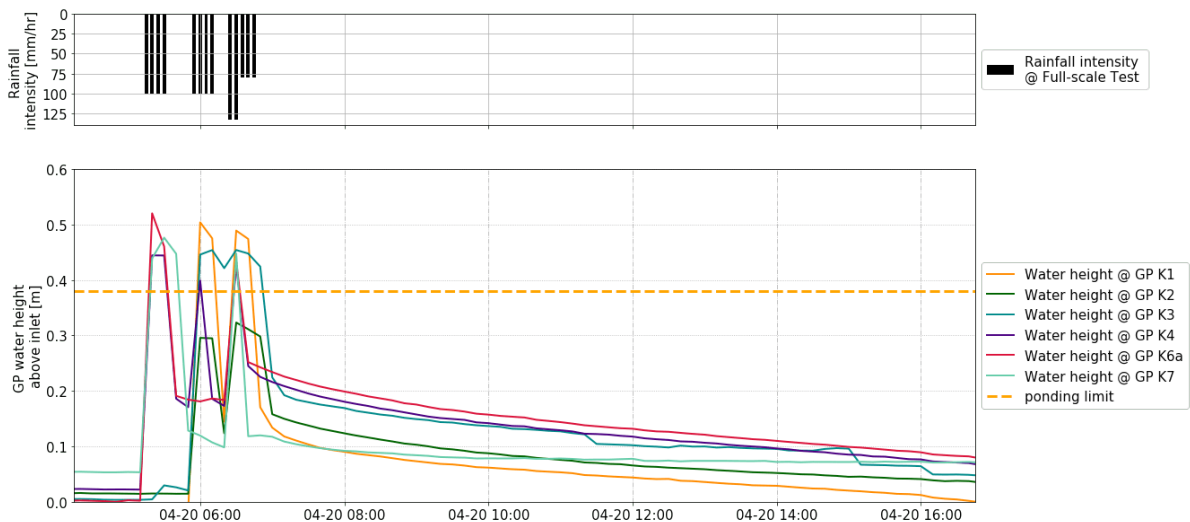


Figure 6.1: Pondering for all gully-pots in response to event 1. The water levels are presented w.r.t. gully-pot pipe invert level.

In Figure 6.1, it is observed ponding was measured at all gully-pots for Event 1. The ponding duration, related to the duration of water on the street, varied between 10 to 30 minutes for each peak with a total of 30 to 50 minutes for the entire event. The ponding times for each gully-pot are summarized in Table 6.2. The ponding can be explained through the capacity of the gully-pots ($30 \text{ m}^3/\text{s}$ per gully-pot) and the high water discharge intensity from the trucks ($150 \text{ m}^3/\text{h}$ divided over 4 gully-pots for section 1, and 3 gully-pots for section 2.).

The ponding depth and duration varied between the gully-pots. The four peaks can be clearly observed in the figure, with the associated peaks at the gully-pots in each section 5.3. K3 remains filled between Peak 2 and Peak 4. Gully-pot K4 shows three peaks, as it received water in both events, due to the high level of ponding and water flowing between the gully-pots. As observed in Figure 6.1, the ponding duration is much longer for K1, K2, and K7, than K4 and K6. This was also observed during field observations at the full-scale test. The ponding in section 1 was much shorter, due to the high flows of water through the gully-pots, and 3 out of 4 functioning gully-pots. In section 2, water flows were only observed at K2, with 1/3 gully-pots functioning.

The Aquaflow system meets the ponding requirement PC1: a maximum ponding duration of 60 minutes for high intensity (>100 mm/hour) storms, with volume 30m^3

Emptying time

Another performance defining metric is the emptying time as defined in section 4.1.2. The emptying time was assessed for all gully-pots as shown in Figure 6.2.

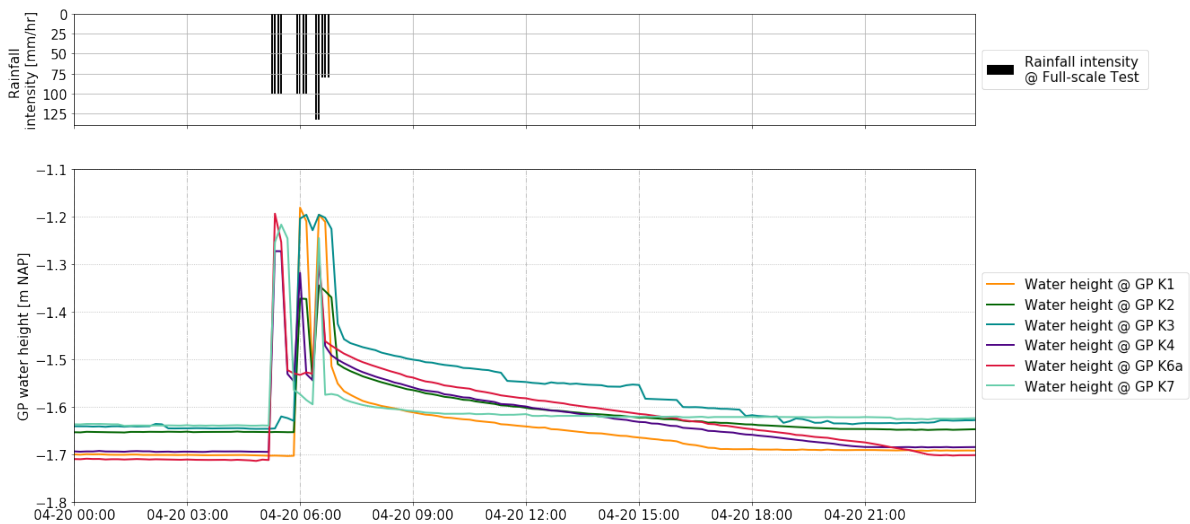


Figure 6.2: Gully-pot water levels w.r.t. m NAP at all locations.

As can be observed in Figure 6.2, all gully-pots emptied in the same manner. The gully-pot water levels show an initial steep decline with water entering the granulate layer through the pipe. After the initial decline, the water levels decrease steadily down to the invert level in a period of 15 hours, with a maximum total emptying time of 17 hours (Table 6.2). After the first peak at K6a, it is observed the water levels remain at -1.52 m NAP, after which the water levels show a steep peak increase for peak 3. The rise and fall of K4, coincides with the rise and fall of the K6a peaks. Between peak 1 and 3, K4 shows a smaller peak due to water flowing from section 2 to section 1 during peak 2. After the third peak, the gully-pot water levels decrease steadily starting from -1.48 m NAP to -1.70 m NAP in 10 hours for K1 and 15 hours for K4 and K6. K1 has a much shorter emptying time with respect to K6. As can be observed in Figure 6.2, the emptying time increases in the downstream direction.

The Aquaflow system is empty within 17 hours, for a maximum filling at the granulate layer of 25 cm above the pipe invert level. The system was not fully-filled for this event, and does not provide information regarding the emptying time for a full system.

Inflow and outflow

The inflow and outflow of the system determines the volume retention, peak delay and peak reduction as defined in section 4.1.3. The response of the inflow at K1 and K6 and the outflow at Manhole MB are shown in Figure 6.3.

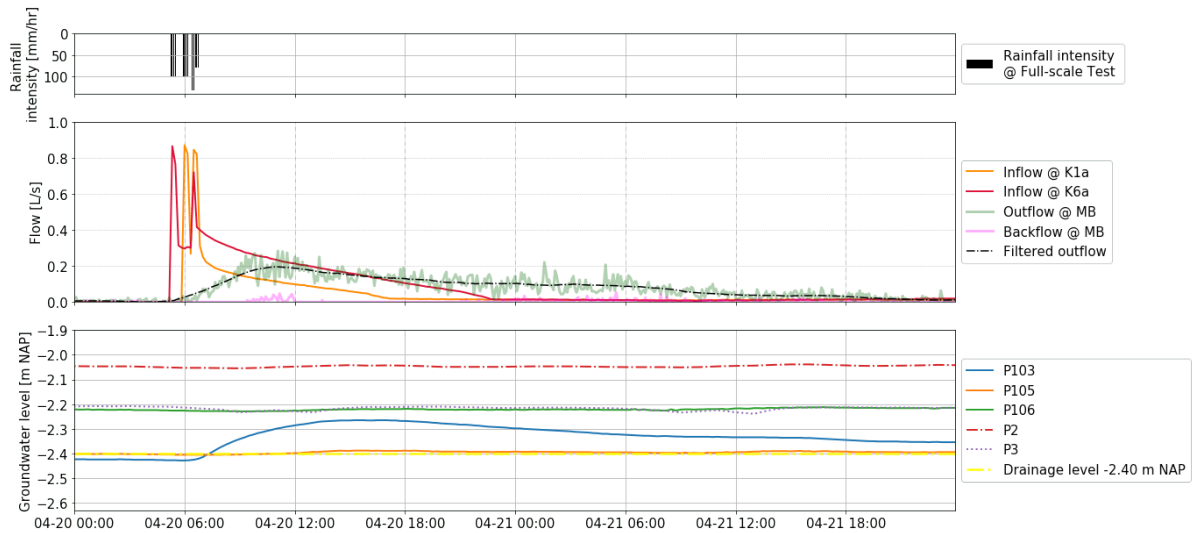
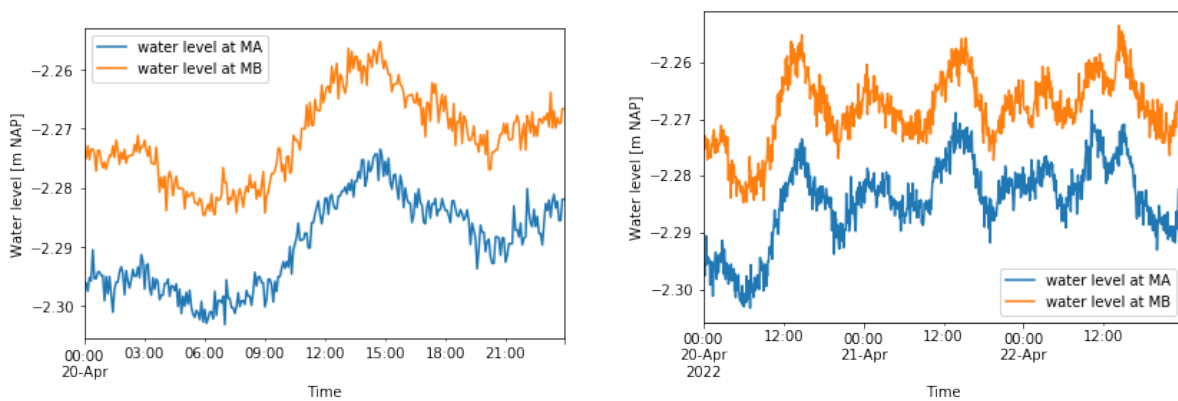


Figure 6.3: Flow and groundwater response to Event 1

The inflow is rapid, due to the high discharge intensity of the full-scale test, and consequently, the rapid gully-pot water rise. The outflow graph response (Outflow @ MB in Figure 6.3) is much more gradual, with a lower maximum. This is in line with the expectations regarding in- and outflow of LID systems, see Figure 4.2. Due to the monitoring interval of five minutes, and the rapid response of the gully-pots, the calculated inflow (14.9 m³) at the gully-pot level is much lower than the actual inflow volume (30 m³). The total outflow is measured at the drainage pipe outlet, with a total volume of 14.85 m³. The total calculated volume retention is 50.5% and the total peak delay is 05:45 hours between the peak in the gully-pots and the peak in the drainage pipe at the end of the system (at Manhole MB). The total duration of the outflow peak is 1 days 05:25:00 (29:25 hours). The performance criteria are met regarding volume retention and peak delay. The total peak reduction is 67.2%. The outflow graph in Figure 6.3 shows the total duration of the peak flow. In addition to outflow measurements, the water levels in the manholes were monitored, showing the rise in water level from approximately 07:00 20-04-2022 to a peak at 15:00 in Figure 6.4a. The peak at the manholes is later than at the flowmeter and coincides with the groundwater table peak at P103.



(a) Manhole water levels at 20-04-2022

(b) Manhole water levels from 20-04-2022 to 21-04-2022.

Figure 6.4: Manhole water level fluctuations in response to event 1, and under natural conditions.

Using the Darcy-Weisbach equation between the two manholes to determine the flow provides insufficient results, due to the natural fluctuations in the manholes, as observed in Figure 6.4. Therefore, the flowmeter results are used for the following events.

The Aquaflow system provides a delay of 5:45 hours for Event 1. This meets the performance criterion

for the peak delay of 1 hour. The total volume retention is 50.5%, the system meets the volume retention performance criterion of 35% retention.

Groundwater recharge

From the results, as shown in Figure 6.3, it is observed the infiltration from the Aquaflow system to the unsaturated zone leads to groundwater recharge. The initial groundwater level prior to the full-scale test was -2.40 m NAP, at the drainage level. The effect of Event 1 on the local groundwater at the test area was also assessed. From the figure, in- and outflow and the groundwater response are observed. At P103, the groundwater responds in the same manner as the outflow graph, with a delay between the groundwater peak and the outflow peak. P103 shows a clear groundwater level increase. At both P105 and P106, the groundwater level fluctuations are minimal. This is explained through the position of P103 in relation to P105 and P106. Both P105 and P106 are located approximately 2 meters from the outflow drain of the Aquaflow system, on the East side of the Aquaflow. P103 is located to the West of the Aquaflow at approximately 10 meters from the outflow drain, with more build-up of water. Additionally, at P105, the piezometer is placed in a clay layer, which also prevents quick recharge at P105 and P106. At P106, the groundwater table is 20 centimeters higher than P105, the distance between these two piezometers is 1 meter, and such high pressure differences seem out of place. Therefore, P105 and P103 are used for groundwater effects of the Aquaflow system.

P2 and P3 are groundwater monitoring locations at the inner-gardens. The groundwater table at the inner gardens is much higher than the road cunet. As can be observed in Figure 6.3, the infiltrated water does not affect the groundwater levels at the inner-gardens. This can be explained through the large distance from the Aquaflow infiltration zone and the local nature of the full-scale test water discharge.

The groundwater recharge is related to the drain pipe outflow. The drain pipe was placed to maintain a drainage level of -2.40 m NAP. Groundwater recharge above this limit results in outflow through the drainage pipe. Approximately 50.5% of the inflow volume is retained in the system, this water is retained in the unsaturated zone below the Aquaflow system, and at the groundwater table at P103. The groundwater levels at P105 and P106 are not affected by the infiltration, where the groundwater table at P105 remains at the drainage level.

The Aquaflow system meets the requirement for groundwater level recharge for the high intensity, high volume rainfall of the full-scale test Event 1. The maximum groundwater table after infiltration is -2.25 m NAP, > 80 cm below the surface level.

Water temperature

The water temperature was monitored at all gully-pots (K1-K7) and both manholes (MA and MB). In Figure 6.5, the gully-pot temperatures are shown. For the gully-pots, water temperature fluctuations indicate inflow from rainwater (temperature decrease) and outflow into the Aquaflow granulate layer (temperature increase). From the figure, the limited performance of gully-pot K3 and K7 is observed, due to the limited temperature fluctuations in the gully-pots in response to the inflow.

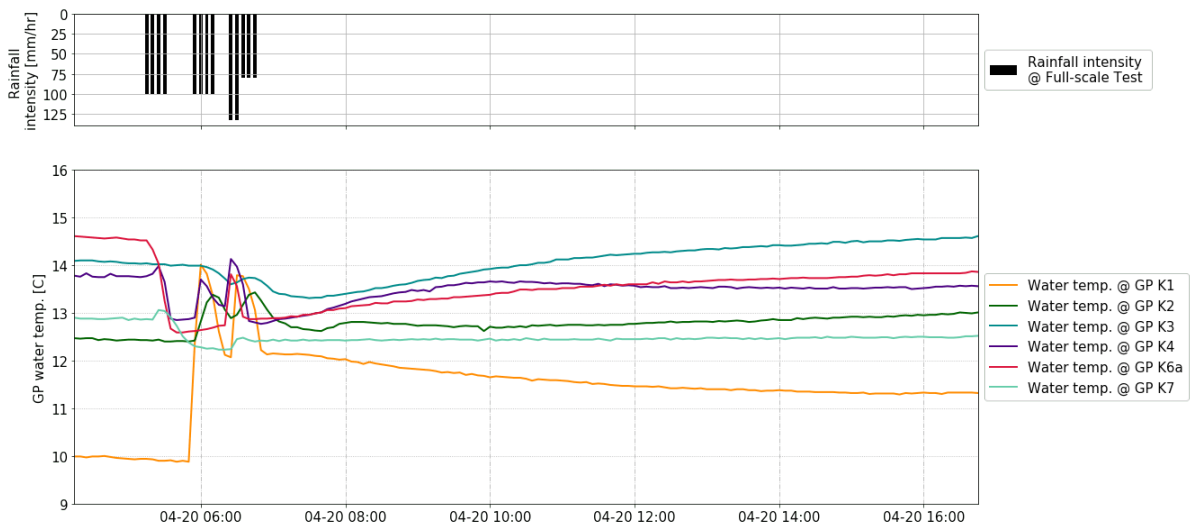


Figure 6.5: Gully-pot water temperature during Event 1

The full-scale test was conducted on 20-04-2022 at the start of spring. The manhole water temperatures are low at the manholes (11-12 degrees Celsius), as shown in Figure 6.6. The infiltrated rainwater therefore causes an increase in manhole water temperature. The manholes are connected to the groundwater, and thus the manhole water temperature is related to the groundwater temperature. This is especially visible at manhole MA, due to the smaller manhole size and lower manhole water depths. At MA, the temperature increases as the outflow peak starts and reaches a steady temperature after the outflow peak ends at approximately 12:00 21-04-2022.

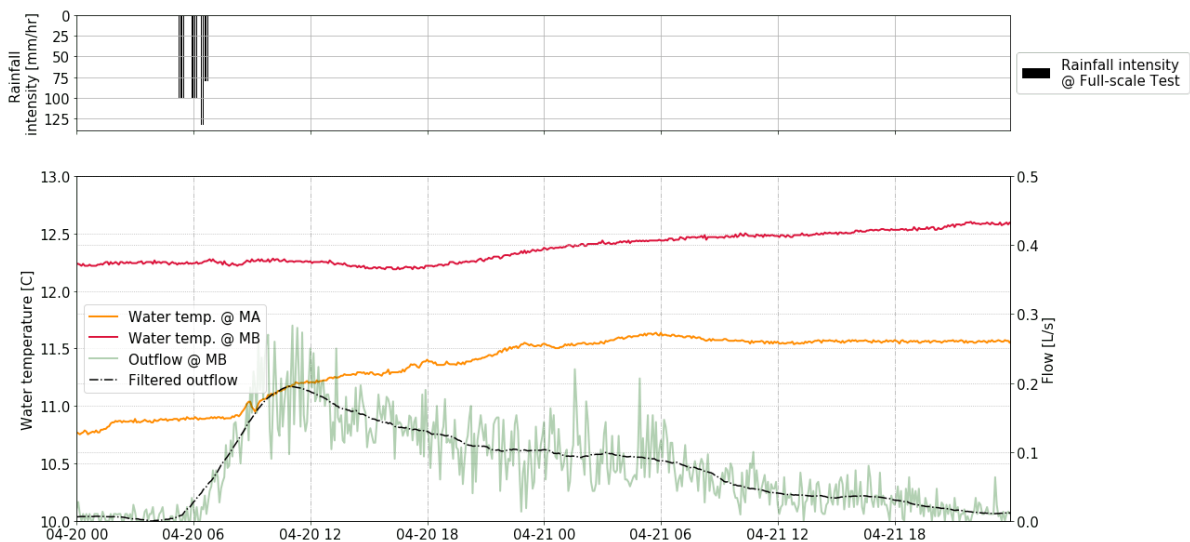


Figure 6.6: Water temperature @ manhole MB and MA for the period around event 1, showing the clear temperature fluctuation at 20-04-2022.

Field observations

During the course of the full-scale test, field observations were conducted. The ponding duration and depth were observed, with more build-up of water in section 2 (figure 6.7d), and quicker emptying at section 1 (figure 6.7a). It could be observed that gully-pot K7, K1 and K3 showed signs of clogging (figure 6.7b), with no visible water flows to these gully-pots. Conversely, at K6 and K4, clear whirlpools were observed, indicating high discharge capacities. The water was discharged onto two sections. Surface water flows could be observed to neighboring gully-pots (Figure 6.7c, showing the spreading of water and increasing the inflow speed to the Aquaflow layer).

Summary Event 1

The results of the Aquaflow response to Event 1 are summarized in Table 6.2.

Table 6.2: Summary Event 1

	K1	K2	K3	K4	K6	K7	Units
<i>Ponding time</i>	30		55	25	20	30	<i>Minutes</i>
<i>Ponding height</i>	0.124		0.075	0.065	0.14	0.09	<i>m</i>
<i>Emptying time</i>	12:35	13:35	12:55	15:40	17:25	21:15	<i>Hours</i>
	System results		Units				
<i>Rain volume</i>	30		<i>m³</i>				
<i>Outflow volume</i>	14.85		<i>m³</i>				
<i>Peak delay</i>	05:45		<i>Hours</i>				
<i>Volume retention</i>	50.5		<i>%</i>				
<i>Peak reduction</i>	67		<i>%</i>				
<i>GW delay @ P103</i>	09:55		<i>%</i>				



Figure 6.7: Field observations during the full-scale test (Event 1)

6.2.2. Event 2: May 20

On May 19 2022, 12.6 mm of rain fell with a maximum intensity of 45 mm/hour. The total associated volume of rain was 18.9 m³, for a runoff coefficient of 1. For the runoff volume entering the Aquaflow system, a runoff coefficient of 1 was selected, to obtain the potential, maximum peak reduction and volume retention.

Ponding

For Event 2, ponding was recorded at K3 and K7. Water levels above the pipe invert level at each gully-pot are shown in Figure 6.8. Aside from K3 and K7, at the remaining gully-pots, water levels remained well below the ponding level, with maximum levels of 18 cm above the invert level. The total ponding time at K3 was 15 minutes. At K7, the total ponding time was 40 minutes. Since the water levels at gully-pots K1, K2, K4 and K6 are a maximum of 18 centimeters, it can be assumed the observed ponding is due to local water build-up at the gully-pots and/or errors in the gully-pot sensors. An explanation for the build-up of water at the gully-pots could be found in clogging of the gully-pots, as also observed during the full-scale test (Figure 6.7b). The gully-pot water temperatures provide additional information regarding this matter.

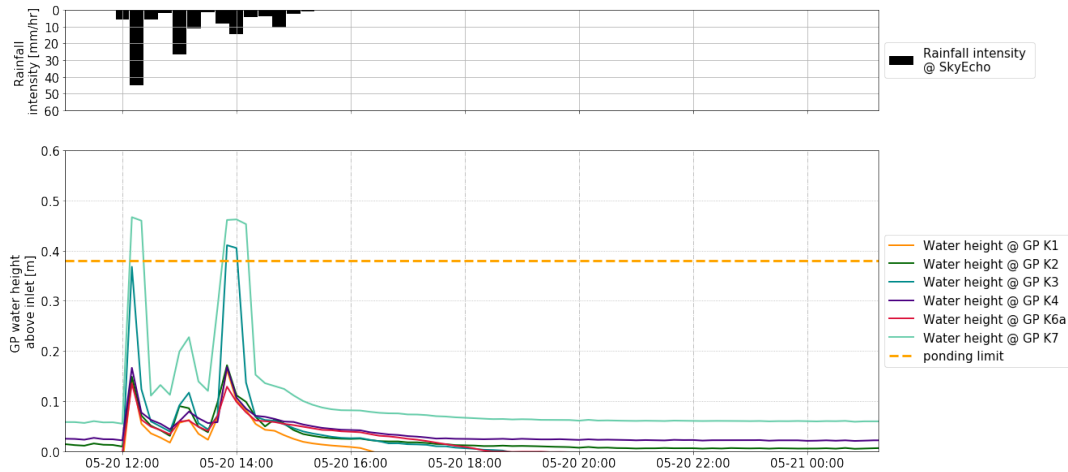


Figure 6.8: Gully-pot water height with respect to invert level of inlet pipe and the surface level, showing the ponding depth and duration.

Event 2 provides information on PC4 for rain events with intensity > 20 mm/hour and water equivalent > 10 mm. The Aquaflow system meets this criterion. However, local ponding at K3 and K7 was observed, due to reduced functioning of these gully-pots.

Emptying time

The emptying time for the gully-pots in terms of water height with respect to meters NAP, are shown in Figure 6.9. The emptying time in response to the rainfall on 20-5-2022 was 5 hours (K4) to 6 hours at K6 (Figure 6.9). The emptying relation in the downstream direction is again observed for this event. And three peaks are observed, showing the system emptying and filling up from new runoff. When looking at the emptying time and gully-pot water levels with respect to m NAP, it shows the lower lying gully-pots empty first. The system empties rapidly, with the system empty within 6 hours.

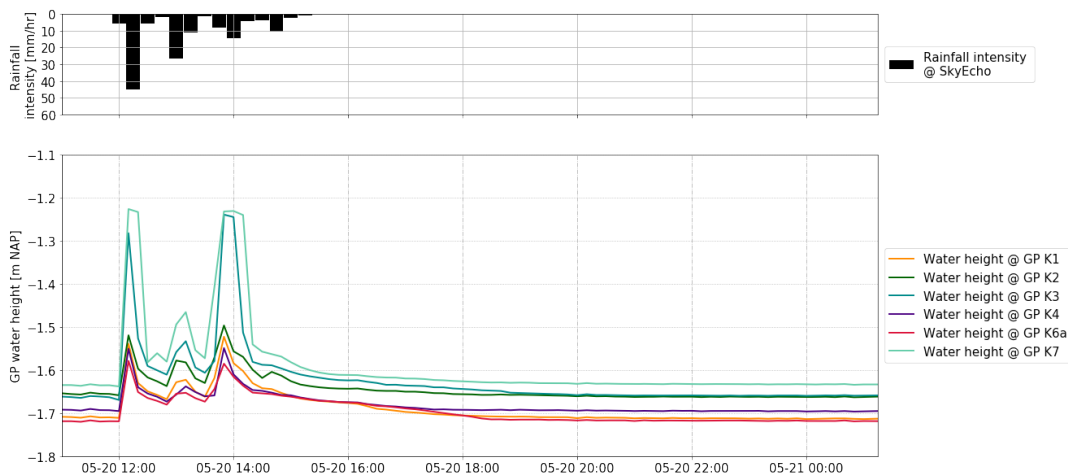


Figure 6.9: Gully-pot water height for event 2, showing the emptying time with respect to meters NAP.

The maximum water level was 18 cm in the gully-pots, and 8 cm in the granulate layer. The system was emptied within 6 hours.

Inflow and outflow

For Event 2, the inflow volume was much lower (9.3 m^3) for a runoff coefficient of 1 ($C=1$). The measured outflow is 2.4 m^3 , resulting in a volume retention of 87.19% and the measured peak reduction is 58.2%. The total outflow volume for event 2 is much lower than event 1, this is due to two factors:

1. The initial groundwater levels at P103 and P105 are below -2.50 m NAP. The drainage level in the area is -2.40 m NAP. Therefore, most rainwater is used to recharge the groundwater level to drainage level.
2. The total inflow volume of Event 2 is 9.3 m³ over 4 hours. During Event 1, 30 m³ was discharged in 1 hour. Therefore, both the intensity and volume of Event 2 are much lower.

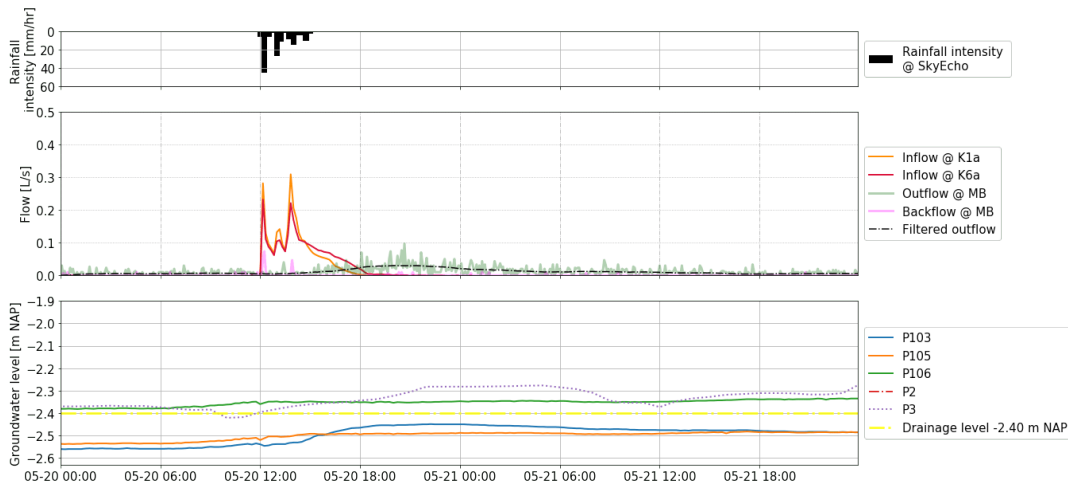


Figure 6.10: In- and outflow at the gully-pots and drain pipe, respectively. Additionally, groundwater level fluctuations are shown in response to event 2.

The flowmeter at Manhole MB measures both positive (outflow) and negative flow (back-flow). Since Event 2 is a natural event, flow from surrounding area is also expected. In Figure 6.10, the outflow and back-flow curves for Event 2 are shown. At the downstream end, at manhole MB, there is a connection to the drainage pipes of the Vrouw-Jannestraat. At the intersection, gully-pots are connected directly to the drainage pipes 3.5. Therefore, at the start of the event runoff enters the drainage pipe directly, thus creating over-pressure, and water flows back into the test location drainage pipe. The interval between the back-flow peak and the inflow peak thus provides additional information into the peak delay, as this indicates the time at which water enters the drainage pipe when gully-pots and drainage pipes are directly connected. This delay coincides with the peak delay measured by comparing gully-pot inflow peaks and drain outflow peaks.

The system meets the performance criteria for both peak delay and volume retention, with a delay of 08:30 hours. The total volume retention is 87.19%.

Groundwater table

In Figure 6.10, the inflow and outflow and groundwater levels are shown for the road cunet, and the inner gardens. The initial groundwater levels at the road cunet (P103 and P105 in Figure 6.10), are more than 10 centimeters below the drainage level (-2.40m NAP). The barometric effect on the groundwater table is observed at the start of the event, at 20-05-2022 12:00. Again, P103 shows a rapid response to the Aquaflow infiltration, in delayed response to the outflow. The outflow volume is low, this can be explained through the low initial groundwater levels, and the limited infiltration volume. Infiltrated water is used to recharge the groundwater table. This can be observed in Figure 6.10, as the groundwater table rises by approximately 5 centimeters after the event to -2.50 m NAP. The groundwater response at P3 is steep and the response is instant with the start of the rain event, due to the instant infiltration from rainwater. However, the time to the groundwater table peak at P3 is much longer than for P103. This is due to the drainage preventing, long term, steep groundwater rise in the road cunet, and the soil structure at P3 (clayey soil).

The maximum groundwater recharge in response to Event 2 is up to -2.45 m NAP at P103 and -2.28 m NAP at P3. The system meets the groundwater table performance criterion.

Water temperature

The water temperature measurements at the gully-pots provide information regarding the discharge potential of the gully-pots, related to the clogging. From Figure 6.11, it can be observed the gully-pots all show a similar response in temperature drop during the event. However, at K3, the gully-pot water temperature fluctuations are very limited, thus providing an explanation for the measured ponding during event 2.

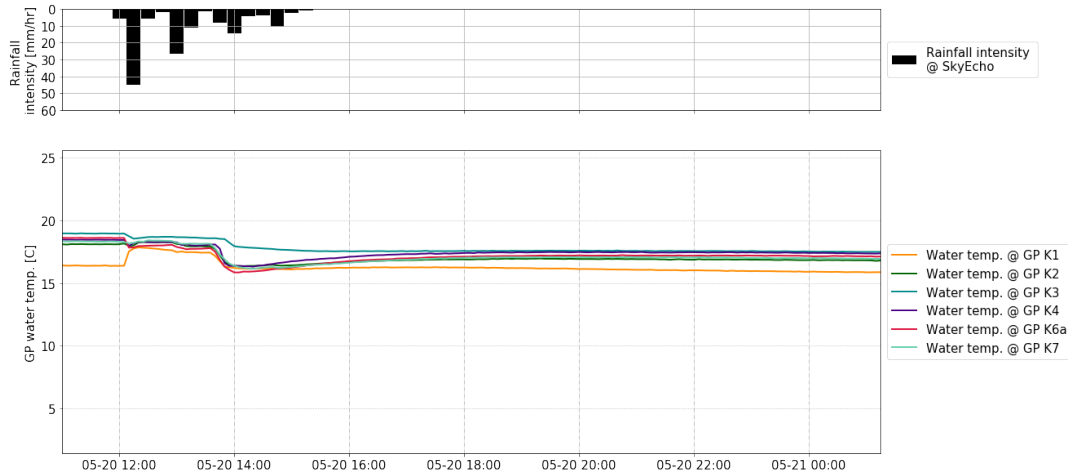


Figure 6.11: Gully-pot water temperatures, providing a solution for the ponding observed at K3, due to clogging.

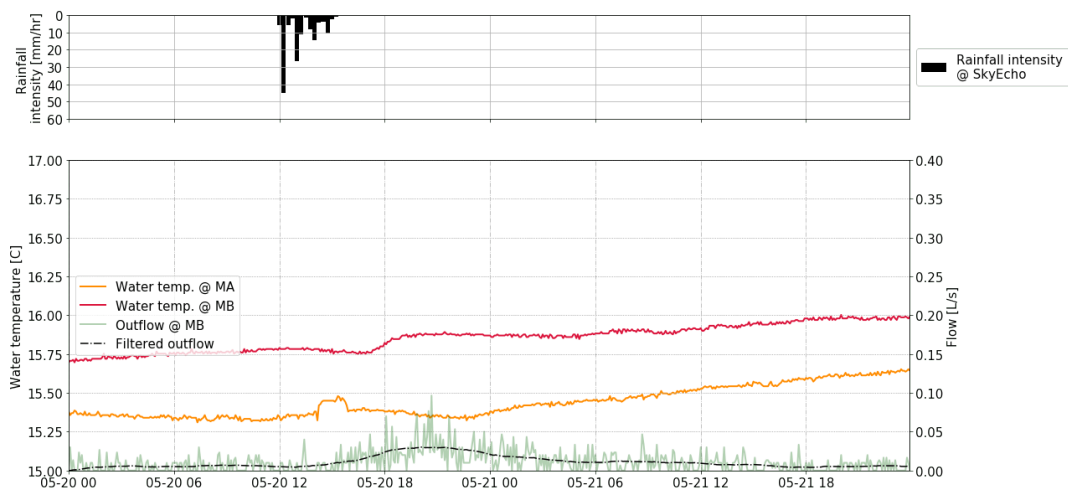


Figure 6.12: Event 2 manhole water temperatures [C] at MA and MB vs. outflow [L/s] at manhole MB

In Figure 6.12, the manhole water temperatures are displayed. The manhole water temperature at MA shows a small spike at 20-05-2022 14:00, possibly indicating the initial flow to the drain pipe. The temperature at manhole MB starts to rise at 18:00, four hours later, when the outflow peak starts.

Event summary

Table 6.3: Summary Table of Event 2.

	K1	K2	K3	K4	K6	K7	
Ponding time	0	0	15	0	0	40	Minutes
Ponding height	0	0	0.03	0	0	0.08	m
Emptying time	04:55	04:55	06:40	04:55	06:05	05:45	Hours
System results		Units					
Rain volume	18.9	m^3					
Outflow volume	2.4	m^3					
Peak delay	08:30	Hours					
volume retention	87.19	%					
Peak reduction	58.2	%					
GW delay @ P103	10:05	Hours					
GW delay @ P3	11:20	Hours					

6.2.3. Event 3: 23 May 2022

Event 3 is characterised by a water equivalent of 15.2 mm with a maximum intensity of 34 mm/hour. The total volume of rain is 22.8 m³ with a runoff coefficient of 1.

Ponding

During Event 3, ponding was registered at K2, K3 and K7, and no ponding was reported at other gully-pots. As shown in Figure 6.13, at K2, ponding was measured for a total duration of 5 minutes, with a maximum depth of 0.07 meters. At K3, ponding was measured for a total of 25 minutes with a maximum depth of 0.06 meters and at K7, ponding was measured for 45 minutes with a maximum depth of 0.11 meters. There is a large difference between the measured ponding at the gully-pots K2, K3 and K7 and the remaining gully-pots, K1, K4 and K6.

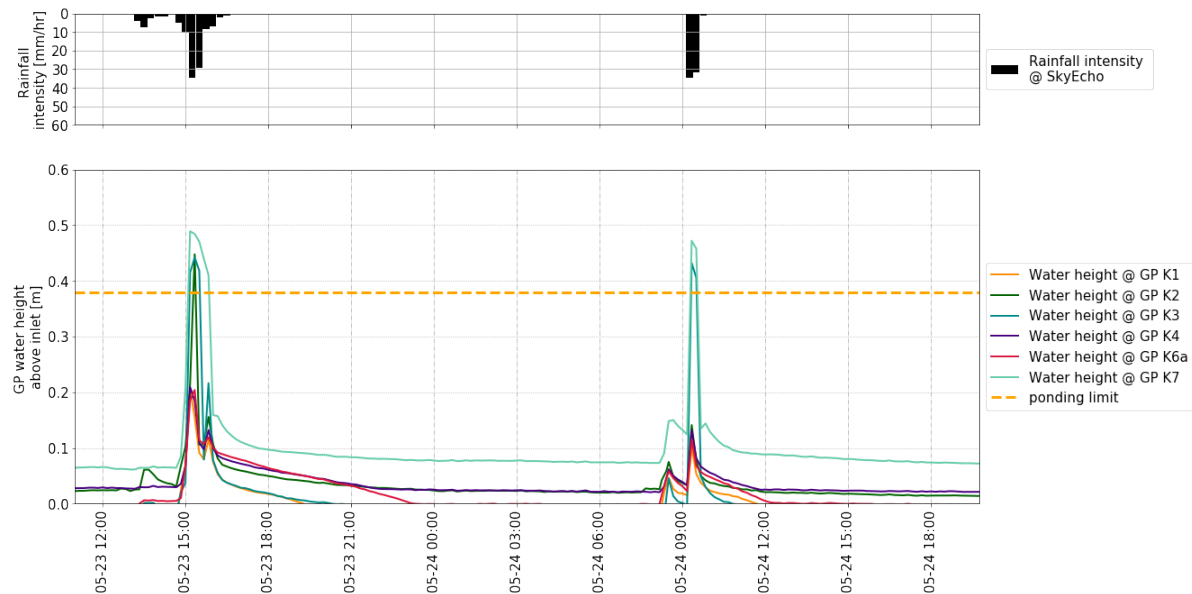


Figure 6.13: Ponding observed during Event 3. The graph shows the water levels at the gully-pots and the water levels exceeding the surface level (=ponding) at K2, K3 and K7.

Based on solely the measurements, the system does not meet the performance criterion for ponding PC4 for events with intensity > 20 mm/hour and rain depth > 10 mm. Ponding was measured at 3/7 gully-pots for a maximum duration of 45 minutes.

Emptying time

Event 3 is characterised by two peaks. The emptying time for the first peak was higher at all gully-pots, and from 5 to 8 hours as measured at the gully-pot level. There is more discrepancy in the emptying response of the gully-pots. Where K1, K4 and K6 show similar response and water levels and K2, K3 and K7 show similar response and water levels. For the first rain event, the emptying time at K1 is shorter than K6 by approximately 1 hour, as observed in previous events. For the second rain event, the emptying time of K6 is quicker than K1. Gully-pot K4 again follows the emptying trend of K6.

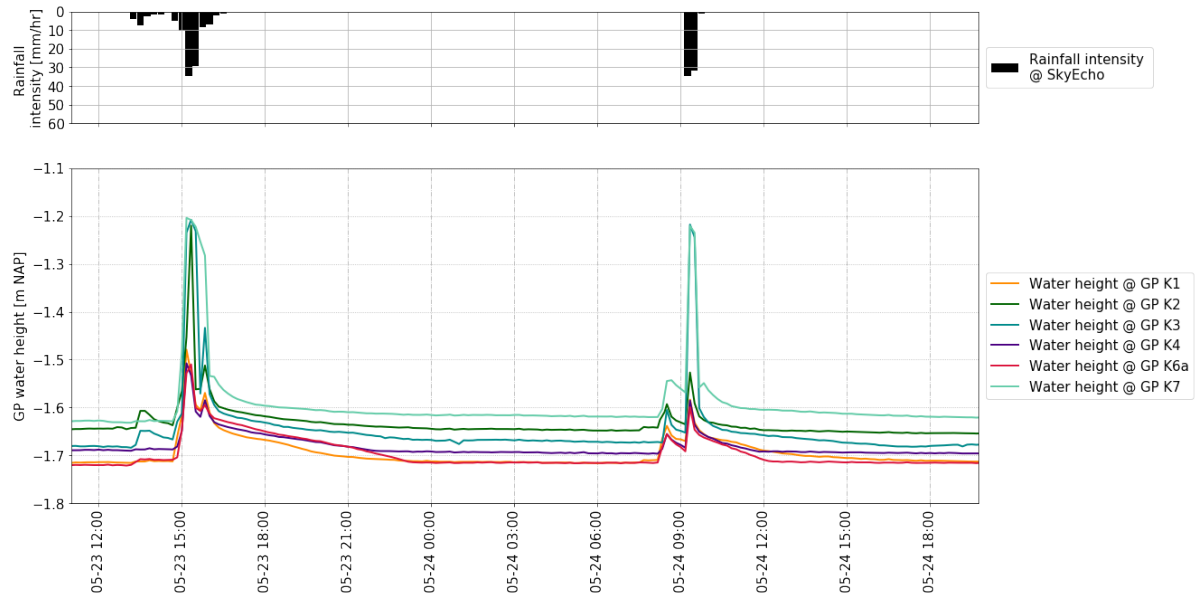


Figure 6.14: Emptying time at all gully-pots for Event 3.

The system has an emptying time from 5 to 8 hours. The maximum water level was 20 cm at the gully-pots, and approximately 11 cm at the granulate layer.

Inflow and outflow

For Event 3, the inflow and outflow peak delay and volume retention were determined. The results are shown in Figure 6.15. Two inflow peaks and two outflow peaks are observed. Additionally, the initial inflow peaks are observed, from the directly connected gully-pots at the intersection. As observed in Event 2, the outflow peak is much lower than the inflow peak. However, the duration is longer. This is likely attributed to the groundwater level rise. After the event, the groundwater table is at the drainage level (-2.40 m NAP). Water above this limit is discharged by the drainage-infiltration-pipe, after which, the groundwater level falls below the drainage level. The total estimated inflow is 13.8 m³. The total measured outflow was 4.4 m³. The total peak delay was 08:25 hours, and the volume retention was 80.74% and the total peak reduction 76%, not including the initial peak, related to the backflow.

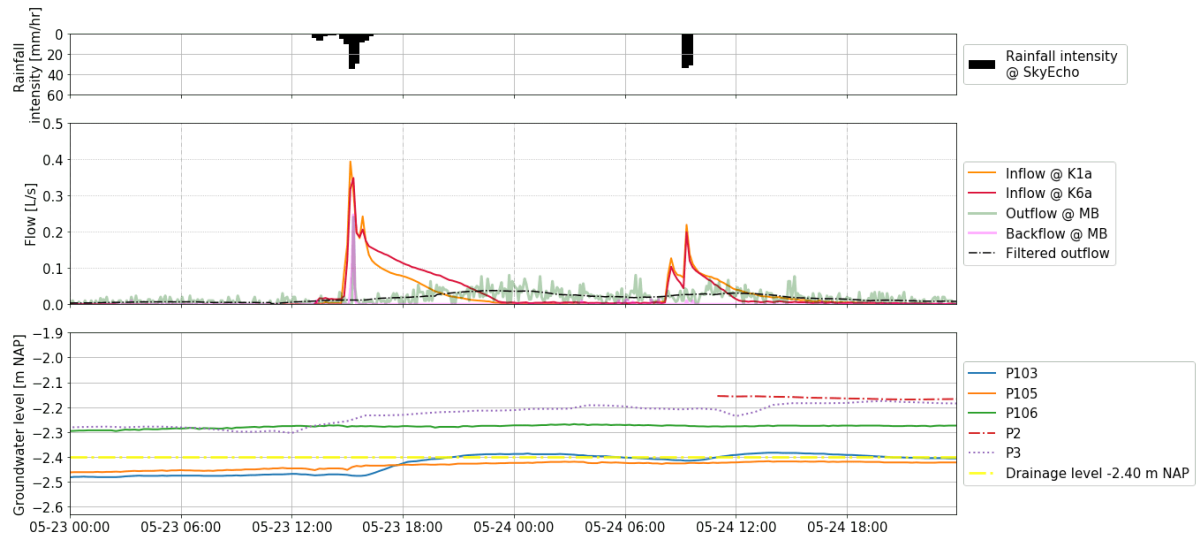


Figure 6.15: Inflow and outflow in response to Event 3, and groundwater table effects.

The peak delay of the system is 08:25 hours, the volume retention is 80.74%. The system meets both requirements related to peak delay and volume retention, respectively.

Groundwater table

The initial groundwater level at Event 3 was -2.48 m NAP. Groundwater levels increased as a result of Event 2 (Section 6.2.2). As a result of the infiltrated water of Event 3, the groundwater table was further recharged to the drainage level (-2.40 m NAP). The excess water was drained by the drainage pipe, as can be observed in Figure 6.15. Again, P103 shows a clear response the gully-pot filling and emptying curve (inflow @ K1a and inflow @ K6a) where P105 and P106 show a more gradual increase. After the event, groundwater levels remain elevated at 2-5 cm below the drainage level. The groundwater response at the inner gardens was only monitored at P3. Here, the groundwater response starts at immediately at the start of the event, while the peak is reached after approximately 16 hours.

The Aquaflow system meets the groundwater recharge performance criterion of water temperatures at least 80 cm below the surface level for Event 3.

Water temperature

In Figure 6.16, the manhole water temperatures are plotted with the inflow and outflow graphs. It can be observed, when the (infiltrated) groundwater reaches the manhole, the water temperature shows a clear drop. At manhole MB, the rise in temperature coincides with the start of the outflow peak. At Manhole MA, at the upstream end of the test area, two temperature drops are observed, showing the effect of the second peak on the inflow into the drainage pipe. From these observations, the time to first water reaching the drainage pipe can be estimated: 3 hours.

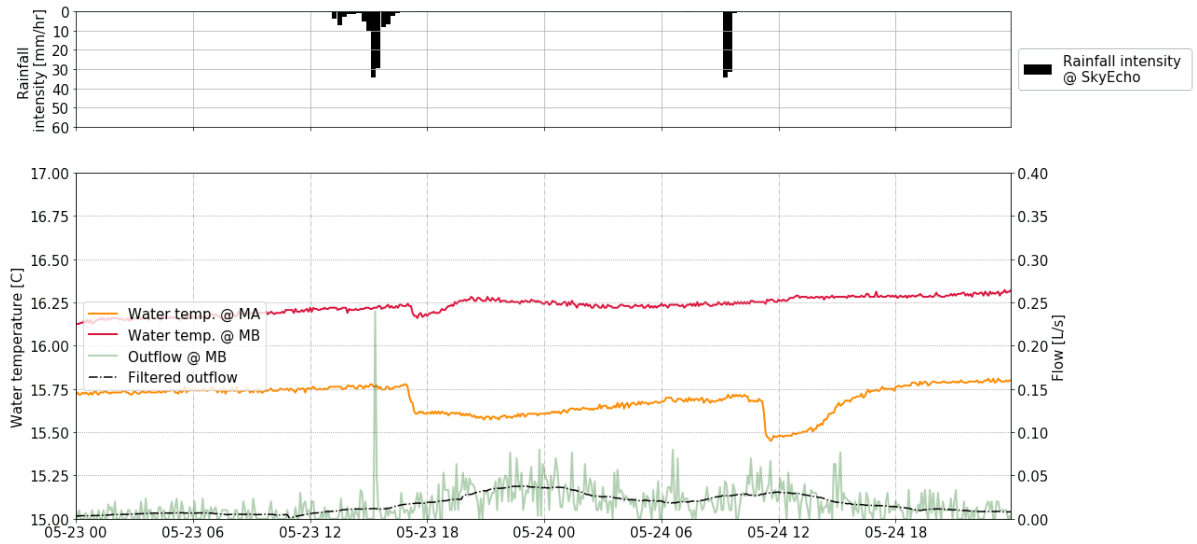


Figure 6.16: Manhole water temperatures in relation to the outflow at Manhole MB.

As for the ponding, the temperatures in the gully-pots as shown in Figure 6.17 show the limited response at K3. This explains the ponding at K3 as likely due to clogging. As for K2 and K7, the response is similar to the remaining gully-pots, so the observed ponding cannot be related to the limited discharge of these gully-pots.

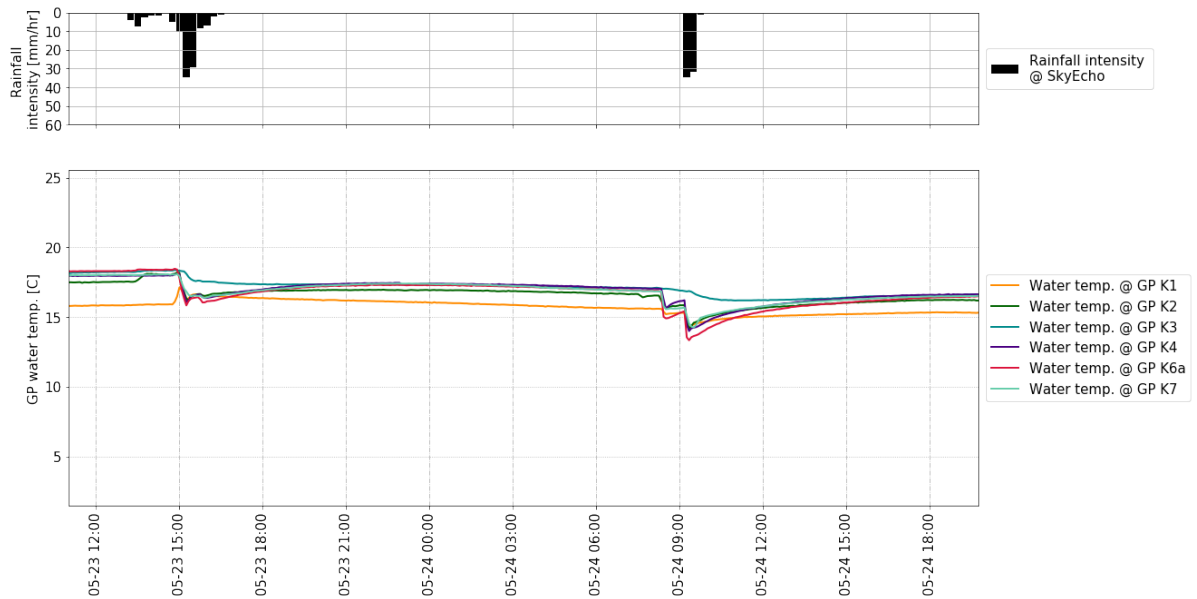


Figure 6.17: Water temperatures at the gully-pots for event 3.

Event summary

Table 6.4: Event 3 summary table

	K1	K2	K3	K4	K6	K7	
Ponding time	0	5	25	0	0	45	Minutes
Ponding height	0	0.06	0.06	0	0	0.109	m
Emptying time	06:25	06:05	06:50	05:25	07:55	08:25	Hours
System results		Units					
Rain volume	22.8	m^3					
Outflow volume	4.4	m^3					
Peak delay	08:25	Hours					
volume retention	80.69	%					
Peak reduction	76.04	%					

6.2.4. Event 4: 5 June 2022

During event 4, 25.6 mm of rain fell in one day (5 June 2022). The total rain volume for a runoff coefficient $C = 1$ was $38.7 m^3$. The maximum intensity was 25.4 mm/hour. In the same manner as the previous events, the monitoring results are discussed for ponding, emptying time, inflow and outflow and groundwater recharge in the following sections.

Ponding

Ponding was measured at K3 and K7 for a total duration of 15 and 55 minutes, respectively (Table 6.5). In Figure 6.18 the gully-pot water levels are plotted for Event 4, showing the ponding at K3 and K7. The remaining gully-pots show little water level increase in response to the event. Although the volume is similar to the full-scale test (Event 1), the gully-pot levels remain low, due to the low intensity of the rainfall. Indicating the gully-pot discharge capacity is sufficient for low intensity rainfall.

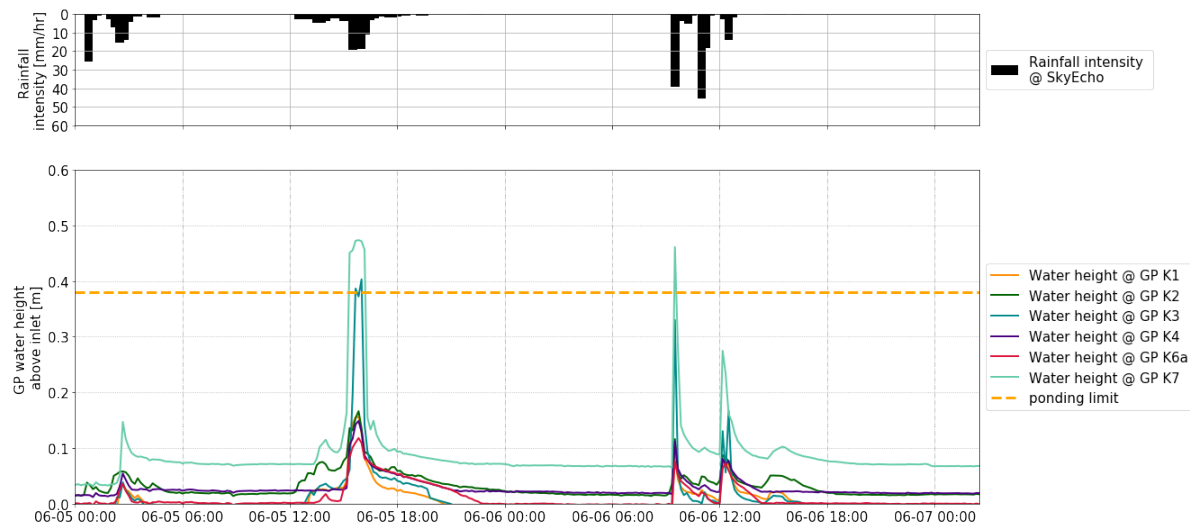


Figure 6.18: Gully-pot water levels in relation to the surface level to show ponding at gully-pots K3 and K7

Ponding was measured at K3 and K7. The maximum filling of the remaining gully-pots system was 0.17. The system meets ponding criterion PC4 for the gully-pots K1, K2, K4 and K6. For events with max intensity > 20 mm/hour and water equivalent > 10 mm.

Emptying time

The emptying time was measured for all gully-pots. The findings are summarized in Table 6.5, with the emptying time ranging from 2:40 (K1) to 6 hours (K6a) and 10:15 (K2)

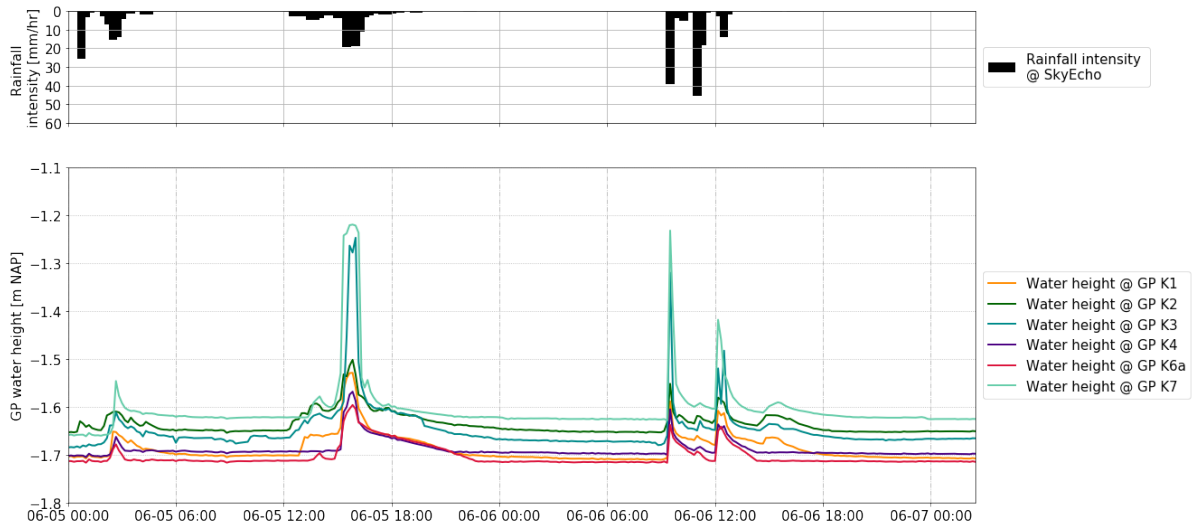


Figure 6.19: Emptying time for event 4 showing the difference in emptying behaviour between the two gully-pots as observed in all events.

The maximum filling of the granulate layer was approximately 8 cm. The emptying time was between 2:40 and 10 hours.

Inflow and outflow

For event 4, the outflow is again very limited. This is due to the low initial groundwater table (-2.50 to -2.55 m NAP). The inflow curve is relatively slow, showing multiple peaks in 48 hours, as shown in Figure 6.35. The total measured outflow is 4.7 m³, where the total inflow was 32 m³ resulting in a volume retention of 85.63%. The total peak reduction was 57.5% with a peak delay of 3:45 hours.

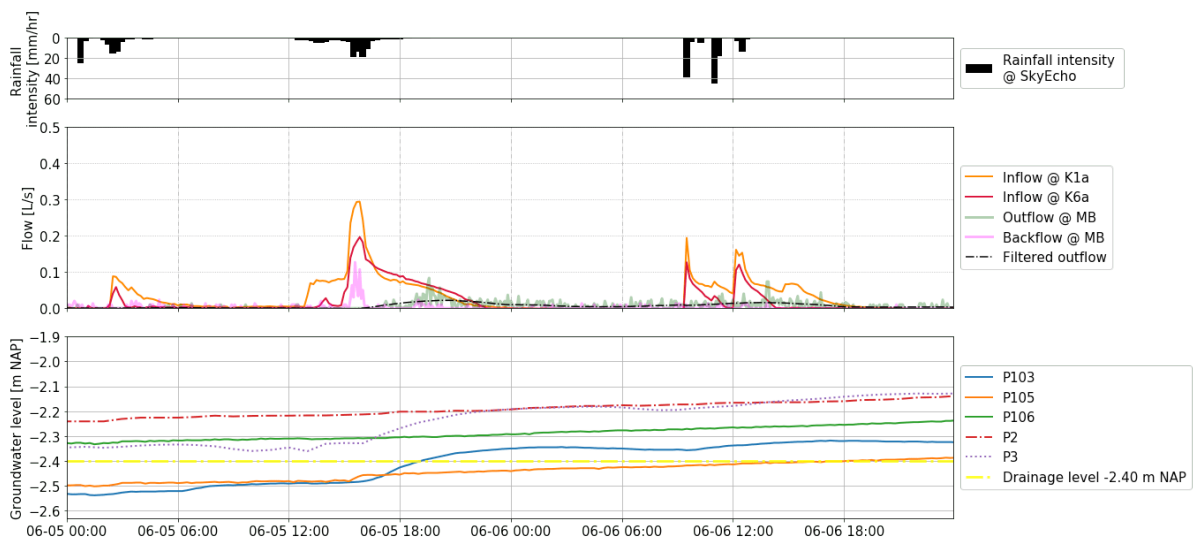


Figure 6.20: Inflow, outflow and groundwater response for event 4

The peak reduction is high for Event 4, with a total peak delay of 3:45 hours. This meets the performance criterion of peak delay at least 1 hour. The total volume retention performance criterion is also met by the Aquaflow system.

Groundwater table

The initial groundwater table was -2.50 m NAP, 10 centimeters below the drainage level, as shown in Figure 6.35. As a result, the infiltrated water is used for groundwater recharge, with little outflow from

the drainage pipe. The outflow starts as the groundwater table rises above the drainage level. After the event, 48 hours later, the groundwater table remains at -2.35 m NAP at both P103 and P105. The groundwater table is more than 80 cm below the surface level.

The Aquaflow system meets the groundwater recharge criterion.

Water temperature

The manhole water temperature shows little fluctuations at manhole MB, apart from the initial response, in combination with the peak in the drain at the start of the outflow peak. Again, the effect of the infiltrated water is observed more clearly at manhole MA, than MB, due to the difference in size.

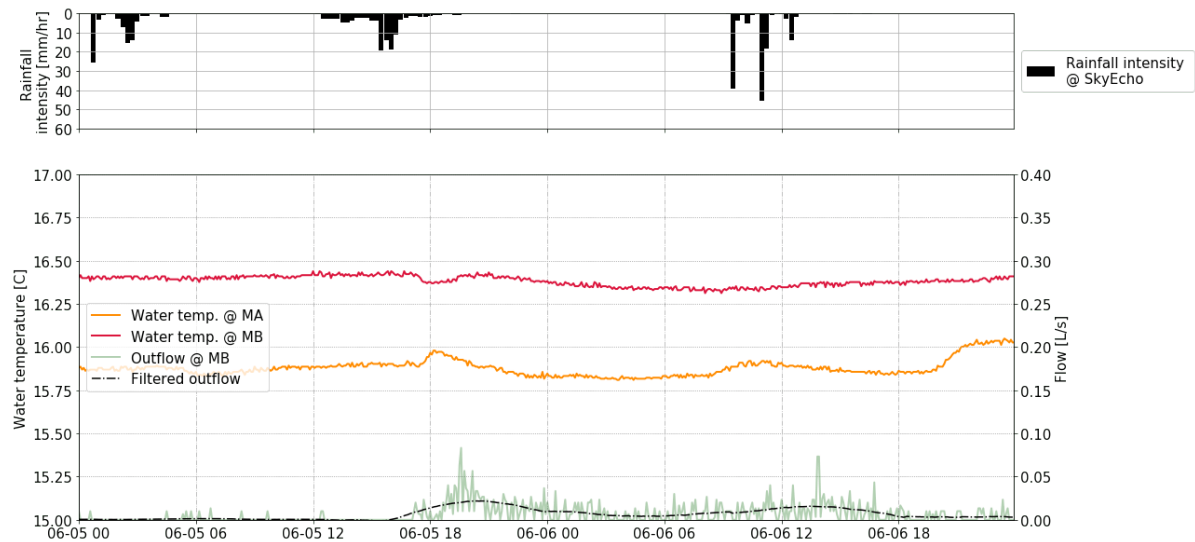


Figure 6.21: Manhole water temperature in relation to inflow and outflow of the system for Event 4.

By assessing the water temperatures at the gully-pots (Figure 6.22), it can be observed K3 shows little to no fluctuations, explaining the ponding at K3.

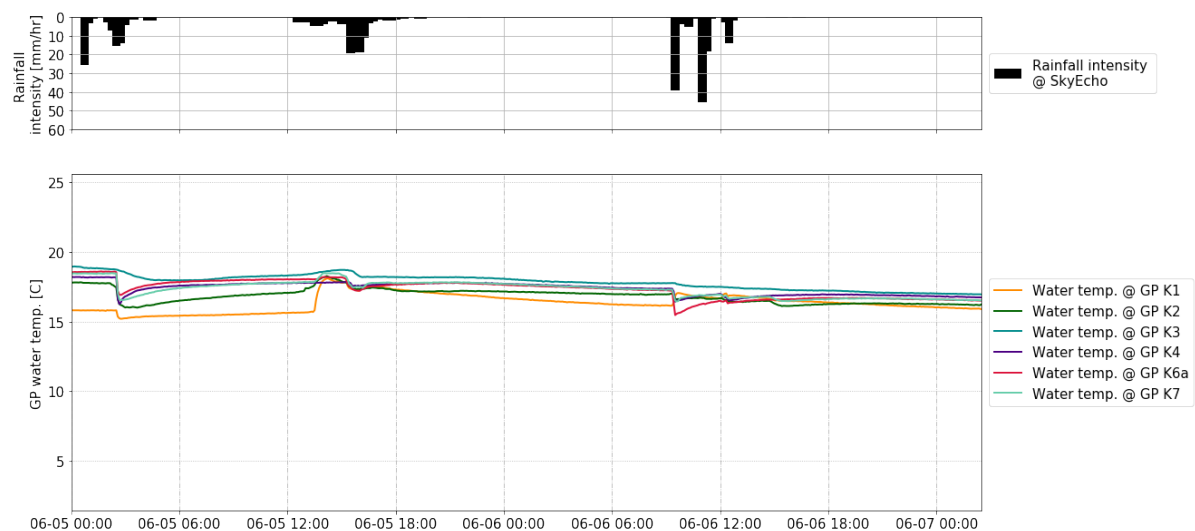


Figure 6.22: Gully-pot water temperatures, showing the limited gully-pot response to the runoff at K3 and K2.

Event summary

Table 6.5: Event 4 summary table

	K1	K2	K3	K4	K6	K7	
Ponding time	0	0	15	0	0	55	Minutes
Ponding height	0	0	0.02	0	0	0.09	m
Emptying time	06:20	10:15	10:20	05:50	06:45	-	Hours
System results		Units					
Rain volume	38.7	m^3					
Outflow volume	1.4	m^3					
Peak delay	03:45	Hours					
volume retention	97.03	%					
Peak reduction	71.6	%					

6.2.5. Event 5: 7 April 2022

Event 5 was selected due to high initial groundwater table (> -2.40 m NAP). The total precipitation was limited, 6 mm with a total volume of $8.7 m^3$ and a maximum intensity of 20 mm/hour. The response is discussed in detail in the following sections.

Ponding

For event 5, ponding was recorded at K2, K3 and K7. The total ponding time at K7 was 25 minutes, 5 minutes at K3 and 5 minutes at K2. The gully-pot water heights with respect to surface level are presented in Figure 6.23. Since the ponding height at K2 was 0.003 m, this value is neglected. The maximum level at K3 as 0.03 meters and at K7, 0.10 meters.

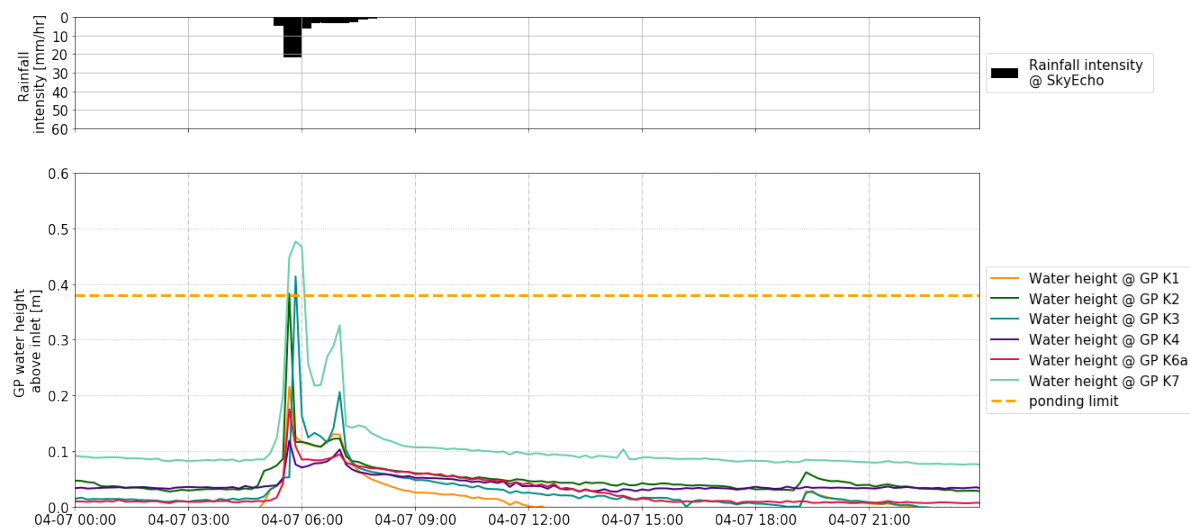


Figure 6.23: Gully-pot water levels with respect to surface level in response to Event 5.

Event 5 provides insight into the performance criterion PC5: no ponding allowed. Based on the measurements, the performance criterion is not met at K2, K3 and K7. The maximum depth in the remaining gully-pots is 22 cm.

Emptying time

The emptying time for event 5 was approximately 4 to 9 hours. The response at each gully-pot follows the emptying response of the aforementioned events: K6 remains filled for longer and emptying is more gradual after peaks; K1 and K3 show a very quick decline in water level after the peaks, after which the emptying becomes more gradual. The results are shown in Figure 6.24. In Table 6.6, the event results are summarized showing the emptying time for all gully-pots.

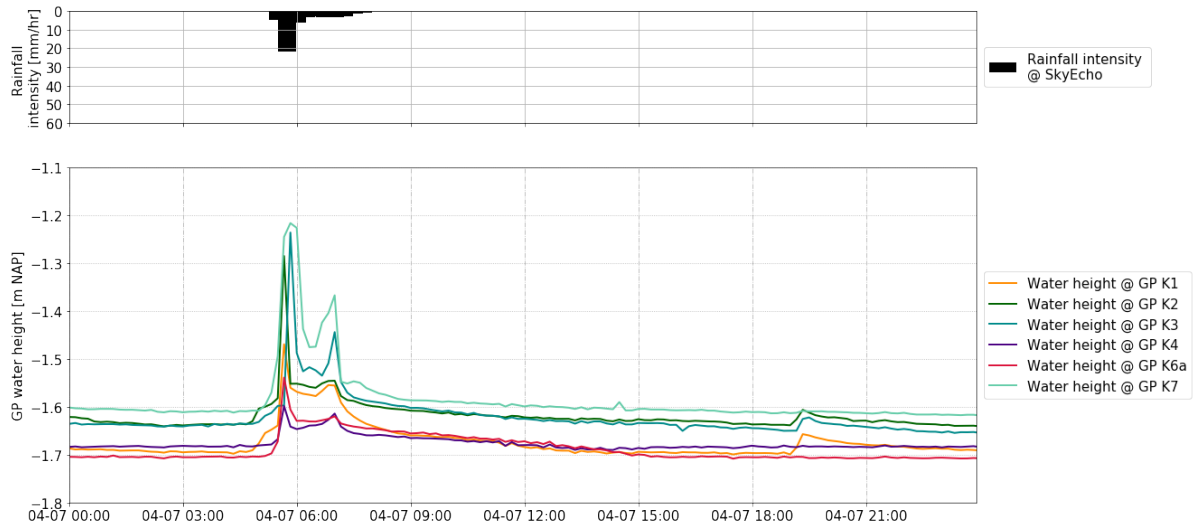


Figure 6.24: Emptying time for all gully-pots in response to Event 5.

The Aquaflow granulate system had a filling depth of approximately 10 cm in response to Event 5. The system was empty within 9 hours (K6).

Inflow and outflow

The inflow and outflow for Event 5, in addition to the groundwater level fluctuations are presented in ???. For this event, the total duration for the timeseries is 9 days, instead of 2, due to the long duration of the outflow and groundwater elevation. There is outflow (0.1 L/s) prior to the start of the event. Following the event, a peak is reached after 07:45 hours. The outflow remains elevated for a long period (> 48 hours). This is due to the high (> 2.40 m NAP) groundwater level at the start of the event. The measured outflow volume is 22 m³. The total rainfall volume was 8.8 m³, thus indicating the additional drainage of groundwater. The total outflow duration coincides with the groundwater elevation, after 9 days, the groundwater table is at drainage level again, at which time the outflow stops.

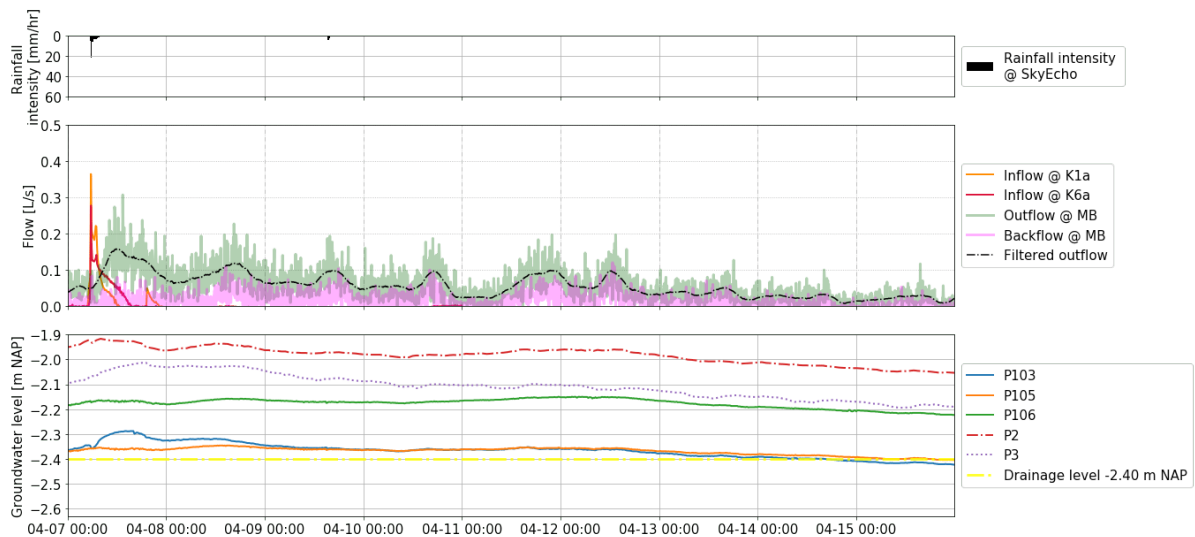


Figure 6.25: Flow and groundwater response for period of 9 days, showing the outflow as long as the groundwater table is above the drainage level.

The Aquaflow system meets the peak delay criterion of 1 hour. For the peak retention, the 35 % volume retention criterion is not met.

Groundwater table

Two days prior to the event, rainfall was recorded which led to an initial increase in groundwater. Aside from affecting the water table as measured at P103, P3 showed an elevated groundwater table for a duration of 50 hours. The groundwater table at P3 responds in similar manner to P103, with more extreme groundwater level increase. This is due to the direct infiltration from the inner gardens and no drainage in the proximity.

The groundwater table recharge criterion is met for Event 5.

Water temperature

From the gully-pot water temperature (Figure 6.26), previous findings regarding the functioning of K3 are further substantiated. The manhole water temperatures, in Figure 6.27, indicate the quick response at Manhole MA and the instance when groundwater reaches the outflow at MB. The period (April) means cold groundwater temperatures and thus the dip in temperature at the start of the outflow peak gives indication of the instance when infiltrated water reaches the flowmeter. After the water is discharged by the drain pipe, water temperatures at Manhole MA reach the initial conditions.

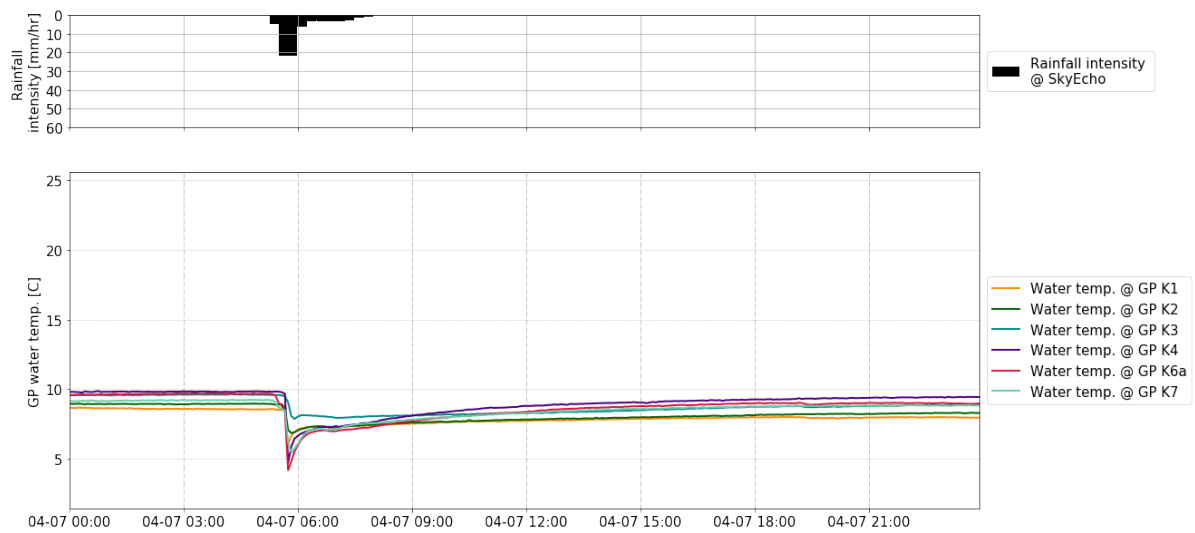


Figure 6.26: Temperature at gully-pots for Event 5.

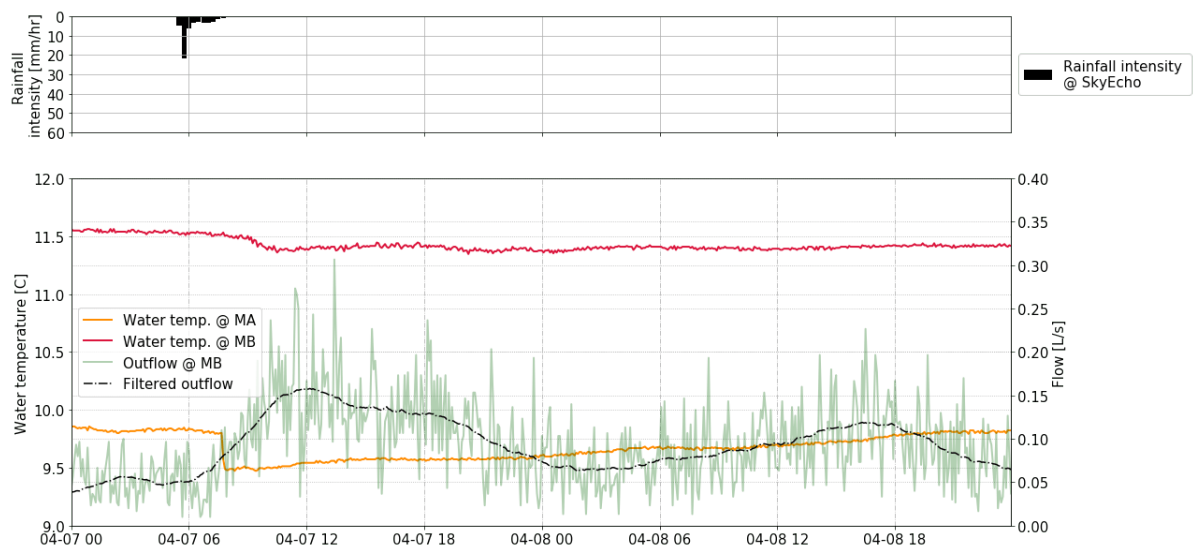


Figure 6.27: Manhole water temperatures for Event 5.

Event summary

Table 6.6: Summary table of the Aquaflow response to Event 5.

	K1	K2	K3	K4	K6	K7	
<i>Ponding time</i>	0	5	5	0	0	25	<i>Minutes</i>
<i>Ponding height</i>	0	0.002	0.03	0	0	0.09	<i>m</i>
<i>Emptying time</i>	05:50	04:00	06:25	05:15	08:45	05:05	<i>Hours</i>
	System results		Units				
<i>Rain volume</i>	8.8	<i>m³</i>					
<i>Outflow volume</i>	22.21	<i>m³</i>					
<i>Peak delay</i>	07:45	<i>Hours</i>					
<i>volume retention</i>	-	<i>%</i>					
<i>Peak reduction</i>	15	<i>%</i>					

6.2.6. Aquaflow response: overview

The 5 selected events provide information regarding the specified performance criteria. The events vary in intensity, rainfall volume, initial groundwater table and initial soil saturation. The findings of the monitoring campaign are summarized in this section. The events are summarized in Table 6.7.

The initial groundwater table was especially low for Event 2, 3 and 4. The initial groundwater table affects the emptying time: lower for lower groundwater tables, and the volume retention: higher for lower groundwater tables. The emptying time relates to the granulate layer. For low water tables, the water infiltrates faster, and thus the granulate layer can empty more quickly. Once the soil becomes saturated, the infiltration rate decreases. The higher volume retention is due to the additional storage space in the unsaturated zone of the road cunet. From the monitoring campaign, the importance of the road cunet was underlined. The granulate layer empties quickly (5-10 hours for events 2-5) and provides sufficient storage ($72m^3$ rainfall storage). The road cunet provides an additional storage buffer when groundwater levels are low and establishes an additional delay factor for the peak runoff. For Event 1, the groundwater table was at the drainage level and for Event 4, the groundwater table was above the drainage level. This negatively affects the peak retention; 50.5% for groundwater table at drainage level; negative for groundwater table above the drainage level.

The rainfall intensity and rainfall volume are important factors of the Aquaflow performance. High rain volumes (Event 1, Event 4) negatively affect the peak delay of the system, due to the large body of water in the Aquaflow system increasing the infiltration rate from the granulate layer. For all events, the peak delay criterion was met, with peak delay ranging from 03:45 to 08:30 hours. The peak delay is mainly affected by the volume of water (Event 1, Event 4) and the initial groundwater table (Event 2, Event 3). Low groundwater tables in combination with low volumes of rain results in a high peak delay between inflow and outflow peaks. High volumes of water results in higher infiltration rates from the Aquaflow system and lower peak delays. The volume retention is high for all events: 50.5% to 97%.

At the surface level, the gully-pot discharge capacity affects the ponding at the surface. For all events, ponding was measured at K3 and K7. At K3, the gully-pot showed signs of clogging (little to no temperature variations, observed in the field). At K7, the gully-pot was affected by subsidence, with initial water levels in the gully-pot above the invert level, under dry conditions. Ponding at K7 can be explained by the limited emptying capacity due to subsidence of the connecting pipe, or due to sensor error, as the water level was high for all events. During field observations, the sensitivity of the gully-pots to clogging was noticeable. At K3, cement was dumped into the gully-pots and at K4 paint was dumped. As a result, the sensors at these gully-pots were broken. Additionally, large amount of build up of leaves, sand from construction and rubble was removed from the gully-pots prior to the monitoring campaign. The clogging of the gully-pots can be beneficial in terms of peak delay, however, the gully-pots are the main connection from surface to the Aquaflow system. Decreasing gully-pot functioning makes the Aquaflow system susceptible to ponding and extreme hindrance in case of high

volume, high intensity events.

Table 6.7: Summary and overview of relevant parameters for full Aquaflo response to the 5 selected events.

	<i>Initial conditions</i>	<i>Peak delay</i>	<i>Volume retention</i>	<i>Peak reduction</i>	<i>Filled time</i>	<i>Volume rain</i>	<i>Volume outflow</i>
	<i>Wet/Dry</i>	%	%	%	<i>Hours</i>	m^3	m^3
<i>Event 1</i>	Dry	05:45	50.5	67	12 to 21	30	14.85
<i>Event 2</i>	Dry	08:30	87.19	58.2	5 to 6	18.9	2.4
<i>Event 3</i>	Wet	08:25	80.69	76.04	6 to 8	22.8	4.4
<i>Event 4</i>	Dry	03:45	97.03	71.6	6 to 10	38.7	1.4
<i>Event 5</i>	Wet	07:45	n.a.	15	5 to 8	8.7	22.21

6.3. Model results

The Hydrus model was created to gain further understanding of the subsurface hydrological response of the Aquaflo system. To do so, the model was calibrated with the full-scale test groundwater observations, and validated with the outflow at the drainage pipe, for the full-scale test. In this section, first, the model calibration and validation results are shown, followed by the modeled response to the rainfall events and the observed differences in the modelled response and the monitored response.

6.3.1. Model calibration and validation: full-scale test

Model calibration

Using observed data from the full scale test, the model was calibrated. The observed data for calibration is presented in Table C.1. To optimize the model performance, the parameters used for calibration were limited. The parameters that were selected to be calibrated were: Q_r , Q_s and K_s for materials Links 1 and Links 2. The inverse solution feature of Hydrus was used with input the groundwater observations of the full-scale test and the selected parameters for calibration. After the inverse solution results were obtained, the model did not show a good fit with the observed data. The parameters were adjusted with trial and error to best fit the groundwater table data, and scaling factors were applied at the Aquaflo layer and the drainage pipe layer. The final results for the model response to the full scale test are shown in Figure 6.28b. The calibrated model parameters are presented in Table 6.8.

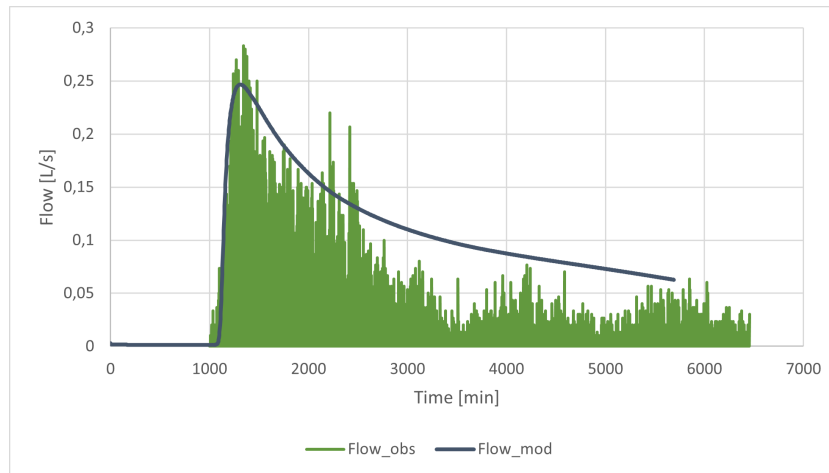
The main performance indicators were the time to peak of the groundwater table at P103 and P105. P106 was not used, as it was observed in the first calibration run, the 20 centimeter height difference between P105 and P106 is not feasible in the model. The groundwater timing of the peaks and height presents the information regarding Aquaflo performance in terms of the delay of the system and potential groundwater recharge. The full-scale test provided information for initial conditions at drainage level, in spring, under dry initial conditions (>7 antecedent dry days). In Figure 6.29a the calibrated model response is shown. The calibrated model parameters are summarized in Table 6.8. For the groundwater prediction, the model achieved a good fit in terms of the initial response, however, the model failed to model the correct height and timing of the peak, with a deviation of 100 minutes and 2.5 cm.

Table 6.8: Calibrated van Genuchten parameters for the three soil types used in the model.

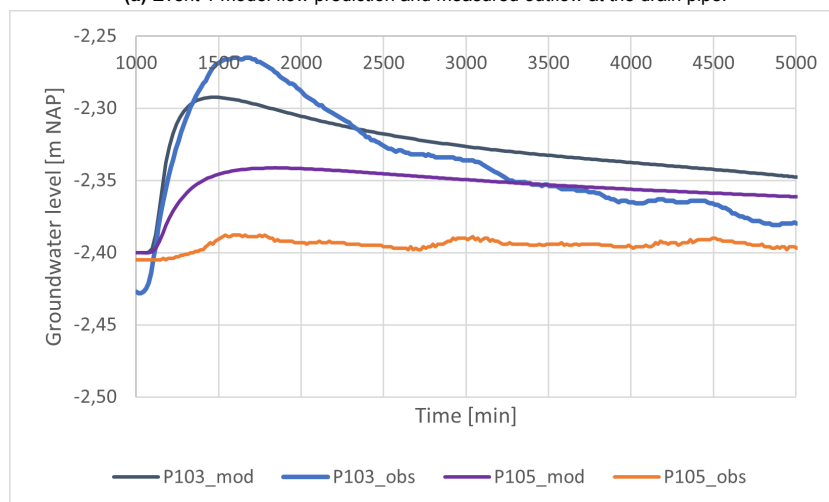
<i>Material</i>	θ_r [-]	θ_s [-]	α [1/cm]	n	K_s [cm/min]	l [-]
<i>Links 1</i>	0.0482	0.333	0.0347	2.8788	0.16	0.5
<i>Material 1</i>	0.05	0.38	0.0342	2.88	0.38	0.5
<i>Clay</i>	0.068	0.38	0.008	1.09	0.003	0.5

Once the calibrated parameters were obtained, the model was validated for the peak outflow. It is observed in Figure 6.29a, the peak occurs at the same time as the modeled peaks, and that the height and the peak rise coincide. The falling limb after the peak of the model at 1330 minutes shows the same rapid decline in both model and observed flow. However, the model fails to produce the low flows

after 2500 minutes, but rather remains elevated at approximately 0.07 L/s. This is due to the elevated groundwater level, above the drainage level of -2.40 m NAP. In this response, the clear difference between real-world situations and designed and modeled situations. Under normal conditions, the water can remain elevated above the drainage period for longer periods of time. This is due to the fact the system is not only connected to the Aquaflo infiltration layer, but also the entire Agniesebuurt area with varying groundwater table, soil conductivity and subsurface structures.



(a) Event 1 model flow prediction and measured outflow at the drain pipe.



(b) Modeled and observed groundwater response for the calibration event.

In Figure 6.29 the spreading of water to the subsurface is shown at $T = 1140, 140$ minutes after the start of the full-scale test. The effect of the observed clay layer at P105 is clearly illustrated with water flowing under it. The zone of influence spreads further to the West (towards P103), due to the presence of the drainage pipe to the right of the Aquaflo system and the presence of the clay layer.

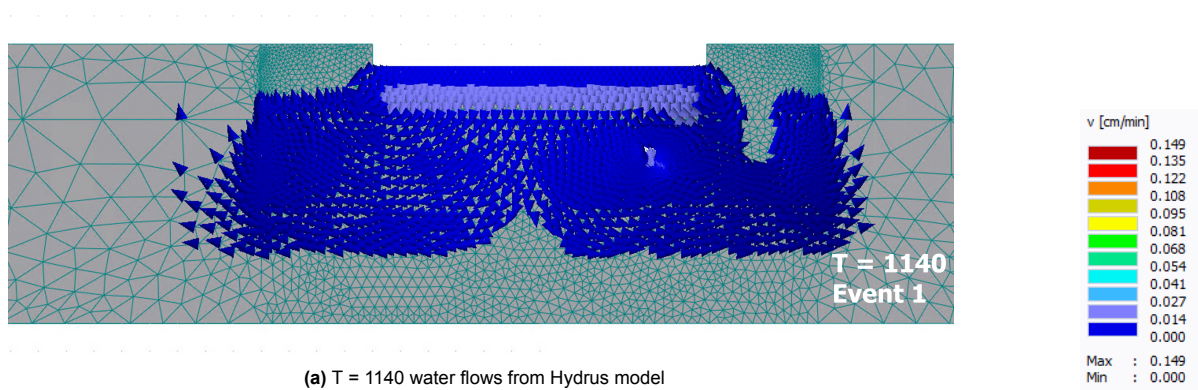


Figure 6.29: Event 1 subsurface flow velocity at T = 1140, 140 minutes after start of the event

6.3.2. Aquaflow event model response

The monitored rainfall at the weather stations was used as input in the calibrated model, as was the initial groundwater conditions (pressure head). For each event, the results are presented in this section in relation to groundwater response, outflow and subsurface flows.

Event 2

Event 2 is characterised by low initial groundwater table -2.55 m NAP. For this event, outflow (total 2.4 m^3) was measured at the flowmeter at manhole MB. The model did not predict any outflow through the drain pipe (Figure 6.31), due to the low groundwater table, and the limited rainfall volume, with groundwater recharge not exceeding the drainage level. The modeled data showed a more gradual peak response, and did not fit the trend of the groundwater peaks. However, the model was able to predict the groundwater recharge after the peak, from T = 2500 minutes. The main difference in the modeled and observed data stems from two possible solutions:

1. The model was designed to fit the overall trend, not the peaks, for a more robust response prediction.
2. Rainfall at the tipping bucket was used as input. The total inflow to the system could be underestimated, due to underestimation of the monitored rainfall data.
3. For the outflow of the model, the observed flow could be due to the initial backflow to the drainage pipe, as shown in Figure 6.31 which then flows out under increased head from the infiltrated water volume. This backflow/outflow process is not included in the model.
4. In the calibrated model, only the Aquaflow system is included. For natural events, the inner gardens create an additional overhead and groundwater flows, possibly explaining the underestimation of the outflow.

In figure A.14, the velocity vectors are shown for the infiltrated water in response to Event 2.

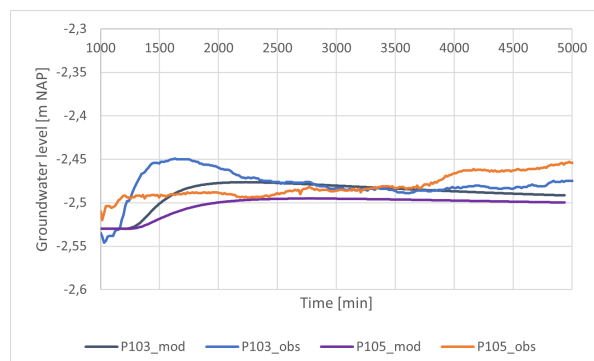


Figure 6.30: Event 2 groundwater response for the modeled (mod) and the observed (obs) groundwater levels. The model does not predict the peak reaction measured at P103, but fits the groundwater level after T = 2500.

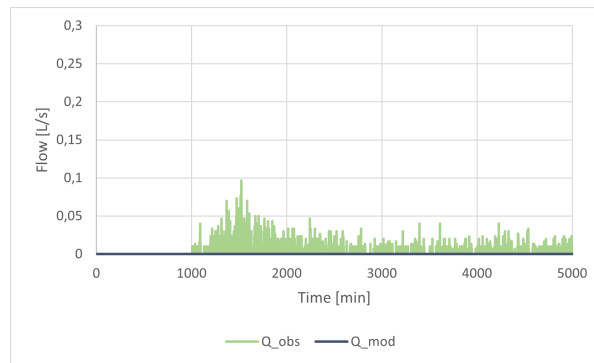


Figure 6.31: Modeled and observed outflow at the drain pipe

Event 3

Event 3 followed Event 2 (three days later) and thus occurred after a period of rain. The initial groundwater table was -2.47 m NAP. For this event, both flow and groundwater levels were modeled. In Figure 6.32, the modeled and observed pressure heads are presented. The model response is more gradual than the actual groundwater response in the timing and height of the peaks. The monitored groundwater responds more rapidly after the peaks. The modeled groundwater at P103 remains elevated after $T = 2500$ minutes, and the observed groundwater at P103 rapidly decreases to -2.46 m NAP.

The modeled flow is very low: approximately 0.02 L/s. For Event 3, the model is not able to mimic the groundwater response and the outflow. In Figure A.15, the flow velocity results are shown for Event 3.

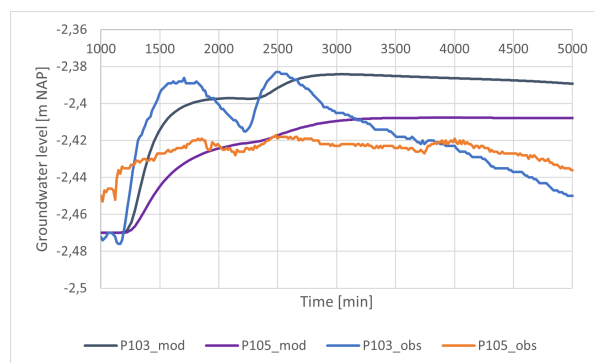


Figure 6.32: Event 3 groundwater head at P103 both modeled (P_{mod}) and observed (P_{obs}).

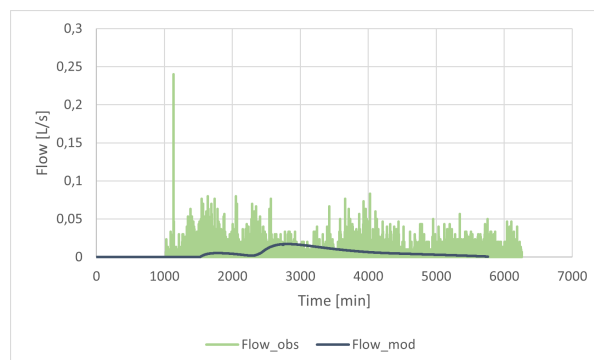


Figure 6.33: Modeled and observed outflow.

Event 4

For Event 4, the groundwater table was well below the drainage level (groundwater table at -2.54 m NAP). The observed and modeled groundwater levels show the same peak response in the timing

and height of the groundwater peak. However, the groundwater level difference is approximately 2 cm initially and increases after $T = 2500$ to approximately 5 cm. The first modeled outflow peak at $T = 2300$ minutes coincides with the peak at the observed flow, when excluding the initial peak at $T = 2100$ minutes due to the backflow at the start of the event. The second peak at $T = 3300$ minutes in the observed data, is modeled at $T = 3800$ minutes in the modeled data. Again, the outflows are very low, and thus susceptible to sensitivity errors.

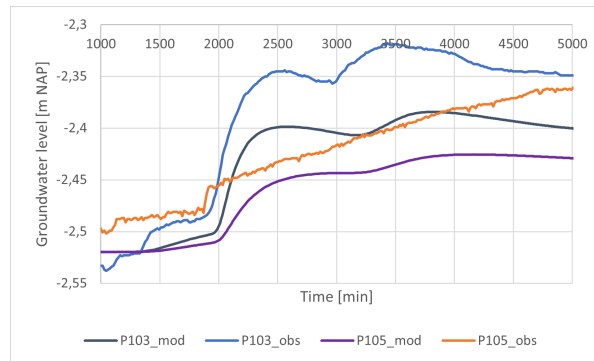


Figure 6.34: Event 4 groundwater response modeled and observed.

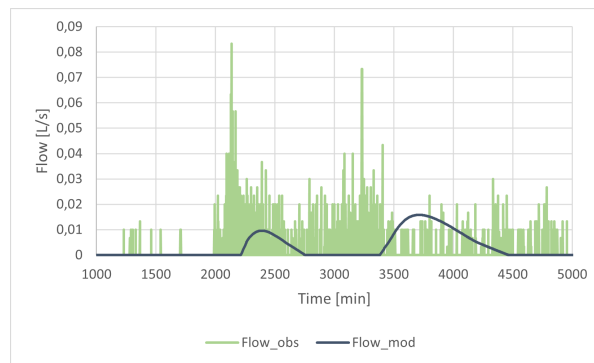


Figure 6.35: Event 4 modeled and observed outflow at the drain pipe.

Event 5

Event 5 provides information regarding subsurface response to wet initial conditions, and the groundwater table above the drainage level (-2.35 m NAP). Both model and results show the initial flow through the DIT pipe, prior to the start of the Event 6.38, due to the elevated groundwater table. The total groundwater velocity vectors in response to the event are summarized in Figure A.16. The timing of the peak is identical in both model and observed data, with higher outliers due to unfiltered data in the observed flow. After the observed peak, the measured flow quickly decreases and shows more peaks at $T = 3200$ and $T = 4800$. The modeled data shows a steady decline, fitting the trend but not the peaks. For the groundwater, the model reproduces the timing of the peak and the height of the peak, with a 3 cm deviation at the peak at $T = 1900$ minutes. After the peak, the groundwater steadily decreases, in the same manner as the modeled data. Again, the trend is modeled, the height of the peaks and degree of fluctuations differs. (Figure 6.37).

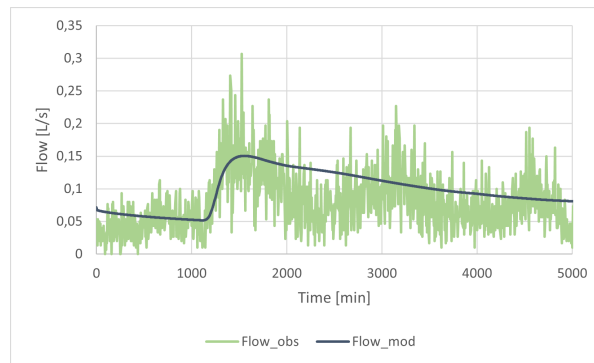


Figure 6.36: Monitored vs. observed outflow at the drainage pipe

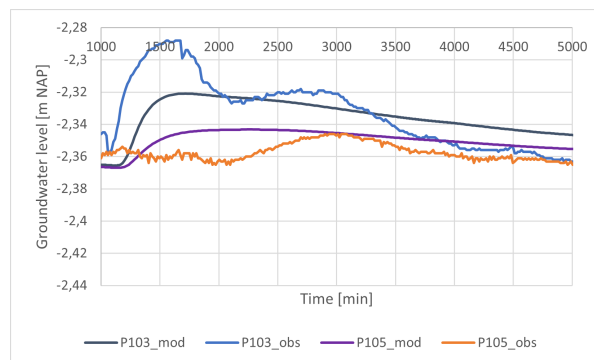


Figure 6.37: Event 5 groundwater table response at P103 and P105 for the modeled and monitored situation.

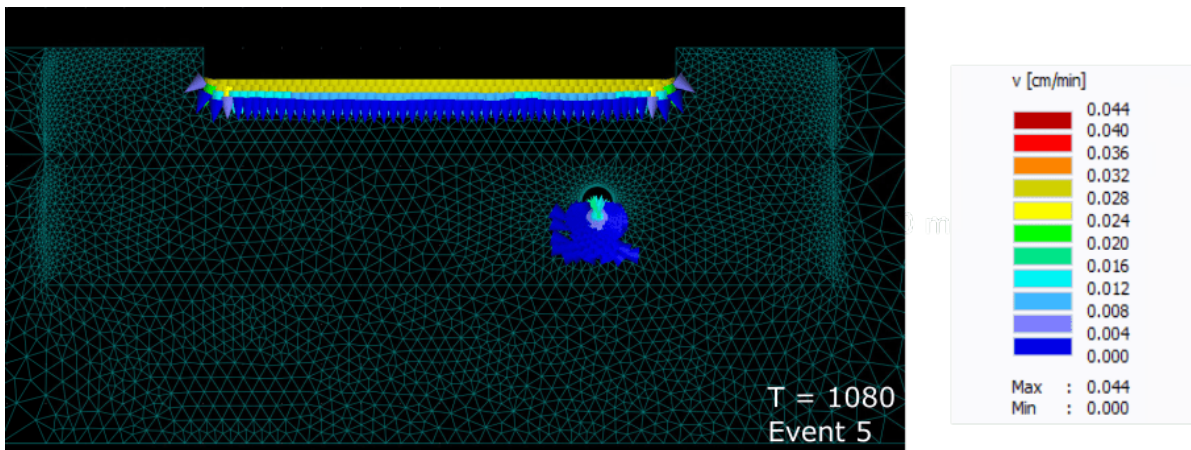


Figure 6.38: Hydrus velocity vector at $T = 1080$, showing the initial groundwater drainage prior to the start of the event.

6.3.3. Hydrus for Aquaflo: overview

The model and the real-world monitored data show inconsistencies. This is due to the following factors:

- The aim of this study was to assess the hydrological performance of the Aquaflo system at the Meester Marrestraat test location. Therefore, extensive monitoring was conducted at the test site and the road cunet. As a result, little is known of the surrounding area (e.g. the inner gardens and the relation of the test area to the Agniesebuurt area). The difference in model response and the monitoring data stems from this lack in knowledge. When calibrating for the full-scale event, the model is calibrated to the local response and input. However, for natural events, water infiltrates at the inner gardens and at the entire Agniesebuurt area.

- The modeled outflow follows the same trend as the observed outflow, and is able to predict the peak of the outflow and thus the peak delay.
- The modeled situation and response describes the potential, ideal response. However, in the natural subsurface, ideal flow-paths occur and the initial conditions can vary due to the presence of trees and different, local differences in soil structures. The differences in modeled groundwater levels and monitored groundwater levels can be attributed to: (i) the groundwater relation to the inner-gardens, with additional groundwater flowing to the road cunet due to pressure heads; (ii) groundwater monitoring efficiency: as described in section 5.1.5, groundwater monitoring is dependent on the barometric pressure (present during natural events), sensor installation (manual installation which could result in measurement errors up to a few cm); (iii) observation nodes are applied at the specified piezometer locations, with the known soil types from the borehole information. However, the precise width of the specific soil, e.g. clay at P105 is not known and affects the modeled groundwater recharge at P105 and P106; (iv) The subsurface is very heterogeneous and therefore, the model is based on too little information to create a fully representative model.
- The input factor for the model was the rainfall as measured at the rain gauge [cm/min] no runoff factor was applied. The rainfall data was used, as the total inflow to the system could not be quantified with the monitoring data. Additionally, the total connected area was estimated at 1500 m³. However, this value depends on the rainfall intensity and the slope of the surface level. This could provide an answer to the difference in groundwater heights for the monitored events.
- The model is built on many assumptions, like the estimated soil parameters, the structure of the soil over a width of 50 meters and the total inflow to the granulate layer. Many factors, like clogging of the gully-pots, clogging of the Aquaflo infiltrating bottom, preferential flow paths in the subsurface and soil moisture content can affect the response of the model, and are not included in the model.
- The road cunet has a high saturated conductivity, which could limit the peak delay. However, when applied in combination with a DIT pipe (with entry resistance), the desired peak delay can be achieved: when applying the predicted soil parameters in combination with the seepage face boundary with no scaling factors in the hydraulic conductivity, no delay was added in the system. Indicating the high conductivity of the road cunet. In the 'real world', the DIT has a lower conductivity than the surrounding sand, therefore indicating the need for a scaling factor. When applied, the road cunet performs well in terms of spreading of the infiltrated water, and recharge of the groundwater table.
- The model performs well in predicting outflow height and outflow peak, when infiltrating volumes are high enough, and the groundwater table is recharged above the drainage level. The model is better in the maintaining the drainage level than the monitored situation.

Conclusions & Recommendations

7.1. Conclusions

This study was carried out to further understand and assess the effects of the Aquaflow infiltrating road foundation on the local hydrologic system. The following conclusions were drawn on the basis of results obtained from the field experiments and from the modelling.

7.1.1. Hydrological performance of the Aquaflow system

- The Aquaflow system performs well in terms of prevention of ponding for high intensity events. The ponding time varies from 20 to 55 minutes for rain events with intensity 100 mm/hour with total duration 60 minutes. The performance criteria related to ponding were met by the Aquaflow system for the monitored events. For PC2, no data was available.
- For high intensity events (100 mm/hour, 60 minutes), the gully-pot discharge capacity is critical.
- For higher intensities (>100 mm/hour) and volumes, ponding can be expected at the gully-pots.
- For low intensity, low volume storms, no ponding was observed at the system and the system performs well.
- Local ponding was measured at gully-pots due to clogging, subsidence and sensor errors.
- The emptying time of the granulate layer ranged from 5 to 8 hours for low volume events, and 6 - 21 hours for high volume events. The road cunet is the most critical component related to emptying time, and provides additional water buffering.
- For all events, the system was emptied within 24 hours. For the measured events, the Aquaflow system was never fully filled.
- Peak delay of the Aquaflow system ranged from 4 hours to 8:30 hours for all rain events. The system performs well in delaying the peak flow to the urban drainage system under all initial conditions.
- The peak delay decreases for high volumes of water.
- The total volume retention of the Aquaflow system was between 50.5% and 97% for all the assessed events. The system met the volume retention criterion of 35% for all events.
- The volume retention is positively affected by low groundwater tables.
- The infiltrated water from the Aquaflow led to groundwater recharge at the test area, for groundwater table below the drainage level. Instant groundwater response was observed for all events. The groundwater levels remained more than 80 cm below the surface level at the Aquaflow site.

7.1.2. Performance limiting factors

- Gully-pots are sensitive to clogging, subsidence and external effects like paint, cement and rubble, which affects the hydrological performance of the Aquaflow system. After 2 years, significant performance reduction could be observed at the gully-pots.

- The DIT pipe performs well in maintaining the drainage level -2.40 m NAP in the area, by draining excess groundwater in case of elevated groundwater table. This affects the total volume retention, as aside from rain volume, excess groundwater is drained from the area (i.e. negative retention). The groundwater furthest from the drain pipe is more strongly affected by the infiltrated water.
- At the start of the rain events, backflow occurs from gully-pots directly connected to the drainage system, this water is subsequently drained by the DIT pipe.
- The Aquaflow granulate layer storage is sufficient to retain the selected events, with 30 m^3 . The maximum filling in the granulate layer was 20 centimeters for 3 hours.

7.1.3. Model performance

- The model performs well in predicting the trend of the outflow and groundwater recharge. The model does not exactly mimic the measurements, due to various environmental effects and applied model boundaries and data limitations. The model can reasonably replicate the system performance.
- From the Hydrus model, parameters for future implementation were found: K_{sat} of the road cunet 0.38 cm/min; inflow resistance at the drainage pipe allows for the groundwater recharge and delay in the system by a factor of 0.05*road cunet conductivity.

7.1.4. Monitoring

- Public precipitation data from KNMI provides information regarding the rain volume and duration. It is recommended to apply a local rain gauge as a control measure, due to variance in precipitation in the city and to limit wrongful data from measurement errors.
- To analyse data at small timescale, local, high temporal resolution weather stations are required.
- Electro-Magnetic flowmeters provide a great solution to measure flow through fully submerged perforated drain pipes (DIT). EM flowmeters can measure both outflow and backflow with high sensitivity.
- Using pressure difference to determine the flow between manholes with horizontal DIT pipes does not provide reliable data regarding the outflow and cannot be used.
- The response in the system is rapid, therefore the monitoring interval needs to be increased to preferably 1 minute.
- To understand the flow through the DIT pipe further, measurements should be conducted in the wet months.
- Monitoring in the gully-pots provides information regarding the inflow to the gully-pots. The monitoring interval should be increased due to the rapid response in the gully-pots.
- Gully-pot measurements are affected by clogging of the gully-pots and external effects and measurements do not provide reliable data regarding Aquaflow granulate layer filling and emptying.
- The monitoring campaign is sensitive to uncertainties in measurement data, parameters, ideal conditions and assumptions.

7.2. Recommendations

This study provides additional information regarding monitoring and modeling of the Aquaflow system and the hydrological performance. From this study, several recommendations can be made for future research and implementation in Rotterdam.

- Monitoring in the wet season to assess the hydrologic performance for elevated groundwater table and high soil saturation.
- Placement of one, preferably multiple, pressure sensors in the granulate layer during construction of the Aquaflow system, to obtain more data regarding the degree of filling, emptying time and movement of water in the granulate layer.
- Placement of a piezometer below the Aquaflow layer, to obtain data of the degree of saturation and groundwater level below the Aquaflow layer.
- Conduct a separate study to determine the effect of the inner gardens on the urban drainage system to assess the flow from the gardens to the DIT pipe.
- Increase the scale of monitoring at the case study area, by including more road sections.

Bibliography

- [Abdalla et al., 2021] Abdalla, E. M. H., Selseth, I., Muthanna, T. M., Helness, H., Alfredsen, K., Gaarden, T., and Sivertsen, E. (2021). Hydrological performance of lined permeable pavements in norway. *Blue-Green Systems*, 3:107–118.
- [AquaflowB.V., 2012] AquaflowB.V. (2012). Waterbergende-weg-goed-gefundeerd-08-2012 (1).
- [AquaflowB.V., 2014] AquaflowB.V. (2014). Aquaflow: snel stromend water onder de weg.
- [AquaflowB.V., 2022] AquaflowB.V (2022). Aquaflow-zuiver-water-bergen-in-wegen-2022-03.
- [atelier GROENBLAUW,] atelier GROENBLAUW. Permeable pavements.
- [Azevedo et al., 2016] Azevedo, J. A., Chapman, L., and Muller, C. L. (2016). Quantifying the daytime and night-time urban heat island in birmingham, uk: A comparison of satellite derived land surface temperature and high resolution air temperature observations. *Remote Sensing*, 8.
- [Balasubramanian and Nagaraju,] Balasubramanian, A. and Nagaraju, D. The hydrologic cycle integrated hydrogeological studies and modeling of river basins in typical hard rock terrains of south india view project educational video documentaries in earth , atmospheric and ocean sciences view project.
- [Barron et al., 2013] Barron, O. V., Barr, A. D., and Donn, M. J. (2013). Effect of urbanisation on the water balance of a catchment with shallow groundwater. *Journal of Hydrology*, 485:162–176.
- [Bernard et al., 2018] Bernard, J., Bocher, E., Petit, G., and Palominos, S. (2018). Sky view factor calculation in urban context: Computational performance and accuracy analysis of two open and free gis tools. *Climate*, 6.
- [Bessembinder et al., 2013] Bessembinder, J., Wolters, D., and van (Lambertus Willem Adriaan) Hove, L. (2013). Regiospecifieke klimaatinformatie voor haaglanden en regio rotterdam : syntheserapport.
- [Bhimanadhuni et al., 2015] Bhimanadhuni, S., Sinha, S. K., and Stolte, M. (2015). Development of a performance index for stormwater pipeline infrastructure.
- [Boers and Rypdal, 2021] Boers, N. and Rypdal, M. (2021). Critical slowing down suggests that the western greenland ice sheet is close to a tipping point.
- [Boomsma and ir Marinus Huurman, 2006] Boomsma, I. W. and ir Marinus Huurman (2006). Permeable paving systems with storing capacity.
- [Brenner, 2019] Brenner, I. (2019). Climate change and the human factor: Why does not everyone realize what is happening? *International Journal of Applied Psychoanalytic Studies*, 16:137–143.
- [Bucci et al., 2017] Bucci, A., Barbero, D., Lasagna, M., Forno, M. G., and De Luca, D. (2017). Shallow groundwater temperature in the turin area (nw italy): vertical distribution and anthropogenic effects. *Environmental Earth Sciences*, 76.
- [by J Šimůnek et al., 1999] by J Šimůnek, Šejna, M., and van Genuchten, M. T. (1999). The hydrus-2d software package for simulating the two-dimensional movement of water, heat, and multiple solutes in variably-saturated media version 2.0.
- [CBS et al., 2020] CBS, PBL, RIVM, and WUR (2020). Jaarlijkse hoeveelheid neerslag in nederland, 1910-2019 [30] (indicator 0508, versie 08 , 24 april 2020).
- [Chahar et al., 2012] Chahar, B. R., Graillot, D., and Gaur, S. (2012). Storm-water management through infiltration trenches. *Journal of Irrigation and Drainage Engineering*, 138:274–281.

- [Chan et al., 2019] Chan, N. W., Tan, M. L., Ghani, A. A., and Zakaria, N. A. (2019). Sustainable urban drainage as a viable measure of coping with heat and floods due to climate change. volume 257. Institute of Physics Publishing.
- [Charlesworth, 2010] Charlesworth, S. M. (2010). A review of the adaptation and mitigation of global climate change using sustainable drainage in cities. *Journal of Water and Climate Change*, 1:165–180.
- [Chen et al., 2014] Chen, M., Zhang, H., Liu, W., and Zhang, W. (2014). The global pattern of urbanization and economic growth: Evidence from the last three decades. *PLoS ONE*, 9.
- [Coupe et al., 2009] Coupe, S. J., Ullate, G., Fresno, E. C., and Rodriguez-hernandez, D. (2009). The storage and protection of rainfall resources stored in permeable paving sustainable drainage systems as sources of landscape and horticultural irrigation water and water for use in evaporative urban heat island mitigation view project the history of water power, drainage, irrigation, navigation and associated engineering in the English north and east Midlands view project the storage and protection of rainfall resources stored in permeable paving.
- [Dar et al., 2021] Dar, M. U. D., Shah, A. I., Bhat, S. A., Kumar, R., Huisingsh, D., and Kaur, R. (2021). Blue green infrastructure as a tool for sustainable urban development. *Journal of Cleaner Production*, 318.
- [Davis et al., 2012] Davis, A. P., Stagge, J. H., Jamil, E., and Kim, H. (2012). Hydraulic performance of grass swales for managing highway runoff. *Water Research*, 46:6775–6786.
- [Dow and DeWalle, 2000] Dow, C. L. and DeWalle, D. R. (2000). Trends in evaporation and Bowen ratio on urbanizing watersheds in eastern United States. *Water Resources Research*, 36:1835–1843.
- [Eiswirth and Hötzl, 1997] Eiswirth, M. and Hötzl, H. (1997). The impact of leaking sewers on urban groundwater.
- [Elkink, 2017] Elkink, A. (2017). Typical green roof construction.
- [Encyclopaedia Britannica,] Encyclopaedia Britannica. Water cycle.
- [Eugenia and Ming, 2003] Eugenia, K. and Ming, C. (2003). Impact of urbanization and land-use change on climate. *NATURE*, 423.
- [Ferré and Warrick, 2005] Ferré, T. P. and Warrick, A. W. (2005). *INFILTRATION*, volume 4. Elsevier.
- [Fletcher et al., 2015] Fletcher, T. D., Shuster, W., Hunt, W. F., Ashley, R., Butler, D., Arthur, S., Trowsdale, S., Barraud, S., Semadeni-Davies, A., Bertrand-Krajewski, J. L., Mikkelsen, P. S., Rivard, G., Uhl, M., Dagenais, D., and Viklander, M. (2015). Suds, lid, bmps, wsud and more – the evolution and application of terminology surrounding urban drainage. *Urban Water Journal*, 12:525–542.
- [Foelsche, 2015] Foelsche, U. (2015). Systematic errors in precipitation measurements with different rain gauge sensors.
- [Foster, 2001] Foster, S. S. D. (2001). The interdependence of groundwater and urbanisation in rapidly developing cities q.
- [Gašparović et al., 2021] Gašparović, M., Zorić, and Singh, S. K. (2021). Urbanisation impact on creation of heat islands in large cities. *International Archives of the Photogrammetry, Remote Sensing and Spatial Information Sciences - ISPRS Archives*, 43:313–318.
- [Gemeente Rotterdam, 2019] Gemeente Rotterdam (2019). Groene daken | Rotterdam.nl.
- [Geneletti and Zardo, 2016] Geneletti, D. and Zardo, L. (2016). Ecosystem-based adaptation in cities: An analysis of European urban climate adaptation plans. *Land Use Policy*, 50:38–47.
- [Geography Notes and Riya, 2018] Geography Notes and Riya, P. (2018). Runoff: Meaning, Types and Factors | Rainfall | Geography.

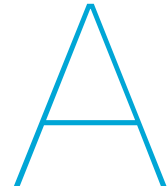
- [Gilissen, 2014] Gilissen, H. K. (2014). The integration of the adaptation approach into eu and dutch legislation on flood risk management.
- [Graham et al., 2012] Graham, A., Day, J., Bray, B., and Mackenzie, S. (2012). *Maximising the potential for people and wildlife Sustainable drainage systems*.
- [Habib et al., 2008] Habib, E. H., Asce, M., Meselhe, E. A., Aduvala, A. V., and Asce, S. M. (2008). Effect of local errors of tipping-bucket rain gauges on rainfall-runoff simulations. *Journal of Hydrologic Engineering* © ASCE.
- [Han et al., 2014] Han, J. Y., Baik, J. J., and Lee, H. (2014). Urban impacts on precipitation. *Asia-Pacific Journal of Atmospheric Sciences*, 50:17–30.
- [Harrington et al., 2022] Harrington, L. J., Ebi, K. L., Frame, D. J., and Otto, F. E. (2022). Integrating attribution with adaptation for unprecedented future heatwaves *enhancedreader.ClimateChange*, 172.
- [Heinen et al., 2020] Heinen, M., Bakker, G., and Wösten, J. (2020). Waterretentie- en doorlatendheidskarakteristieken van boven- en ondergronden in nederland: de starringreeks : Update 2018.
- [Hilberts et al., 2005] Hilberts, A. G., Troch, P. A., and Paniconi, C. (2005). Storage-dependent drainable porosity for complex hillslopes. *Water Resources Research*, 41:1–13.
- [Hordon, 1998] Hordon, R. M. (1998). *hydrological cycleHydrological cycle*, pages 367–371. Springer Netherlands, Dordrecht.
- [Huff and Changnon, 1973] Huff, F. A. and Changnon, S. A. (1973). precipitation modillcallon.
- [Huisman, 1998] Huisman, P. (1998). *Water in the Netherlands*. Netherlands Hydrological Society, managing checks and balances edition.
- [Ilgen et al., 2019] Ilgen, S., Sengers, F., and Wardekker, A. (2019). City-to-city learning for urban resilience: The case of water squares in rotterdam and mexico city. *Water (Switzerland)*, 11.
- [Interreg 2 Mers Seas Zeeën 2014-2020,] Interreg 2 Mers Seas Zeeën 2014-2020. SPONGE 2020 | 2 Mers Seas Zeeën.
- [Jacobson, 2011] Jacobson, C. R. (2011). Identification and quantification of the hydrological impacts of imperviousness in urban catchments: A review. *Journal of Environmental Management*, 92:1438–1448.
- [Kalvová et al., 2003] Kalvová, J., Halenka, T., Bezpalcová, K., and Nemešová, I. (2003). Köppen climate types in observed and simulated climates. *Studia Geophysica et Geodaetica*, 47:185–202.
- [Kim and Kim, 2021] Kim, H. and Kim, G. (2021). An effectiveness study on the use of different types of lid for water cycle recovery in a small catchment. *Land*, 10.
- [Klungniam, 2016] Klungniam, C. (2016). The effects of urbanization on urban hydrology characteristics.
- [KNMI, 2015] KNMI (2015). Climate scenarios for the netherlands '14.
- [KNMI, 2022] KNMI (2022). Neerslagtekort / Droogte.
- [Kreienkamp et al., 2021] Kreienkamp, F., Philip, S. Y., Tradowsky, J. S., Kew, S. F., Lorenz, P., Arrighi, J., Belleflamme, A., Bettmann, T., Caluwaerts, S., Chan, S. C., Ciavarella, A., Cruz, L. D., de Vries, H., Demuth, N., Ferrone, A., Fischer, E. M., Fowler, H. J., Goergen, K., Heinrich, D., Henrichs, Y., Lenderink, G., Kaspar, F., Nilson, E., and Otto, F. E. L. (2021). Rapid attribution of heavy rainfall events leading to the severe flooding in western europe during july 2021.
- [Kuchment, 2004] Kuchment, L. S. (2004). *THE HYDROLOGICAL CYCLE AND HUMAN IMPACT ON IT*. Encyclopedia of Life Support Systems (EOLSS).
- [Kumar, 2021] Kumar, P. (2021). Climate change and cities: Challenges ahead. *Frontiers in Sustainable Cities*, 3.

- [Leimgruber et al., 2018] Leimgruber, J., Krebs, G., Camhy, D., and Muschalla, D. (2018). Sensitivity of model-based water balance to low impact development parameters. *Water (Switzerland)*, 10.
- [Lenzholzer et al., 2020] Lenzholzer, S., Carsjens, G. J., Brown, R. D., Tavares, S., Vanos, J., Kim, Y. J., and Lee, K. (2020). Awareness of urban climate adaptation strategies—an international overview. *Urban Climate*, 34.
- [Li et al., 2016] Li, C., Liu, M., Hu, Y., Gong, J., and Xu, Y. (2016). Modeling the quality and quantity of runoff in a highly urbanized catchment using storm water management model. *Polish Journal of Environmental Studies*, 25:1573–1581.
- [Li et al., 2018] Li, C., Liu, M., Hu, Y., Shi, T., Zong, M., and Walter, M. T. (2018). Assessing the impact of urbanization on direct runoff using improved composite cn method in a large urban area. *International Journal of Environmental Research and Public Health*, 15.
- [Likos et al., 2014] Likos, W. J., Lu, N., and Godt, J. W. (2014). Hysteresis and uncertainty in soil water-retention curve parameters. *Journal of Geotechnical and Geoenvironmental Engineering*, 140.
- [Liu and Niyogi, 2019] Liu, J. and Niyogi, D. (2019). Meta-analysis of urbanization impact on rainfall modification. *Scientific Reports*, 9.
- [Lucas et al., 2009] Lucas, S. A., Coombes, P. J., Lucas, S. A., and Coombes, P. J. (2009). The performance of infiltration trenches constructed to manage stormwater runoff from an existing urbanised catchment peri-urban processes view project integrated water resources view project the performance of infiltration trenches constructed to manage stormwater runoff from an existing urbanised catchment.
- [Maheshwari et al., 2020] Maheshwari, B., Pinto, U., Akbar, S., and Fahey, P. (2020). Is urbanisation also the culprit of climate change? – evidence from australian cities. *Urban Climate*, 31.
- [Marchioni and Becciu, 2014] Marchioni, M. and Becciu, G. (2014). Permeable pavement used on sustainable drainage systems (suds): A synthetic review of recent literature. volume 139, pages 183–194. WITPress.
- [Marsalek et al., 2006] Marsalek, J., Jiménez-Cisneros, B. E., Malmquist, P.-A., Karamouz, M., Goldenfum, J., and Chocat, B. (2006). Urban water cycle processes and interactions; 2006.
- [Mauree et al., 2019] Mauree, D., Naboni, E., Coccolo, S., Perera, A. T., Nik, V. M., and Scartezzini, J. L. (2019). A review of assessment methods for the urban environment and its energy sustainability to guarantee climate adaptation of future cities. *Renewable and Sustainable Energy Reviews*, 112:733–746.
- [McGrane, 2016] McGrane, S. J. (2016). Impacts of urbanisation on hydrological and water quality dynamics, and urban water management: a review. *Hydrological Sciences Journal*, 61:2295–2311.
- [Mees and Driessen, 2011] Mees, H. L. P. and Driessen, P. P. (2011). Adaptation to climate change in urban areas: Climate-greening london, rotterdam, and toronto. *Climate Law*, 2:251–280.
- [Ministerie van Infrastructuur en Waterstaat, 2021] Ministerie van Infrastructuur en Waterstaat (2021). Normaal Amsterdams Peil (NAP).
- [Mobron et al., 2022] Mobron, N., van Hille, T., and Prins, J. (2022). Hydrologische en thermische effecten van extensief groen dak op winkelcentrum alexandrium. *H2O*.
- [Nabiliek, 2016] Nabiliek, K., e. a. (2016). Cities in europe - facts and figures on cities and urban areas.
- [Oke, 2006] Oke, T. R. (2006). Towards better scientific communication in urban climate. *Theoretical and Applied Climatology*, 84:179–190.
- [Oo et al., 2019] Oo, H. T., Zin, W. W., and Kyi, C. C. T. (2019). Assessment of future climate change projections using multiple global climate models. *Civil Engineering Journal*, 5:2152–2166.
- [Pagano and Sorooshian, 2002] Pagano, T. and Sorooshian, S. (2002). *Encyclopedia of global environmental change*. Wiley.

- [Paithankar and Taji, 2020] Paithankar, D. N. and Taji, S. G. (2020). Investigating the hydrological performance of green roofs using storm water management model. volume 32, pages 943–950. Elsevier Ltd.
- [Patz et al., 2014] Patz, J. A., Frumkin, H., Holloway, T., Vimont, D. J., and Haines, A. (2014). Climate change: Challenges and opportunities for global health. *JAMA - Journal of the American Medical Association*, 312:1565–1580.
- [PBL, 2019] PBL (2019). Sterke groei in steden en randgemeenten verwacht.
- [Pieneman and Goedbloed, nd] Pieneman, J. and Goedbloed, D. (n.d.). Bijlage i: Resultaten watersysteemanalyse rotterdam.
- [Poeter et al., 2020] Poeter, E., Fan, Y., Cherry, J., Wood, W., and Mackay, D. (2020). Groundwater in our water cycle: Getting to know earth's most important fresh water source.
- [Puertas et al., 2014] Puertas, D. G. L., Woldearegay, K., Mehta, L., Beusekom, M. V., Pérez, M. A., and Steenberg, F. V. (2014). Roads for water: The unused potential. *Waterlines*, 33:120–138.
- [Rahman et al., 2020] Rahman, M. A., Stratopoulos, L. M., Moser-Reischl, A., Zölch, T., Häberle, K. H., Rötzer, T., Pretzsch, H., and Pauleit, S. (2020). Traits of trees for cooling urban heat islands: A meta-analysis. *Building and Environment*, 170.
- [Ramirez et al., 2021] Ramirez, R. B. M., Weir, B., Miller, B., and Weir, B. (2021). Climate change: Here are the top climate stories of 2021, a year of extremes.
- [Rasmussen and Crawford, 1997] Rasmussen, T. C. and Crawford, L. A. (1997). Identifying and removing barometric pressure effects in confined and unconfined aquifers. *Ground Water*, 35:502–511.
- [Ress et al., 2020] Ress, L. D., Hung, C. L. J., and James, L. A. (2020). Impacts of urban drainage systems on stormwater hydrology: Rocky branch watershed, columbia, south carolina. *Journal of Flood Risk Management*, 13.
- [Ribeiro et al., 2019] Ribeiro, H. V., Rybski, D., and Kropp, J. P. (2019). Effects of changing population or density on urban carbon dioxide emissions. *Nature Communications*, 10.
- [RIONED, 2019] RIONED (2019). Bui01 - Bui10.
- [Ripple et al., 2020] Ripple, W. J., Wolf, C., Newsome, T. M., Barnard, P., and Moomaw, W. R. (2020). World scientists' warning of a climate emergency scientist signatories from 153 countries (list in supplemental file s1).
- [Ripple et al., 2021] Ripple, W. J., Wolf, C., Newsome, T. M., Gregg, J. W., Lenton, T. M., Palomo, I., Eikelboom, J. A., Law, B. E., Huq, S., Duffy, P. B., and Rockström, J. (2021). World scientists' warning of a climate emergency 2021. *BioScience*, 71:894–898.
- [Rotterdam, 2021] Rotterdam, G. (2021). Van buis naar buitenruimte.
- [Santos et al., 2019] Santos, L. F., Galvão, A. F., and Cardoso, M. A. (2019). Performance indicators for urban storm water systems: A review. *Water Policy*, 21:221–244.
- [Sarkar et al., 2018] Sarkar, S., Butcher, J. B., Johnson, T. E., and Clark, C. M. (2018). Simulated sensitivity of urban green infrastructure practices to climate change. *Earth Interactions d*, 22.
- [Satoh et al., 2022] Satoh, Y., Yoshimura, K., Pokhrel, Y., Kim, H., Shiogama, H., Yokohata, T., Hanasaki, N., Wada, Y., Burek, P., Byers, E., Schmied, H. M., Gerten, D., Ostberg, S., Gosling, S. N., Eric, J., Boulange, S., and Oki, T. (2022). The timing of unprecedented hydrological drought under climate change. *NATURE COMMUNICATIONS*, 13.
- [Savitzky and Golay, 1964] Savitzky, A. and Golay, M. J. (1964). Smoothing and differentiation of data by simplified least squares procedures. *Analytical Chemistry*, 36:1627–1639.

- [Schaap et al., 2001] Schaap, M. G., Leij, F. J., and Genuchten, M. T. V. (2001). rosetta: a computer program for estimating soil hydraulic parameters with hierarchical pedotransfer functions. *Journal of Hydrology*, 251:163–176.
- [Singh et al., 2020] Singh, J., Karmakar, S., Paimazumder, D., Ghosh, S., and Niyogi, D. (2020). Urbanization alters rainfall extremes over the contiguous united states. *Environmental Research Letters*, 15.
- [Soltani and Sharifi, 2017] Soltani, A. and Sharifi, E. (2017). Daily variation of urban heat island effect and its correlations to urban greenery: A case study of adelaide. *Frontiers of Architectural Research*, 6:529–538.
- [Spane, 1999] Spane, F. A. (1999). Effects of barometric fluctuations on well water-level measurements and aquifer test data.
- [Steenefeld et al., 2011] Steenefeld, G. J., Koopmans, S., Heusinkveld, B. G., Hove, L. W. V., and Holtslag, A. A. (2011). Quantifying urban heat island effects and human comfort for cities of variable size and urban morphology in the netherlands. *Journal of Geophysical Research Atmospheres*, 116.
- [Steensen et al., 2022] Steensen, B. M., Marelle, L., Hodnebrog, and Myhre, G. (2022). Future urban heat island influence on precipitation. *Climate Dynamics*, 58:3393–3403.
- [Støvring et al., 2018] Støvring, J., Dam, T., and Jensen, M. B. (2018). Hydraulic performance of lined permeable pavement systems in the built environment. *Water (Switzerland)*, 10.
- [susdrain,] susdrain. Permeable pavement.
- [Sörensen and Emilsson, 2019] Sörensen, J. and Emilsson, T. (2019). Evaluating flood risk reduction by urban blue-green infrastructure using insurance data. *Journal of Water Resources Planning and Management*, 145:04018099.
- [Toreti et al., 2022] Toreti, A., Masante, D., Navarro, J. A., Bavera, D., Cammalleri, C., Jager, A. D., Ciollo, C. D., Essenfelder, A. H., Maetens, W., Magni, D., Mazzeschi, M., Spinoni, J., and Felice, M. D. (2022). *Drough in Europe*, volume EUR 31147 EN. Publications Office of the European Union.
- [U.S. EPA, 2008] U.S. EPA (2008). Heat Island Compendium.
- [USGS, 2020] USGS (2020). Evaluating the potential benefits of permeable pavement on the quantity and quality of stormwater runoff | U.S. Geological Survey.
- [Vieux and Vieux, 2005] Vieux, B. and Vieux, J. (2005). Rainfall accuracy considerations using radar and rain gauge networks for rainfall-runoff monitoring. *Journal of Water Management Modeling*.
- [Vijayaraghavan, 2016] Vijayaraghavan, K. (2016). Green roofs: A critical review on the role of components, benefits, limitations and trends. *Renewable and Sustainable Energy Reviews*, 57:740–752.
- [Wakode et al., 2018] Wakode, H. B., Baier, K., Jha, R., and Azzam, R. (2018). Impact of urbanization on groundwater recharge and urban water balance for the city of hyderabad, india. *International Soil and Water Conservation Research*, 6:51–62.
- [Wang and Guo, 2020] Wang, J. and Guo, Y. (2020). Dynamic water balance of infiltration-based stormwater best management practices. *Journal of Hydrology*, 589.
- [Wang et al., 2017] Wang, J. P., Hu, N., François, B., and Lambert, P. (2017). Estimating water retention curves and strength properties of unsaturated sandy soils from basic soil gradation parameters. *Water Resources Research*, 53:6069–6088.
- [Watts et al., 2021] Watts, N., Amann, M., Arnell, N., Ayeb-Karlsson, S., Beagley, J., Belesova, K., Boykoff, M., Byass, P., Cai, W., Campbell-Lendrum, D., Capstick, S., Chambers, J., Coleman, S., Dalin, C., Daly, M., Dasandi, N., Dasgupta, S., Davies, M., Napoli, C. D., Dominguez-Salas, P., Drummond, P., Dubrow, R., Ebi, K. L., Eckelman, M., Ekins, P., Escobar, L. E., Georgeson, L., Golder, S., Grace, D., Graham, H., Hagggar, P., Hamilton, I., Hartinger, S., Hess, J., Hsu, S. C., Hughes, N.,

- Mikhaylov, S. J., Jimenez, M. P., Kelman, I., Kennard, H., Kiesewetter, G., Kinney, P. L., Kjellstrom, T., Kniveton, D., Lampard, P., Lemke, B., Liu, Y., Liu, Z., Lott, M., Lowe, R., Martinez-Urtaza, J., Maslin, M., McAllister, L., McGushin, A., McMichael, C., Milner, J., Moradi-Lakeh, M., Morrissey, K., Munzert, S., Murray, K. A., Neville, T., Nilsson, M., Sewe, M. O., Oreszczyn, T., Otto, M., Owfi, F., Pearman, O., Pencheon, D., Quinn, R., Rabhaniha, M., Robinson, E., Rocklöv, J., Romanello, M., Semenza, J. C., Sherman, J., Shi, L., Springmann, M., Tabatabaei, M., Taylor, J., Triñanes, J., Shumake-Guillemot, J., Vu, B., Wilkinson, P., Winning, M., Gong, P., Montgomery, H., and Costello, A. (2021). The 2020 report of the lancet countdown on health and climate change: responding to converging crises. *The Lancet*, 397:129–170.
- [WMO, 2021] WMO (2021). State of Climate in 2021: Extreme events and major impacts.
- [Xiao et al., 2017] Xiao, Q., McPherson, E. G., Zhang, Q., Ge, X., and Dahlgren, R. (2017). Performance of two bioswales on urban runoff management. *Infrastructures*, 2.
- [Yang et al., 2021] Yang, D., Yang, Y., and Xia, J. (2021). Hydrological cycle and water resources in a changing world: A review. *Geography and Sustainability*, 2:115–122.
- [Zhao and Wang, 2013] Zhao, D. and Wang, G. (2013). Removing barometric pressure effects from groundwater level and identifying main influential constituents. *Science China Technological Sciences*, 56:129–136.
- [Zhou et al., 2004] Zhou, L., Dickinson, R. E., Tian, Y., Fang, J., Li, Q., Kaufmann, R. K., Tucker, C. J., and Myneni, R. B. (2004). Evidence for a significant urbanization effect on climate in china.
- [© atelier GROENBLAUW, Marlies van der Linden,] © atelier GROENBLAUW, Marlies van der Linden. Section scheme of a bioswale during rainfall .
- [Ícaro Vasconcelos do Nascimento et al., 2018] Ícaro Vasconcelos do Nascimento, de Assis Júnior, R. N., de Araújo, J. C., de Alencar, T. L., Freire, A. G., Lobato, M. G. R., da Silva, C. P., Mota, J. C. A., and do Nascimento, C. D. V. (2018). Estimation of van genuchten equation parameters in laboratory and through inverse modeling with hydrus-1d. *Journal of Agricultural Science*, 10:102.
- [Šimůnek et al., 2012] Šimůnek, J., Genuchten, M. T. V., and Šejna, M. (2012). Hydrus: Model use, calibration, and validation. *Transactions of the ASABE*, 55:1261–1274.



Appendix A: Subsurface

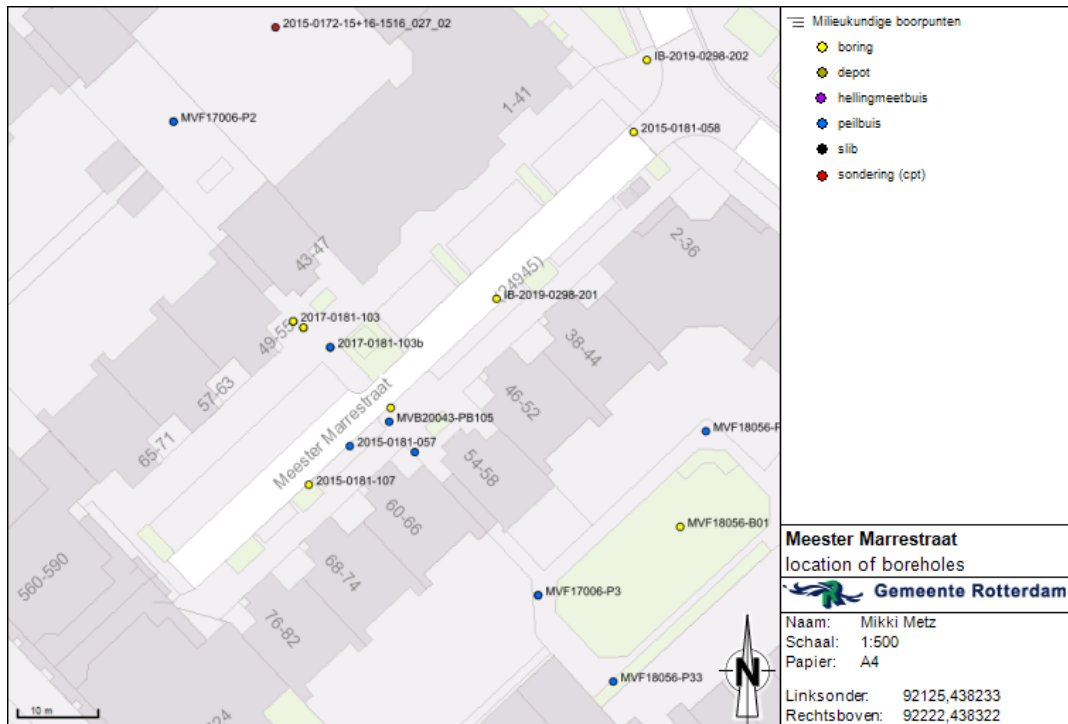
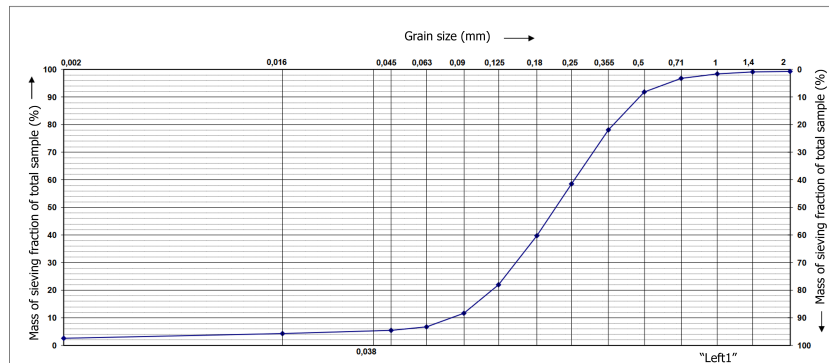
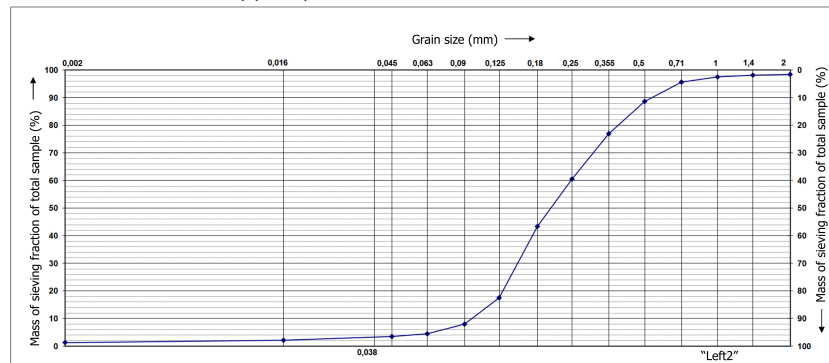
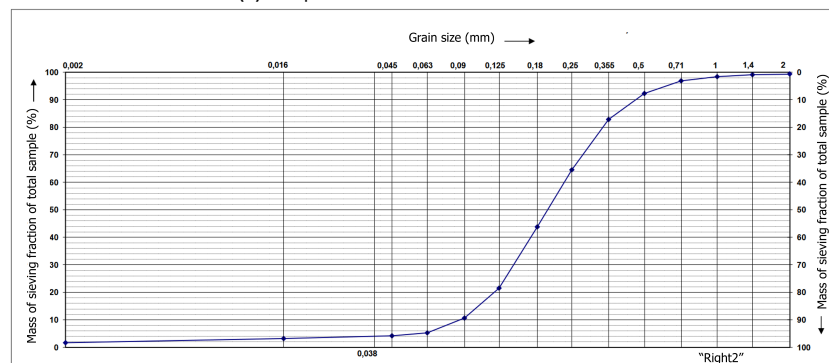


Figure A.1: Borehole locations in the test area for summarized data in Table A.1

Table A.1: Borehole summary at the test location for boreholes depths ranging from 2 to 3 meters.

Location	P107	Soil	57	Soil	105	Soil	103b	Soil	201	Soil	58	Soil
Depth	3		2.5		2		2		2.5		3	
Top layer	3 m	Sand	2 m	Sand	0.7 m	Sand	2 m	Sand	2.5 m	Sand	3 m	Sand
Middle			0.7 m	Clay	0.8 m	Clay						
Bottom					0.5 m	Sand						

**(a)** The particle size distribution at location L1**(b)** The particle size distribution at location L2**(c)** The particle size distribution at location R2**Figure A.2:** Sampled soil particle size distribution**Figure A.3:** Grain Size Distribution test results for three monitoring locations L1, L2 and R2 as shown in Figure 5.11.

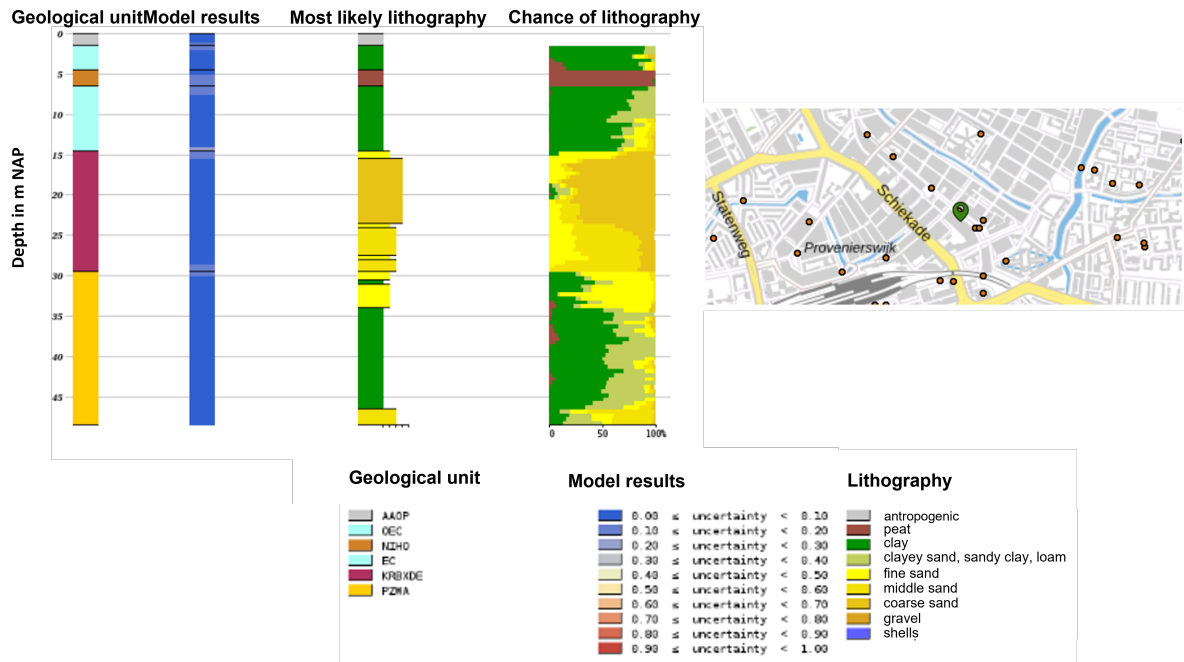


Figure A.4: Borehole location 1

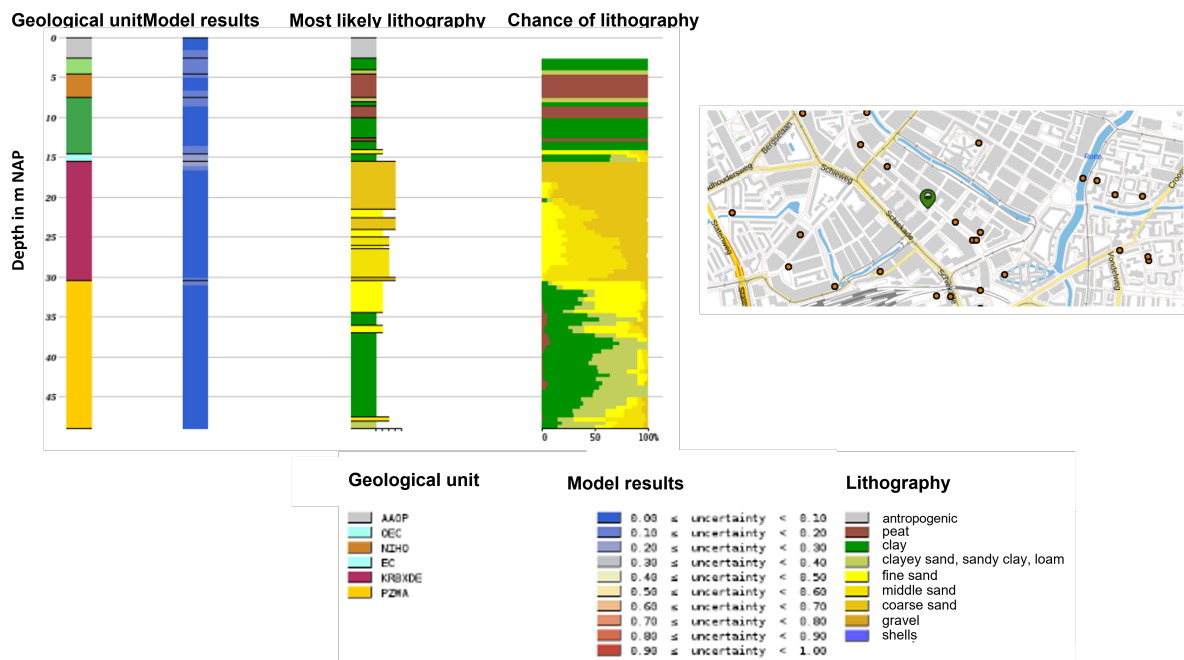


Figure A.5: Borehole location 2

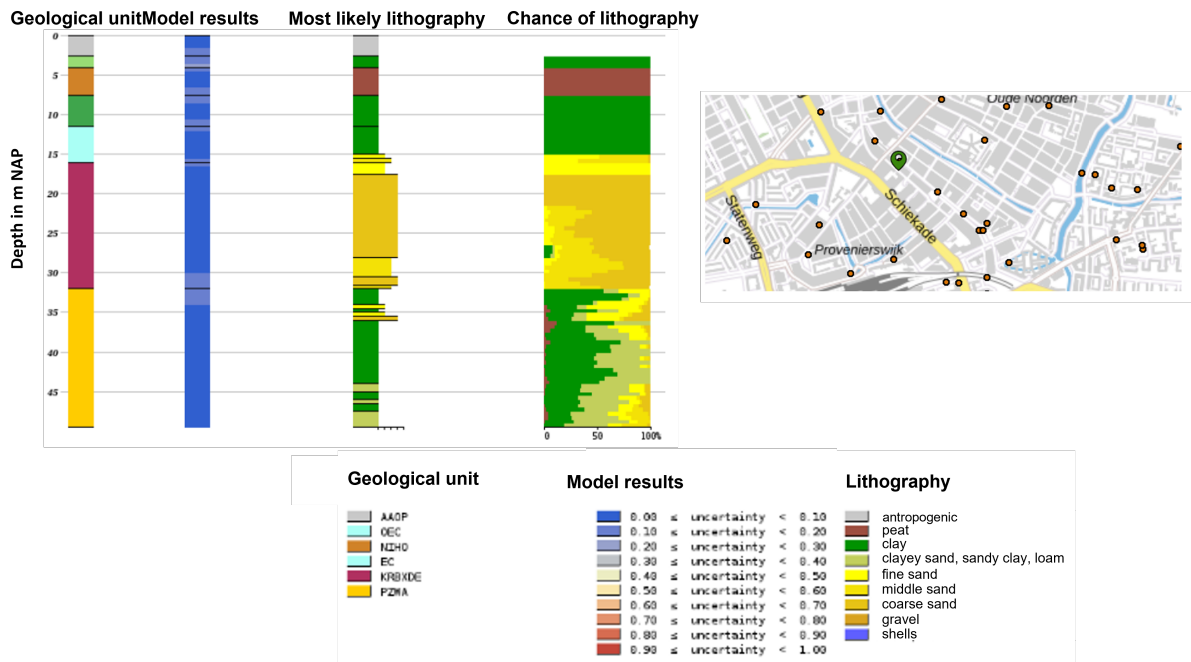


Figure A.6: Borehole location 3

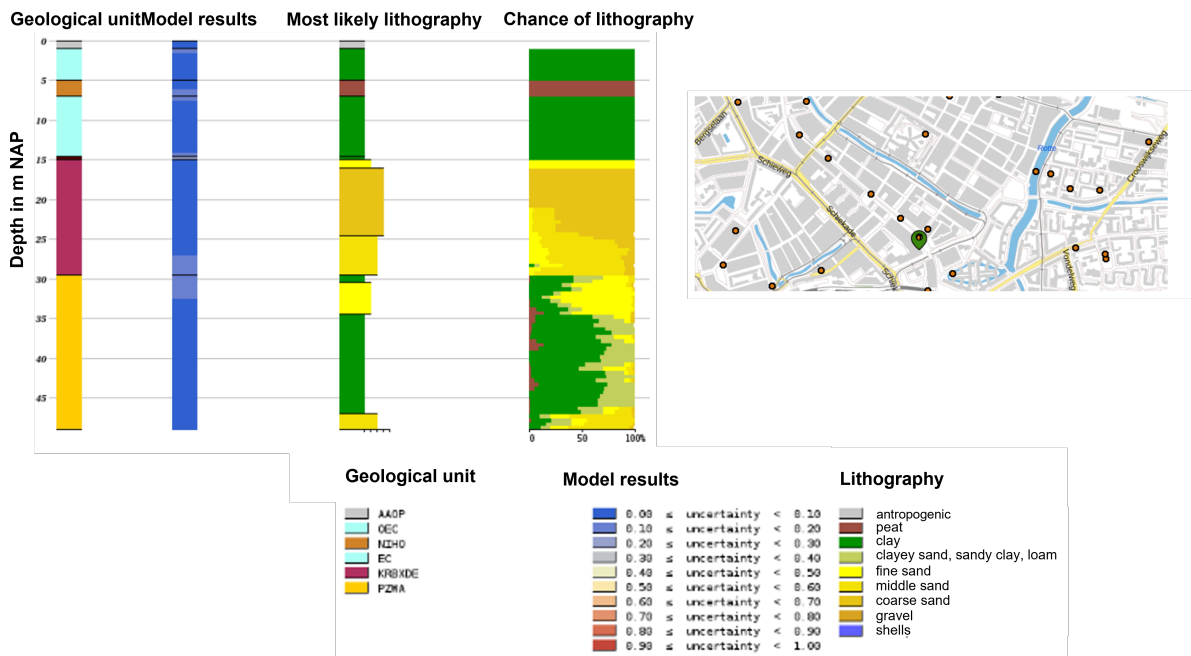


Figure A.7: Borehole location 4

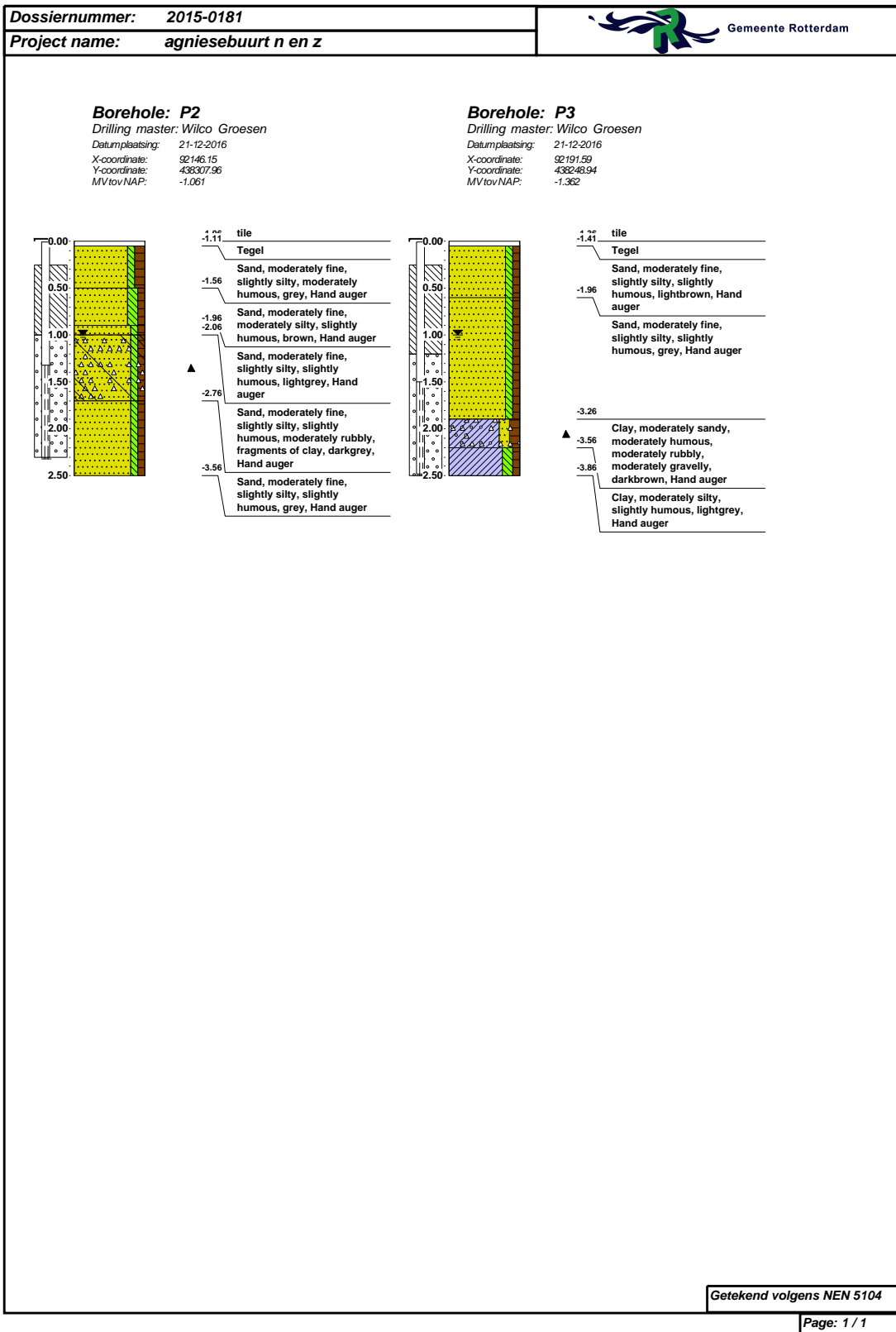


Figure A.8: Soil data from piezometer location P2 and P3

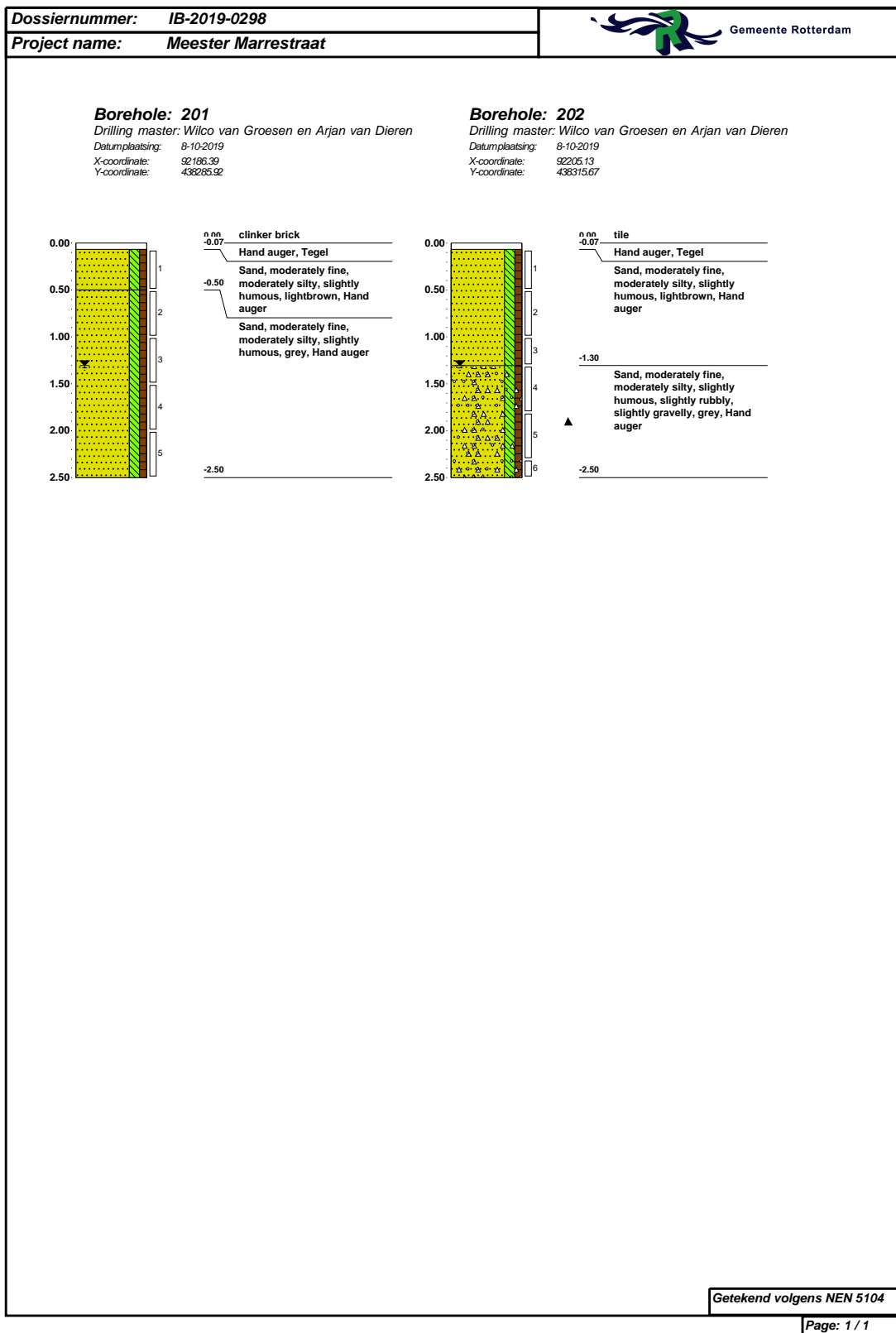


Figure A.10: Soil data from piezometer location P201 and P202

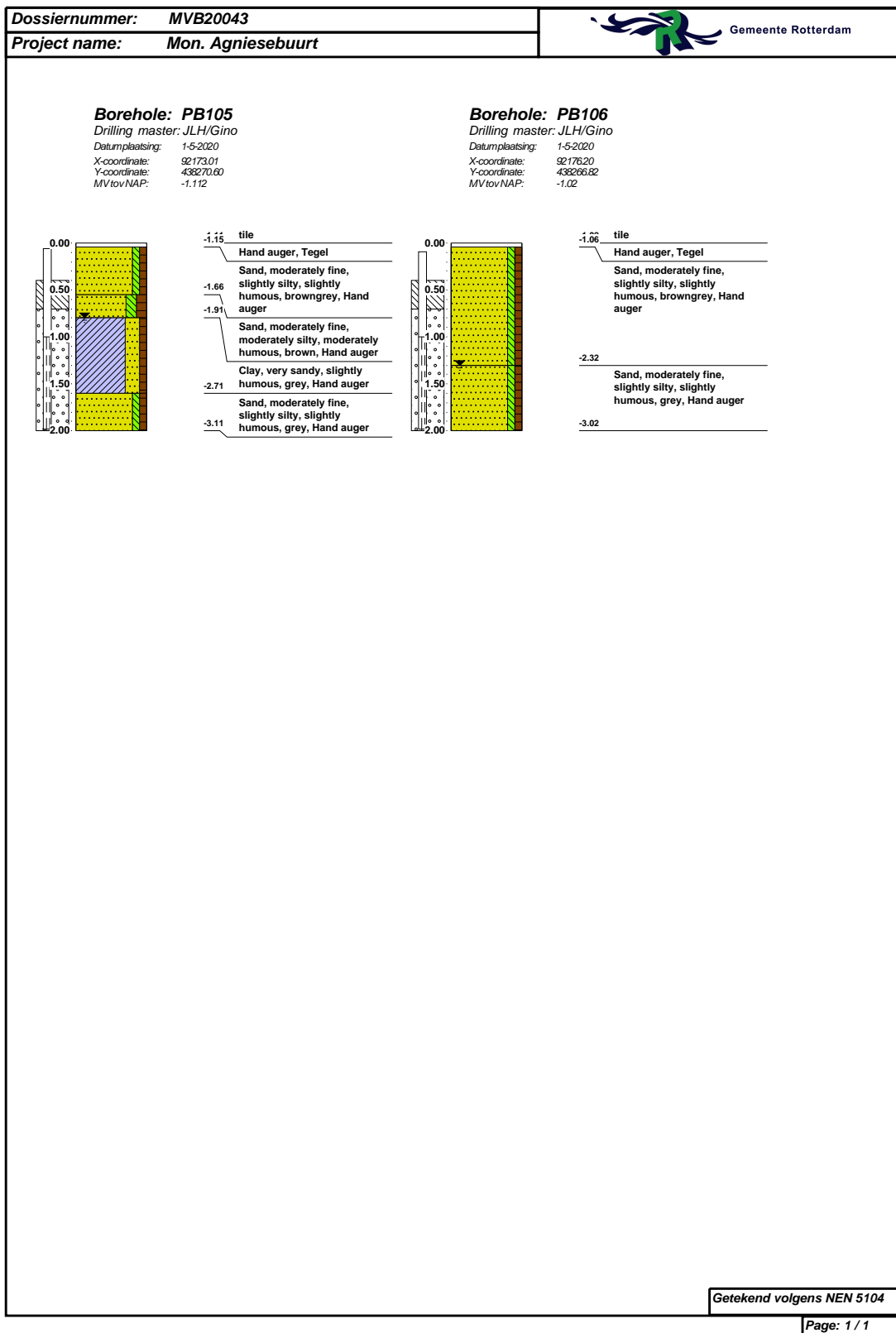


Figure A.11: Soil data from piezometer location P105 and P106

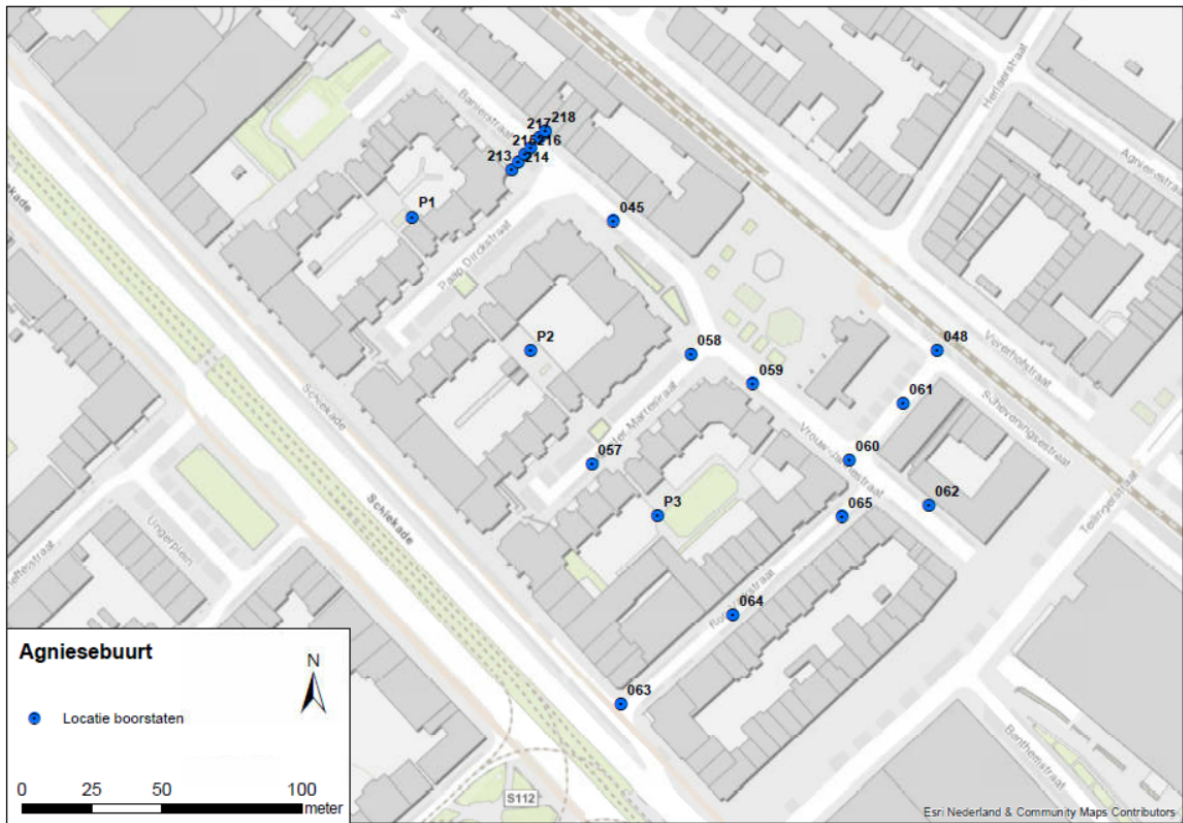
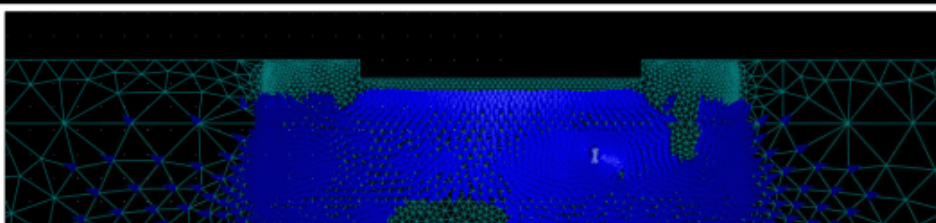
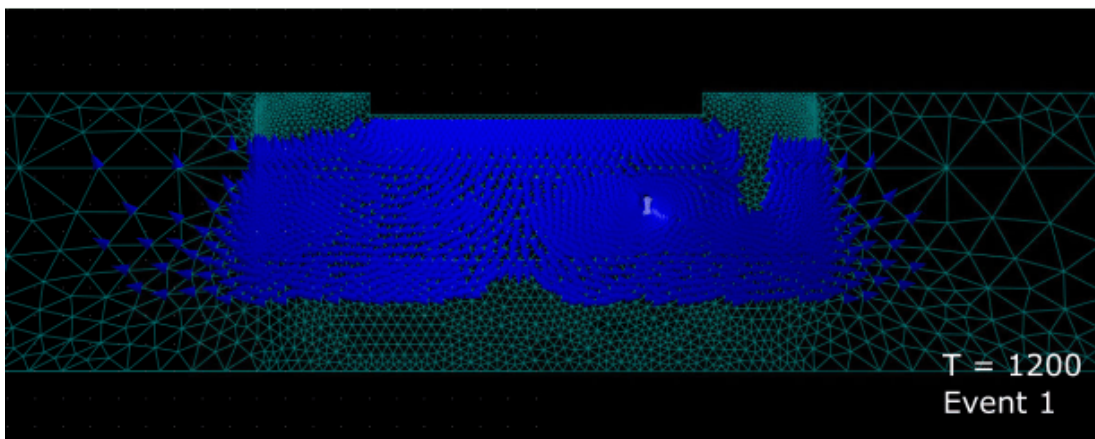
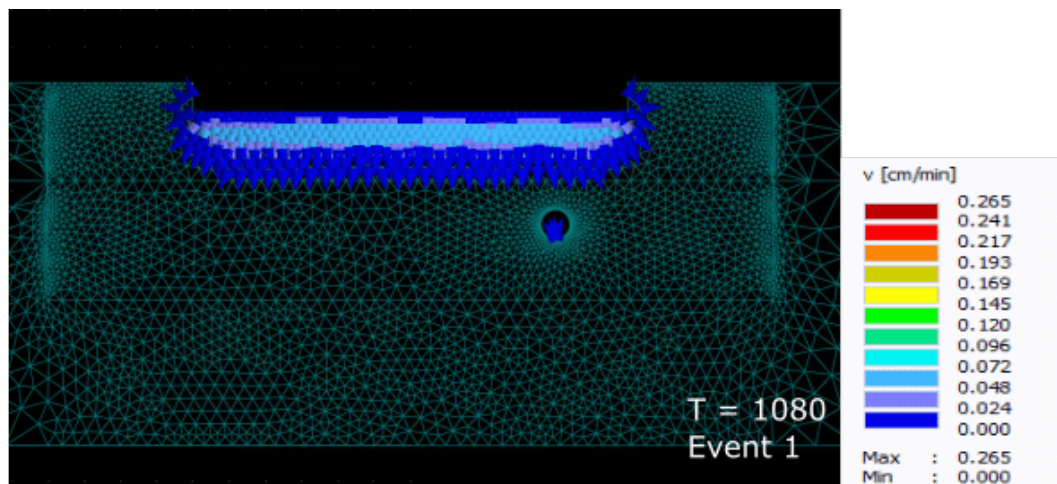


Figure A.12: Soil monitoring locations



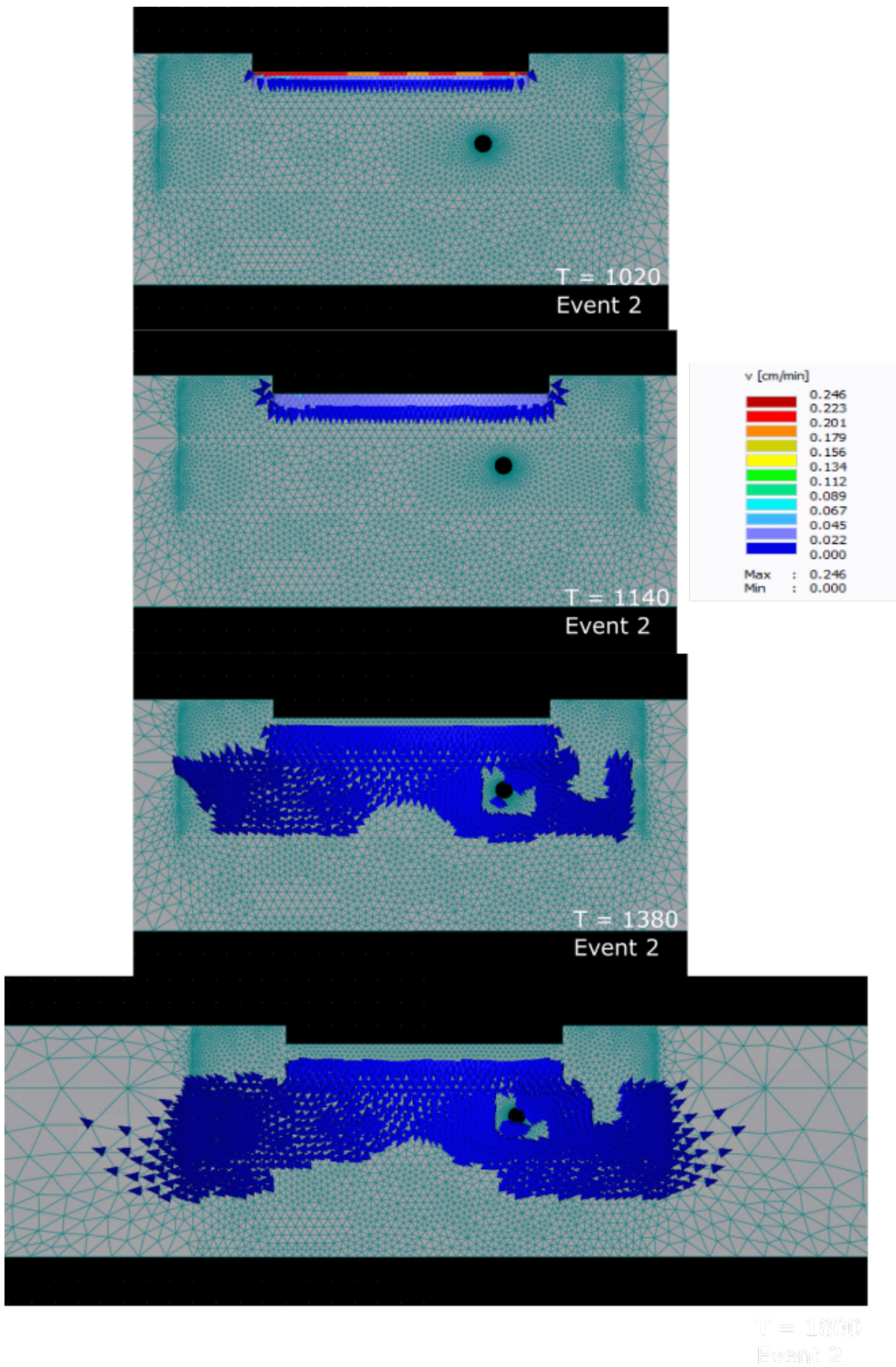


Figure A.14: Hydrus flow velocity for Event 2

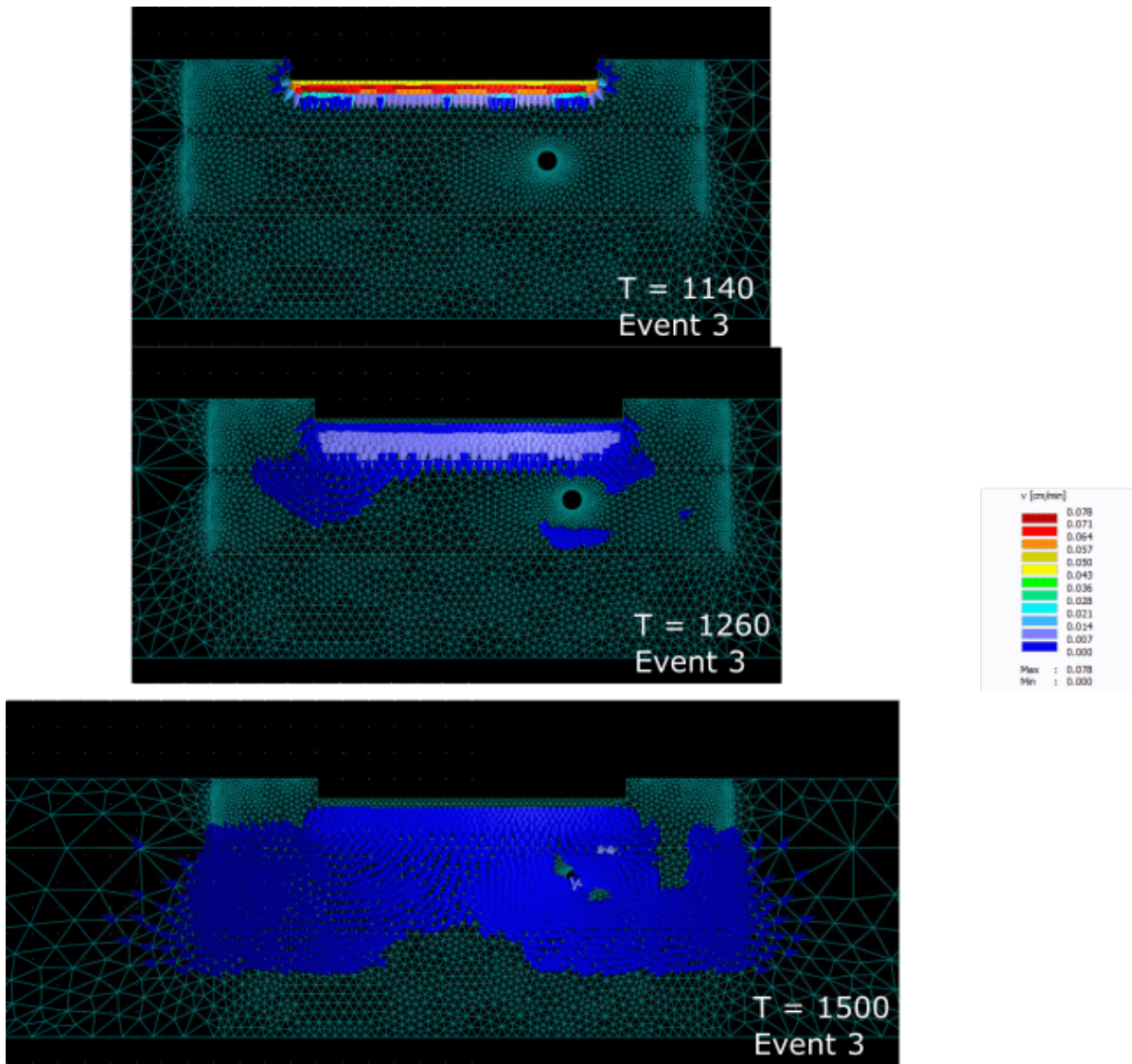
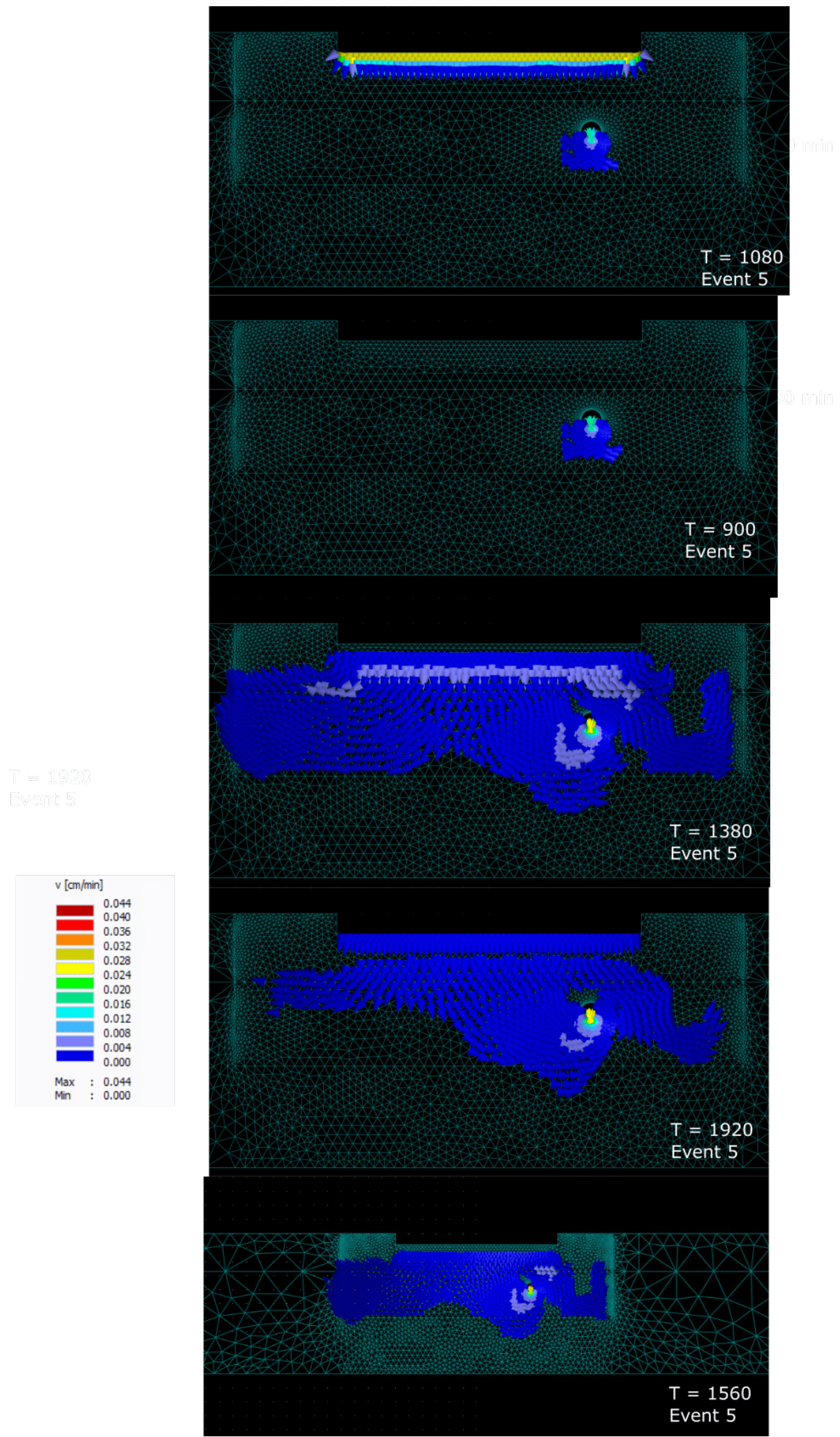


Figure A.15: Hydrus flow velocity for Event 3



B

Rainfall analysis

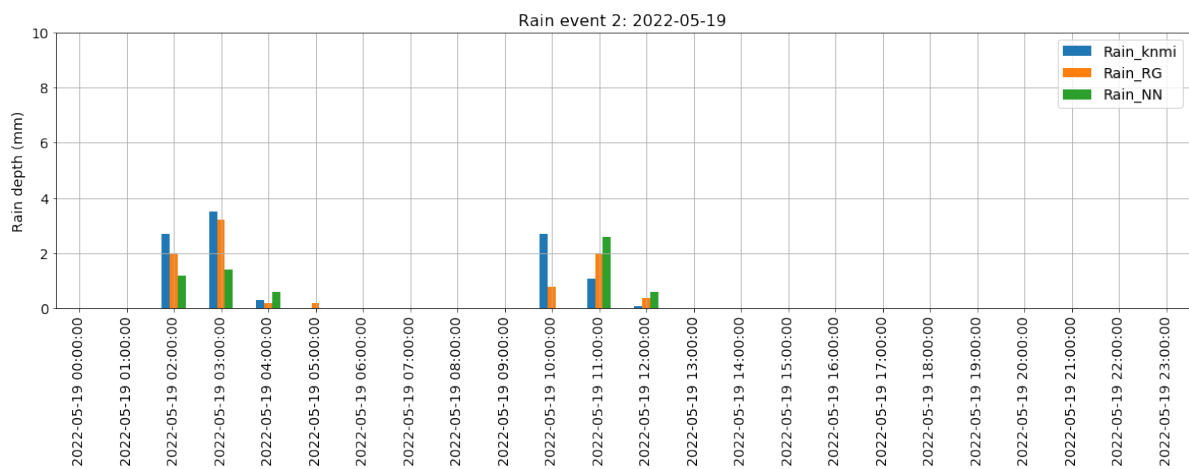


Figure B.1: Event 1 rain [mm] comparison

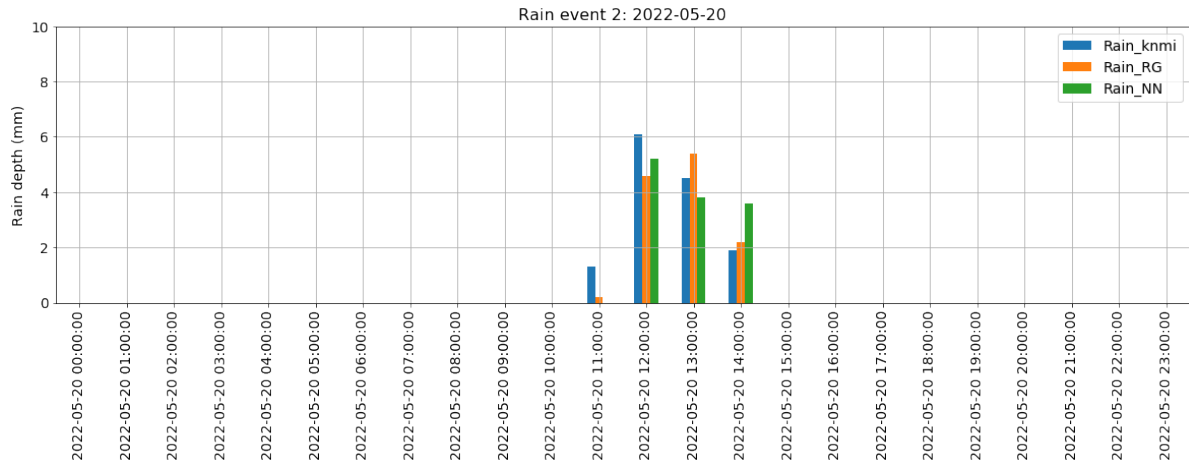


Figure B.2: Event 2-b rain [mm] comparison

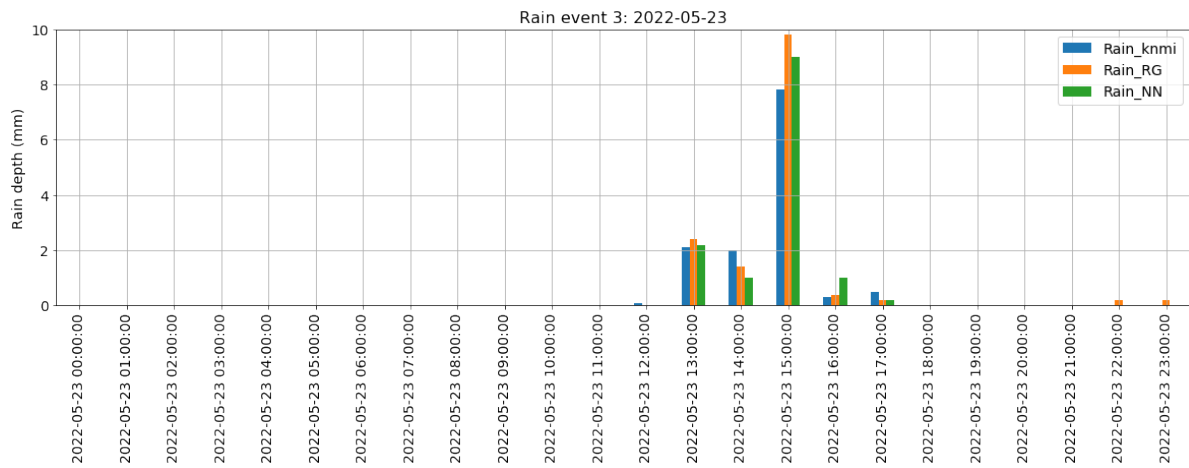


Figure B.3: Event 3 rain [mm] comparison

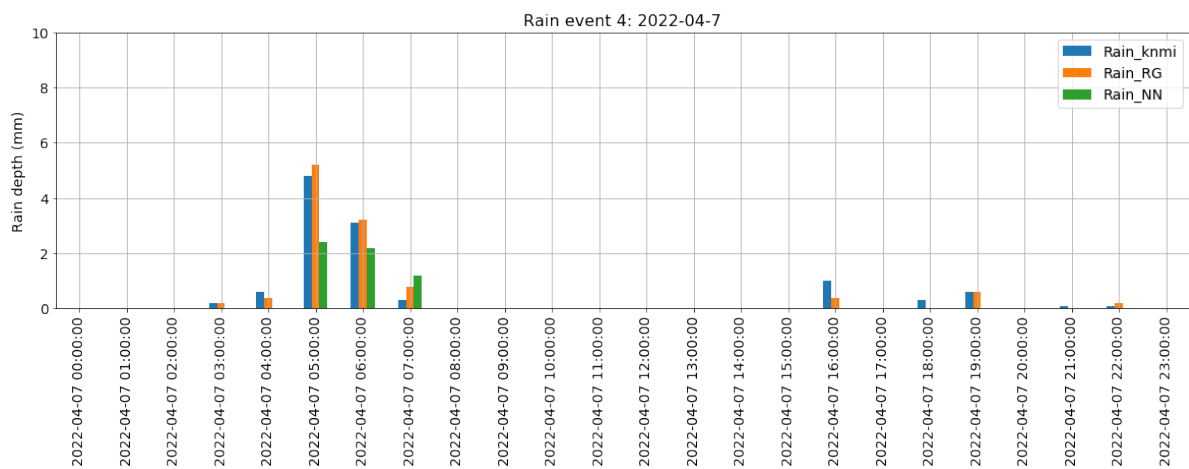
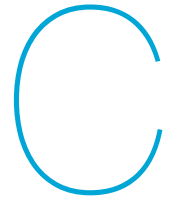


Figure B.4: Event 4 rain [mm] comparison



Hydrus

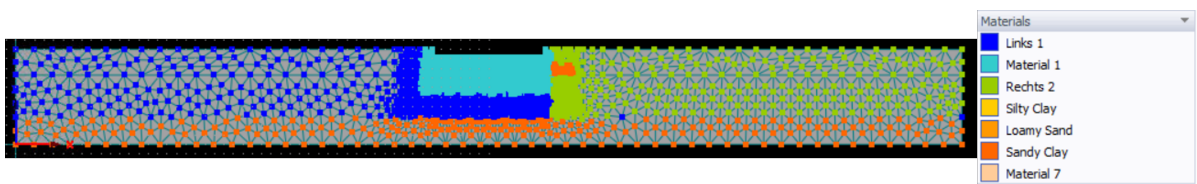


Figure C.1: Material Distribution Hydrus

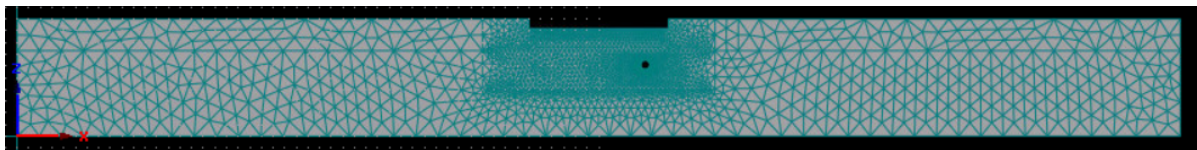


Figure C.2: FE-Mesh Hydrus

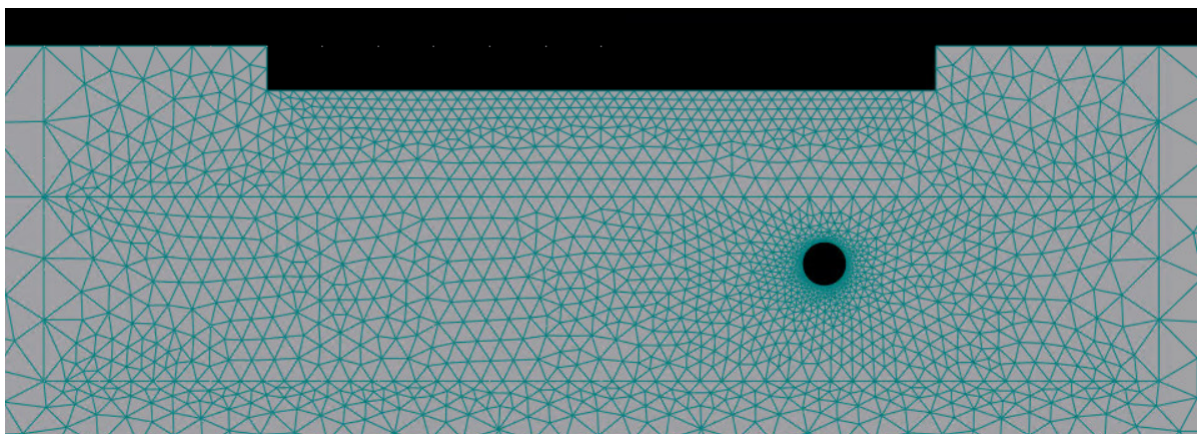


Figure C.3: Zoomed in FE-Mesh Hydrus

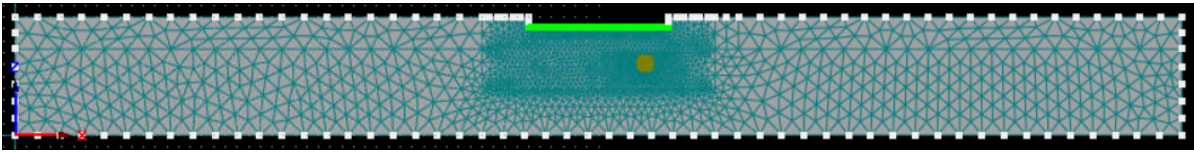


Figure C.4: Boundary Conditions Hydrus

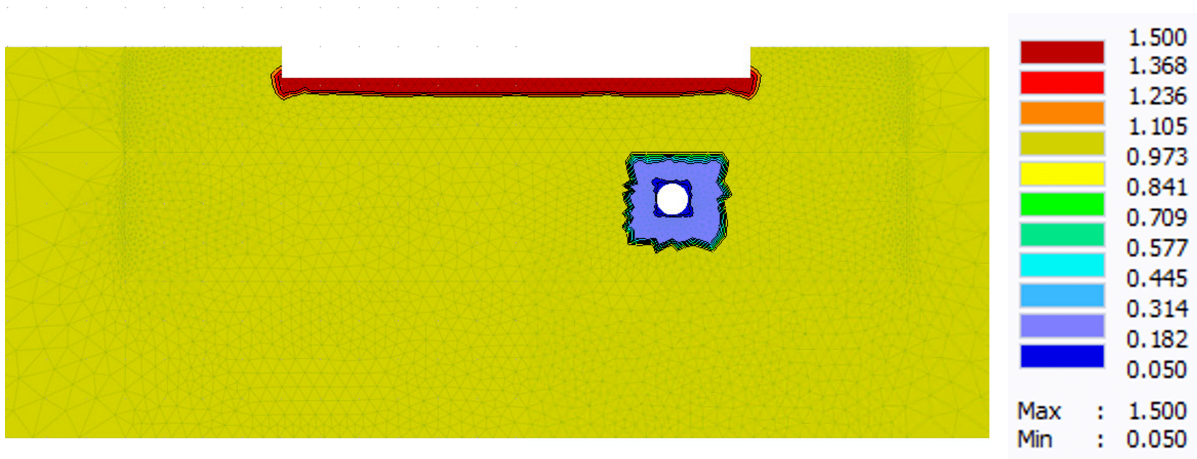


Figure C.5: Scaling Factor applied in the model

Table C.1: Observation point heads over time from full scale test piezometer locations P103 (obs 1 and obs 2) and P105 (obs3).

<i>X (time [mins])</i>	<i>Y (head [cm])</i>	<i>Observation point (Piezometer)</i>
1	0	1
1000	0	1
1420	12	1
1540	15	1
2020	10	1
2720	7	1
3440	5	1
4160	3	1
4880	0	1
1	0	2
1000	0	2
1420	12	2
1540	15	2
2020	10	2
2720	7	2
3440	5	2
4160	3	2
4880	0	2
1	0	3
1000	0	3
1420	0	3
1540	2	3
2020	1	3
2720	1	3
3440	1	3
4160	1	3
4880	1	3